DOKUZ EYLÜL UNIVERSITY
GRADUATE SCHOOL OF NATURAL AND APPLIED SCIENCES

EMPLOYING THE FRACTIONAL AUTOCORRELATION AND CROSS – CORRELATION OPERATIONS IN TARGET DETECTION AND RANGE ESTIMATION USING POLYPHASE PULSE COMPRESSION WAVEFORMS

by
Erten ERÖZDEN

September, 2006
İZMİR

EMPLOYING THE FRACTIONAL AUTOCORRELATION AND CROSS – CORRELATION OPERATIONS IN TARGET DETECTION AND RANGE ESTIMATION USING POLYPHASE PULSE COMPRESSION WAVEFORMS

A Thesis Submitted to the
Graduate School of Natural and Applied Sciences of Dokuz Eylül University
In Partial Fulfillment of the Requirements for the Degree of Master of Science in Electrical and Electronics Engineering

by
Erten ERÖZDEN

September, 2006
İZMİR

M.Sc THESIS EXAMINATION RESULT FORM

We have read the thesis entitled **"EMPLOYING THE FRACTIONAL AUTOCORRELATION AND CROSS – CORRELATION OPERATIONS IN TARGET DETECTION AND RANGE ESTIMATION USING POLYPHASE PULSE COMPRESSION WAVEFORMS"** completed by **Erten ERÖZDEN** under supervision of **Asst. Prof. Dr. Olcay AKAY** and we certify that in our opinion it is fully adequate, in scope and in quality, as a thesis for the degree of Master of Science.

.....

Asst. Prof. Dr. Olcay AKAY
Supervisor

.....

Asst. Prof. Dr. Yavuz ŞENOL
(Jury Member)

.....

Asst. Prof. Dr. Serdar ÖZEN
(Jury Member)

Prof.Dr. Cahit HELVACI
Director
Graduate School of Natural and Applied Sciences

ACKNOWLEDGMENTS

I would like to thank my advisor Asst. Prof. Dr. Olcay AKAY for his valuable guidance and patient support during the course of this thesis work. I also wish to express my sincere appreciation to my friend Edip BİNER for the valuable insights he has provided. Lastly and mostly, I thank my family for their never – ending support.

Erten ERÖZDEN

EMPLOYING THE FRACTIONAL AUTOCORRELATION AND CROSS – CORRELATION OPERATIONS IN TARGET DETECTION AND RANGE ESTIMATION USING POLYPHASE PULSE COMPRESSION WAVEFORMS

ABSTRACT

Radars are mostly used for detection and ranging of a target. The transmitted signal is generally a sinusoidal waveform. However, it is known that linear frequency modulated (LFM) signals are commonly employed in radars to perform pulse compression. Beside the LFM signal, step LFM and polyphase coded signals such as, Frank, P1, P2, P3 and P4 codes are also used for a similar purpose. Since the instantenous frequency of the LFM signal is changing in time linearly, it has a linear support region on the time-frequency plane. Using this property of the LFM, we can detect it using the Radon – ambiguity transform as suggested in some previous works. It was also proposed and shown that LFM signals can be detected using the fractional autocorrelation function. Using the similarity of ambiguity functions of polyphase coded signals with the LFM ambiguity function we suggested to detect these codes applying the fractional autocorrelation function. In this thesis, we show that fractional autocorrelation also works for the detection and ranging applications of these codes via simulations using the MATLAB numeric analysis software package.

In radars, estimation of a target's position can also be accomplished using cross – correlation of the received and transmitted waveforms. We suggested using fractional cross – correlation for estimating the delay of the received waveform when the transmitted signal is the LFM, step LFM or polyphase codes. We compare the performance of conventional and fractional cross – correlations through various simulations.

Keywords : Fourier transform, Fractional Fourier transform, fractional autocorrelation, fractional cross – correlation, ambiguity function, polyphase codes,

LFM signal, step LFM signal, Frank code, P1 code, P2 code, P3 code, P4 code.

ÇOK FAZLI DARBE SIKIŞTIRMA DALGA ŞEKİLLERİNİ KULLANARAK KESİRLİ OTOKORELASYON VE ÇAPRAZ KORELASYON İŞLEMLERİNİN HEDEF TESPİTİ VE MESAFE KESTİRİMİNDE UYGULANMASI

ÖZ

Radarlar genellikle hedef tesbiti ve hedef uzaklığının belirlenmesi için kullanılır. Gönderilen sinyal genellikle sinusoidal bir sinyaldir. Fakat, radarlarda darbe sıkıştırmaya yatkın olan doğrusal frekans modulasyon (DFM) sinyali de gönderilen sinyal olarak sıklıkla kullanılır. DFM sinyali yanında basamaklı DFM ve çok fazlı kodlamalı sinyaller olarak adlandırılan Frank, P1, P2, P3 ve P4 sinyalleri de benzer amaçla kullanılabilir. DFM sinyalinin anlık frekansı zamanla değiştiği için zaman – frekans düzleminde doğrusal bir izdüşümü oluşturur. DFM'nin bu özelliğinden yararlanıp Radon – Belirsizlik Fonksiyonu kullanılarak DFM sinyalinin tesbiti yapılabilir. Fakat, DFM'yi kesirli otokorelasyon fonksiyonunu kullanan bir yöntemle de tesbit edebileceğimiz yakın zamanda önerilmiştir. Basamaklı DFM ve çok fazlı kodlamalı sinyallerin DFM'ye benzeyen özelliğini kullanarak, bu sinyalleri de kesirli otokorelasyon yöntemiyle tesbit edebileceğimizi MATLAB numerik analiz yazılım paketi üzerinde yaptığımız simülasyonlarla gösteriyoruz.

Radarlarda hedefin yerinin tespitini gönderilen ve algılanan sinyallerin çapraz korelasyonu yardımıyla yapabiliriz. Biz, DFM, basamaklı DFM ve çok fazlı kodlamalı sinyalleri kullanarak hedefin yerinin tespitini kesirli çapraz korelasyon ile yapabileceğimiz yeni bir yöntem öneriyoruz. Klasik ve kesirli çapraz korelasyon yöntemlerinin performanslarını çeşitli simülasyon örnekleri aracılığıyla yapıyoruz.

Anahtar sözcükler : Fourier dönüşümü, kesirli Fourier dönüşümü, kesirli otokorelasyon, kesirli çapraz korelasyon, belirsizlik fonksiyonu, çok faz kodlamalı sinyaller, DFM sinyali, basamaklı DFM sinyali, Frank kodu, P1 kodu, P2 kodu, P3 kodu, P4 kodu.

CONTENTS

Page

CHAPTER ONE
INTRODUCTION

1.1 Introduction

Radars are used in many areas of our daily lives. Basicly, a radar is an electronic system used for detection and range determination of targets. However, modern radars go beyond this scope and they can also classify or identify targets, and even produce the images of target objects. Radars usually transmit a signal and receive back a reflected signal that is corrupted by noise. By processing the received signal the existence of a target can be determined. After the detection of the target, its range and velocity properties can be estimated.

One of the most commonly employed methods for detection is the matched filter which optimally maximizes the output signal to noise ratio (SNR). The output of the matched filter can be computed using cross – correlation of the received signal and the delayed replica of the transmitted signal. If the input signal were the same with the transmitted signal, then the output of the matched filter would be the autocorrelation function (Mahafza, 2000).

Linear frequency modulated (LFM) signals are one of the oldest and most useful pulse compression waveforms due to their high range resolution and tolerance to Doppler for ease in receiver processing. Radon – Wigner transform (RWT) detects lines in the Wigner time – frequency plane by computing the line integrals for a set of angles and positional offsets in the transform (Kay & Boudreaux – Bartels, 1985), (Li, 1987), (Wood & Barry, 1994). Radon – ambiguity transform (RAT) is another method that detects unknown LFM signals by computing a series of line integrals through the origin of the ambiguity plane (Wang, et. al. 1998). Since the LFM has an ambiguity function, which is a line passing through the origin of the ambiguity plane, only those line integrals are computed. Detection of LFM signals can be performed more efficiently using fractional autocorrelation (Akay & Boudreaux – Bartels, 2001). The other pulse compression signals used in radars, step LFM and polyphase-

coded signals such as, Frank, P1, P2, P3 and P4, can also be detected using the RAT (Jennison, 2003).

In this thesis, we investigate the performance of a detector that is implemented using the fractional autocorrelation function for detection of LFM, step LFM and polyphase-coded signals. The fractional Fourier transform (FrFT) which is the generalization of the classical Fourier transform (FT) was developed in recent years (Almeida, 1994). Properties of the FrFT were derived and its relationship with time – frequency representations were established. A fast approximate discrete FrFT algorithm was also developed (Özaktaş, et. al., 1996). The FrFT was alternatively defined via unitary and Hermitian fractional operators (Akay & Boudreaux – Bartels, 1998) following the concepts of unitary equivalence (Baraniuk & Jones, 1995) and covariant and invariant transforms (Sayeed & Jones, 1996). Fractional cross – correlation and autocorrelation functions which are the generalizations of classical cross – correlation and autocorrelation functions were defined using the unitary fractional operator. A detection statistic which is based on fractional autocorrelation was also proposed for detection of LFM signals (Akay & Boudreaux – Bartels, 2001). In this thesis, we extend the work of Akay and Boudreaux – Bartels for detection of other pulse compression radar waveforms; step LFM signals and polyphase coded signals. Performance of this detector is also investigated. Furthermore, we utilize fractional cross – correlation for range estimation.

In Chapter 2, a theoretical study of the FrFT is provided. After providing a brief introduction to the FT and the Fourier series, definitions of classical cross – correlation and autocorrelation are given. The FrFT which is the generalization of the classical FT is formulated and its fundamental properties are listed briefly. Definitions of fractional cross – correlation and fractional autocorrelation are derived using the fractional operators. Some alternative definitions of fractional cross – correlation and autocorrelation are also formulated.

In Chapter 3, principles of a radar system are introduced, and a simple optimal detection scenario is formulated. The matched filter and the radar ambiguity function

are also introduced. The concept of pulse compression and LFM, step LFM, polyphase coded signals such as Frank, P1, P2, P3 and P4 codes, are described and their ambiguity function plots are illustrated.

In Chapter 4, using fractional autocorrelation a detection statistic is formulated for the detection of pulse compression waveforms defined in Chapter 3. Performance of this detector is investigated through simulations at different SNR values and at different signal pulse durations.

In Chapter 5, range estimation is performed by estimating the delay parameter using fractional cross – correlation. Performance of fractional cross – correlation is compared with its conventional counterpart.

Finally, our conclusions are given in Chapter 6.

CHAPTER TWO

FUNDAMENTALS OF THE FRACTIONAL FOURIER TRANSFORM AND FRACTIONAL CORRELATION

In this chapter, fundamentals of the fractional Fourier transform and fractional correlation is given. In Sections 1 and 2, the Fourier representation of periodic signals and finite energy signals along with autocorrelation are discussed. In Section 3, the fractional Fourier transform is studied. Then, in last section, definitions of fractional cross – correlation and fractional autocorrelation functions are introduced using the unitary fractional shift operator.

2.1 Frequency Analysis of Continuous - Time Signals

We can represent a signal in different forms using transform techniques by which the interesting properties of signals could be displayed explicitly. Fourier analysis is the basic tool for signals whose frequency content does not change in time. For signals whose frequency content changes with time (such as biomedical signals, speech signals, etc.), the classical Fourier analysis is not adequate. Hence, other tranforms such as the short-time Fourier transform and the Wigner distribution are defined for analysis of so – called nonstationary signals (Cohen, 1995), (Qian & Chen, 1996), (Poularikas, 2000).

Using the Fourier transform, a time domain signal can be represented in frequency domain. This signal representation basically involves the decomposition of the time domain signal onto sinusoidal (or complex exponential) basis functions. With this decomposition, the time domain signal is represented with respect to its frequency content.

2.1.1 Fourier Series for Continuous – Time Periodic Signals

The basic mathematical representation of periodic signals is the Fourier series. It represents any well behaving periodic signal as a linear weighted sum of harmonically related sinusoids or complex exponentials. Jean Baptiste Joseph Fourier, a French mathematician, used such trigonometric series expansions in describing the phenomenon of heat conduction and temperature distribution through solid bodies. His techniques find application in a variety of problems encompassing many different fields including optics, system theory, and electromagnetics (Proakis & Manolakis, 1996).

A linear combination of harmonically related complex exponentials of the form

$$s(t) = \sum_{k=-\infty}^{\infty} a_k \exp(j2\pi k f_0 t) \tag{2.1}$$

is a periodic signal with fundamental period $T_P = \frac{1}{f_0}$. Hence, we can think of the exponential signals

$$\left\{ \exp(j2\pi k f_0 t) \qquad k = 0, \pm 1, \pm 2, \ldots \right\}, \tag{2.2}$$

as the basic "building blocks" from which we can construct periodic signals of various types by proper choice of the fundamental frequency, f_0, and the coefficients $\{a_k\}$. The fundamental period, T_P, of $s(t)$ is determined by f_0 and the coefficients, $\{a_k\}$, specify the shape of the waveform.

The Fourier series coefficients can be calculated by the following integral equation;

$$a_k = \frac{1}{T_P} \int_{T_P} s(t) \exp(-j2\pi k f_0 t) dt. \tag{2.3}$$

Note that the integration is performed within only one period of the periodic signal $s(t)$. The only conditions for the periodic signal $s(t)$ to have a valid Fourier

series representation are the Dirichlet conditions. They can be stated as follows (Proakis & Manolakis, 1996):

- The signal $s(t)$ has a finite number of discontinuities in any period,
- The signal $s(t)$ contains a finite number of maxima and minima within any period,
- The signal $s(t)$ is absolutely integrable in any period.

2.1.2 Fourier Transform for Continuous Time Aperiodic Signals

An aperiodic signal $s(t)$ with finite duration can be represented using the Fourier transform (FT) as

$$S(f) = \int_{-\infty}^{\infty} s(t)\exp(-j2\pi ft)dt. \tag{2.4}$$

$S(f)$ is a function of the continuous frequency variable, f. The Fourier transform facilitates the frequency analysis of continuous-time aperiodic signals.

The inverse FT is given by the following integration;

$$s(t) = \int_{-\infty}^{\infty} S(f)\exp(j2\pi ft)df. \tag{2.5}$$

2.2 Correlation of Continuous – Time Deterministic Signals

The objective in the computation of correlation between two signals is to measure the degree to which these two signals are similar and thus to extract some information that depends to a large extent on the application. Correlation of signals is often utilized in applications of radar, sonar, and digital communications (Proakis & Manolakis, 1996). In radar applications, correlation is mostly used to detect the presence of a target and to extract its range information.

Cross – correlation of two time domain signals $s(t)$ and $h(t)$ is defined as (Poularikas, 2000)

$$s(t) \star h(t) = \int_{-\infty}^{\infty} s(\tau) h^*(\tau - t) d\tau \tag{2.6}$$

where τ is called the time shift or lag.

For the special case of $h(t) = s(t)$, we have the autocorrelation of $s(t)$ given as

$$R_s(t) = s(t) \star s(t) = \int_{-\infty}^{\infty} s(\tau) s^*(\tau - t) d\tau \tag{2.7}$$

where $R_s(t)$ is employed to represent the autocorrelation of $s(t)$.

At this point, we would like to mention some useful properties of the autocorrelation function. Firstly, the autocorrelation function attains its maximum when the time lag is equal to zero. Secondly, according to Wiener-Khinchin theorem, the power spectrum of a signal can be obtained as the FT of its auto – correlation function. That is;

$$\left|S(f)\right|^2 = \int R_s(\tau) \exp(-j2\pi f \tau) d\tau. \tag{2.8}$$

2.3 The Fractional Fourier Transform – A Generalization of Fourier Transform

The fractional Fourier transform (FrFT), which is the generalization of the classical FT was introduced around 1980s in quantum mechanics (Namias, 1980), (McBride and Kerr, 1987). Recently, it has been studied by some signal processing researchers. The transform, its useful properties and its relationship with the Wigner distribution, the ambiguity function and other quadratic time – frequency representations were excessively studied in Almeida's paper (Almedia, 1994). After Almedia's work, the FrFT drew the attention of some researchers working on time – frequency representations. Özaktaş and his collegues used the FrFT in optimal noise filtering (Özaktaş et. al., 1997) and they also developed a fast approximate discrete FrFT algorithm (Özaktaş et. al., 1996), (Özaktaş et. al., 2000). Akay and Boudreaux – Bartels then defined the FrFT in terms of the unitary and Hermitian fractional operators and formulated the fractional convolution and correlation operations (Akay & Boudreaux – Bartels, 2001).

The fractional Fourier transform generalizes the classical FT with an angle parameter ϕ[1]. When the angle parameter $\phi = 0$, the FrFT reduces to the identity transform and we get back the signal itself. When $\phi = \frac{\pi}{2}$, the FrFT simplifies to the classical FT operation. For any other values of the angle ϕ, we essentially obtain a different signal representation with respect to the fractional domains of the time – frequency plane. The FrFT can also be interpreted as a rotation in the time – frequency plane and it is related with most of the time – frequency representations (Almeida, 1994).

The FT, perhaps the most frequently used tool in signal processing, gives us information about the spectral content of a signal. However, when the signal has a frequency content that is changing with time, we often use time – frequency representations such as the short time Fourier transform and the Wigner distribution. Researchers developed numerous other time – frequency distribution functions beside these two well – known representations (Cohen, 1995).

In time – frequency representations, one normally uses a plane with two orthogonal axes, horizontal axis corresponding to time and vertical axis corresponding to frequency. If we consider the signal $s(t)$ as represented along the time axis, its Fourier transform $S(f)$ is represented along the frequency axis (see Figure 2.1(a)). Thus, the classical FT can be thought as an operator which rotates the signal in the counterclockwise direction by an angle of $\frac{\pi}{2}$ on the time – frequency plane.

Analogously, the FrFT can be considered as an operator that rotates the signal on the time – frequency plane by an angle ϕ. At this angle we have another

---

[1] Some researchers use an order parameter "a" instead of the angle parameter. Both can be used equivalently since they can be related as $\phi = a\frac{\pi}{2}$. We prefer to use the angle parameter ϕ in this thesis.

representation of the signal and we have a new domain, which we call the *fractional domain*, "r", as shown in Figure 2.1(b). This can also be thought as the counterclockwise rotation of the signal by an angle ϕ. Notice that for all possible values of [1]the angle ϕ, we have a different representation of the signal. This new representation is termed the fractional Fourier transformed signal.

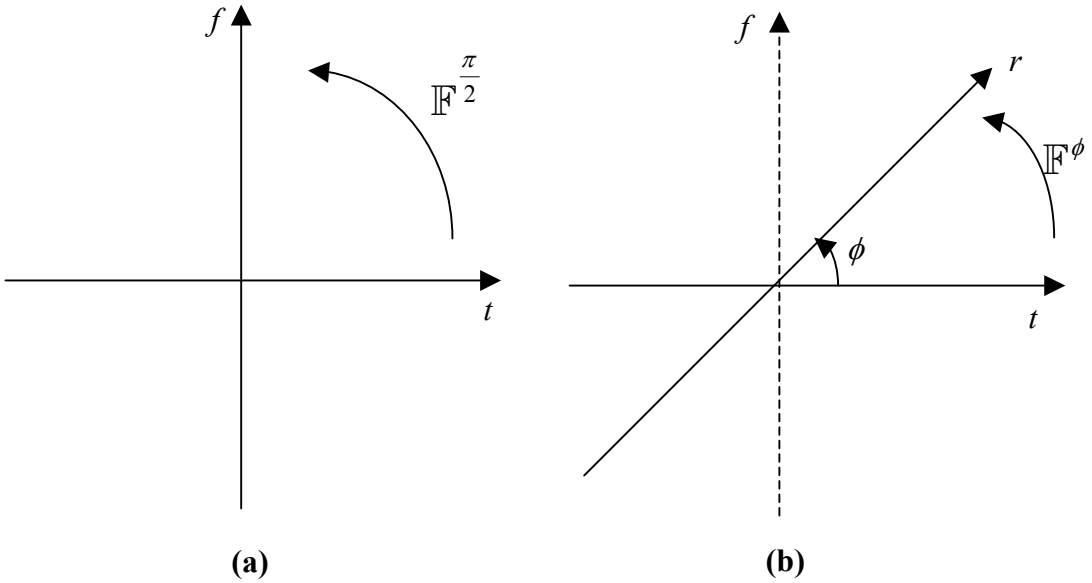

Figure 2.1: (a) Time, frequency and (b) fractional domains.

Mathematically, the FrFT of a signal $s(t)$ is defined as (Almeida, 1994)

$$(\mathbb{F}^{\phi}s)(r) = S^{\phi}(r) = \int_{-\infty}^{\infty} s(t)K^{\phi}(t,r)dt \quad [1]$$

$$= \begin{cases} \sqrt{1 - j\cot\phi}\,\exp(j\pi r^2\cot\phi)\int s(t)\exp(j\pi t^2\cot\phi - j2\pi tr\csc\phi)dt, & \phi \neq n\pi, n \in \mathbb{Z} \\ s(r), & \phi = (2n)\pi \\ s(-r), & \phi = (2n+1)\pi. \end{cases} \quad (2.9)$$

Here, $\mathbb{F}^{\phi}$ is the FrFT operator associated with ϕ, $S^{\phi}(r)$ is the fractional Fourier transformed signal, $K^{\phi}(t,r)$ is the transformation kernel and n is an integer.

[1] From now on, the integral limit values accepted -∞ and +∞ if not specified otherwise.

The transformation kernel is defined as,

$$K^{\phi}(t,r)=\begin{cases}\sqrt{1-j\cot\phi}\exp[j\pi(t^2+r^2)\cot\phi-j2\pi rt\csc\phi], & \phi\neq n\pi\\ \delta(t-r), & \phi=(2n)\pi\\ \delta(t+r), & \phi=(2n+1)\pi.\end{cases} \tag{2.10}$$

Many properties of the FrFT are derived from the kernel defined in (2.10).

When $\phi=0$, the FrFT reduces to the identity transform, since in this case the kernel $K^{\phi}(t,r)$ becomes the impulse function $K^{2n\pi}(t,t')=\delta(t-t')$. Thus, we obtain the identity transform as,

$$\left(\mathbb{F}^{0}s\right)(t)=S^{0}(t)=\int s(t')\delta(t-t')dt'=s(t). \tag{2.11}$$

When $\phi=\dfrac{\pi}{2}$, the FrFT reduces to the classical FT, since the kernel in this case becomes an exponential function as $K^{\pi/2+2n\pi}(t,f)=\exp(-j2\pi tf)$. Thus, this special case of the FrFT is obtained as the classical FT;

$$\left(\mathbb{F}^{\frac{\pi}{2}}s\right)(f)=S^{\frac{\pi}{2}}(f)=\int s(t)\exp(-j2\pi tf)dt=S(f). \tag{2.12}$$

For odd integer multiples of π, the kernel becomes $K^{\pi+2n\pi}(t,t')=\delta(t+t')$. Hence, for $\phi=\pi$, the FrFT simply becomes an axis reversal transformation. That is;

$$\left(\mathbb{F}^{\pi}s\right)(t)=S^{\pi}(t)=\int s(t')\delta(t+t')dt'=s(-t). \tag{2.13}$$

For $\phi=\dfrac{3\pi}{2}+2n\pi$, the FrFT simplifies to the inverse conventional FT. In this case the kernel becomes $K^{3\pi/2+2n\pi}(t,f)=\exp(j2\pi tf)$ and the FrFT is given by

$$\left(\mathbb{F}^{\frac{3\pi}{2}}s\right)(f)=S^{\frac{3\pi}{2}}(f)=\int s(t)\exp(j2\pi tf)dt=S(-f). \tag{2.14}$$

For $\phi\neq n\pi$, the FrFT, as given in (2.9), can be calculated in four steps shown in Figure 2.2 (Akay, 2000):

- A product by a chirp (complex exponentials with linear frequency modulation) signal in the input domain t,

- A classical Fourier transform with its argument scaled as $\frac{r}{\sin\phi}$,
- Another product by a chirp signal in the output domain r,
- A product by the complex amplitude factor $\sqrt{1-j\cot\phi}$.

Thus, in summary, computing the FrFT of the signal $s(t)$ corresponds to expressing it in terms of an orthonormal basis formed by chirps, i.e. complex exponentials with linear frequency modulation.

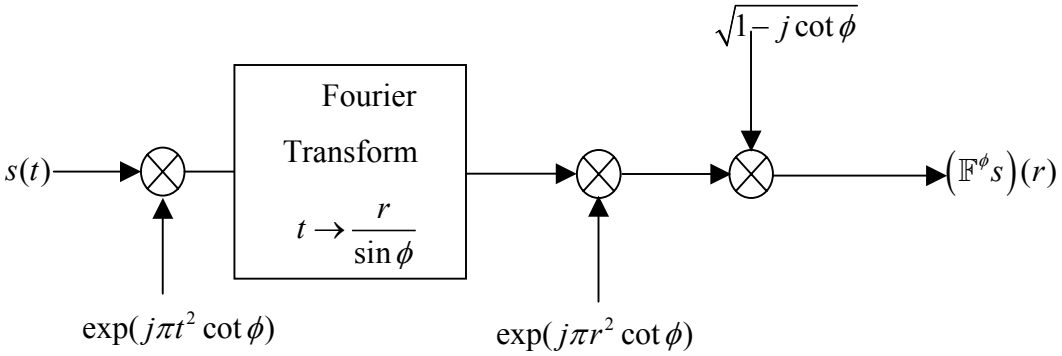

Figure 2.2: FrFT calculation steps.

Since chirps have constant magnitude, this immediately allows us to make a rather general statement about the existence of the transform. In fact, if $s(t)$ is in the space of square integrable functions, or is a generalized function, its product by a chirp is also square integrable, or is a generalized function, respectively. Therefore, the FrFT exists under the same conditions as with the classical FT (Almeida, 1994).

2.3.1 Fundamental Properties of the Fractional Fourier Transform

Fundamental properties of the FrFT as derived in (Almeida 1994) are summarized below;

$$K^{\phi}(t,r) = K^{\phi}(r,t) \qquad \text{(Symmetry)} \qquad (2.15)$$

$$K^{-\phi}(t,r) = \left[K^{\phi}(t,r)\right]^{*} \qquad \text{(Self-reciprocity)} \qquad (2.16)$$

$$K^{\phi+2n\pi}(t,r) = K^{\phi}(t,r) \qquad n \in \mathbb{Z} \qquad \text{(Periodicity)} \tag{2.17}$$

$$K^{\phi}(-t,r) = K^{\phi}(t,-r) \qquad \text{(Axis reversal)} \tag{2.18}$$

$$\int K^{\phi_1}(t,t')K^{\phi_2}(t',r)dt' = K^{\phi_1+\phi_2}(t,r) \qquad \text{(Additivity)} \tag{2.19}$$

$$\int K^{\phi}(t,r)[K^{\phi}(t,r')]^{*}dt = \delta(r-r') \qquad \text{(Completeness)} \tag{2.20}$$

$$\int K^{\phi}(t,r)[K^{\phi}(t',r)]^{*}dr = \delta(t-t') \qquad \text{(Orthonormality).} \tag{2.21}$$

Proofs of these properties can be performed using the transformation kernel in (2.10). As a result of the property given in (2.19), the FrFT has the additivity property which is expressed as (Almeida, 1994)

$$\left(\mathbb{F}^{\phi_1}\left\{\left(\mathbb{F}^{\phi_2}s\right)(r')\right\}\right)(r) = \left(\mathbb{F}^{\phi_1+\phi_2}s\right)(r). \tag{2.22}$$

As a result of the completeness and orthonormality properties in (2.20) and (2.21), the FrFT is a unitary transformation. Using the self – reciprocity property in (2.16) and the orthonormality property in (2.21), it can be shown that the inverse of the FrFT with an angle ϕ corresponds to an FrFT with angle -ϕ (Almeida, 1994)

$$s(t) = \int S^{\phi}(r)K^{-\phi}(t,r)dr. \tag{2.23}$$

Using the operator theory notation the inverse FrFT can be written as

$$s(t) = \left(\mathbb{F}^{-\phi}\left\{S^{\phi}(r)\right\}\right)(t) = \left(\mathbb{F}^{-\phi}\left\{\left(\mathbb{F}^{\phi}s\right)(r)\right\}\right)(t). \tag{2.24}$$

Due to its unitarity, the FrFT preserves inner products and satisfies a relation similar to Parseval's relation of the classical FT (Almeida, 1994). For two signals $s_1(t)$ and $s_2(t)$,

$$\int s_1(t)s_2^{*}(t)dt = \int S_1^{\phi}(r)[S_2^{\phi}(r)]^{*}dr. \tag{2.25}$$

Thus, we can conclude that the FrFT is an energy preserving transformation. That is;

$$\int |s(t)|^2 dt = \int |S^{\phi}(r)|^2 dr. \tag{2.26}$$

Any further properties of the FrFT can be found in (Akay, 2000).

2.4 Fractional Operators and Fractional Correlation Functions

2.4.1 Hermitian Time, Hermitian Frequency and Unitary Time, Unitary Frequency Operators

A signal can be represented in many forms if we express it with respect to sets of complete and orthogonal bases spanning the vector space that the signal belongs to. Hermitian operators have been used in quantum mechanics to derive expansion functions in order to represent signals with respect to different physical variables (Cohen, 1995). Hermitian operators later have been adopted by the signal processing community. For the fundamental physical variables of time, t, and frequency, f, the Hermitian time, $\mathcal{T}$, and Hermitian frequency, $\mathcal{F}$, operators are defined as (Baraniuk & Jones, 1995), (Sayeed & Jones, 1996)

$$\left(\mathcal{T}s\right)(t) = ts(t), \tag{2.27}$$

$$\left(\mathcal{F}s\right)(t) = \frac{1}{j2\pi}\frac{d}{dt}s(t). \tag{2.28}$$

An important property of Hermitian operators is that the eigenfunctions of Hermitian operators form a complete and orthogonal basis set for the underlying vector space. Thus, any Hermitian operator naturally defines a signal representation as a signal expansion onto its eigenfunctions.

The eigenfunctions of $\mathcal{T}$ are impulse functions, $u_T(t,t') = \delta(t-t')$, and the signal representation defined by them is simply the identity transform,

$$S_T(t') = \int s(t)\delta(t-t')dt = s(t'). \tag{2.29}$$

Similarly, the eigenfunctions of $\mathcal{F}$ are complex exponentials, $u_{\mathcal{F}}(t,f) = \exp(j2\pi ft)$ and the signal representation defined by them is the classical FT,

$$S_{\mathcal{F}}(f) = \int s(t)\exp(-j2\pi ft)dt. \tag{2.30}$$

Unitary operators can also be used to define signal transforms. They can be obtained by exponentiating Hermitian operators. Thus, eigenfunctions of unitary operators also form complete and orthogonal basis functions for the signal space. The unitary operator representations of time, $\mathbf{T}_\tau$, and frequency, $\mathbf{F}_\nu$, are defined as

$$(\mathbf{T}_\tau s)(t) = s(t-\tau), \tag{2.31}$$

$$\left(\mathbf{F}_\nu s\right)(t) = s(t)\exp(j2\pi\nu t). \tag{2.32}$$

Using, Stone's theorem (Sayeed & Jones, 1996) the relations between the unitary and Hermitian time and frequency operators are expressed as,

$$\mathbf{T}_\tau = \exp(-\mathrm{j}2\pi\tau\mathcal{F}) \qquad \text{and} \qquad \mathbf{F}_\nu = \exp(\mathrm{j}2\pi\nu\mathcal{T}). \tag{2.33}$$

As a result of these equivalency relations, we can say that time and frequency variables are duals of each other.

2.4.2 Hermitian and Unitary Fractional Operators

The unitary frequency – shift operator, $\mathbf{F}_\nu$ is unitarily equivalent to the unitary time – shift operator, $\mathbf{T}_\tau$, as demonstrated by the relationship (Baraniuk & Jones, 1995), (Sayeed & Jones, 1996)

$$\mathbf{F}_\nu = \mathbb{F}^{-\frac{\pi}{2}}\mathbf{T}_\nu\mathbb{F}^{\frac{\pi}{2}}. \tag{2.34}$$

Here, $\mathbb{F}^{\frac{\pi}{2}}$ is the classical FT operator. To derive the time domain definition of the unitary frequency – shift operator, $\mathbf{F}_\nu$, according to (2.34), we first go to frequency domain using the operator $\mathbb{F}^{\frac{\pi}{2}}$, then translate (shift) the frequency domain signal using $\mathbf{T}_\nu$. The final inverse FT operator, $\mathbb{F}^{-\frac{\pi}{2}}$, takes the translated frequency domain signal back to the time domain. This unitary equivalence property can be generalized to other variables and corresponding operators (Baraniuk & Jones, 1995).

The unitary fractional – shift operator, $\mathbf{R}_{\rho}^{\phi}$, of the fractional variable, r, associated with angle ϕ, measured counterclockwise from the time axis, can be defined similar to (2.34) (Akay, 2000),

$$\mathbf{R}_{\rho}^{\phi} = \mathbb{F}^{-\phi}\mathbf{T}_{\rho}\mathbb{F}^{\phi}. \tag{2.35}$$

Here, $\mathbb{F}^{\phi}$ and $\mathbb{F}^{-\phi}$ are the forward and inverse FrFT operators, respectively. Using (2.35) the explicit formulation of the unitary fractional – shift operator is obtained as (Akay, 2000)

$$\left(\mathbf{R}_{\rho}^{\phi}s\right)(t) = s(t-\rho\cos\phi)\exp[-j2\pi(\frac{\rho^2}{2})\cos\phi\sin\phi + j2\pi t\rho\sin\phi] \tag{2.36}$$

with $\rho \in \mathbb{R}$. $\mathbf{R}_{\rho}^{\phi}$ describes a shift of the signal support by a radial distance ρ along the arbitrary orientation ϕ of the time – frequency plane.

The unitary fractional – shift operator, $\mathbf{R}_{\rho}^{\phi}$, can alternatively be expressed using the unitary time – shift operator, $\mathbf{T}_{\tau}$, and the unitary frequency – shift operator, $\mathbf{F}_{\nu}$, via

$$\left(\mathbf{R}_{\rho}^{\phi}s\right)(t) = \exp(-j\pi\rho^2\cos\phi\sin\phi)(\mathbf{F}_{\rho\sin\phi}\mathbf{T}_{\rho\cos\phi}s)(t). \tag{2.37}$$

Just as the FrFT simplifies to the identity transform for $\phi = 0$ and to the classical FT for $\phi = \frac{\pi}{2}$, the unitary fractional shift operator, $\mathbf{R}_{\rho}^{\phi}$, also reduces to the unitary time – shift operator, $\mathbf{T}_{\tau}$, in (2.31) and to the unitary frequency – shift operator, $\mathbf{F}_{\nu}$, in (2.32) for $\phi = 0$ and $\phi = \frac{\pi}{2}$, respectively (Akay, 2000).

Applying Stone's theorem and the concept of duality along with the unitary fractional shift operator $\mathbf{R}_{\rho}^{\phi}$, the Hermitian fractional – shift operator, $\mathcal{R}^{\phi}$, is derived as (Akay, 2000)

$$\mathcal{R}^{\phi} = \cos\phi\mathcal{T} + \sin\phi\mathcal{F}. \tag{2.38}$$

Note that similar to the unitary fractional shift operator, for the special cases of $\phi = 0$ and $\phi = \frac{\pi}{2}$, the Hermitian fractional operator, $\mathcal{R}^{\phi}$, also reduces to the Hermitian time and frequency operators, respectively.

2.4.3 Fractional Cross – Correlation and Fractional Autocorrelation

In Section 2.2, we defined the cross – correlation and autocorrelation functions, which are frequently used in linear time – invariant (LTI) system applications of signal processing. The classical FT is a useful tool in this context, since the LTI correlation simply corresponds to a multiplication in the frequency domain.

Because the FrFT is a generalization of the classical FT into arbitrary orientations of the time – frequency plane, a generalization of correlation also exists and it is derived by the fractional operator theory methods summarized in Section 2.4.2. Using the unitary fractional shift operator $\mathbf{R}_{\rho}^{\phi}$, the fractional cross – correlation and fractional autocorrelation operations can be defined (Akay, 2000).

Fractional cross – correlation of functions $s(t)$ and $h(t)$ associated with angle ϕ is obtained by computing the inner product of the signal $s(t)$ with the fractionally shifted version of the function $h(t)$ as

$$\begin{aligned}\left(s \star_{\phi} h\right)(\rho) &= \left\langle s, \mathbf{R}_{\rho}^{\phi} h \right\rangle \\ &= \exp(j2\pi \frac{\rho^2}{2} \cos\phi \sin\phi) \int s(\beta) h^{*}(\beta - \rho\cos\phi) \exp(-j2\pi\beta\rho\sin\phi) d\beta. \end{aligned} \tag{2.39}$$

Here $\langle\ ,\ \rangle$ defines the inner product operator, ρ is the fractional lag variable and $\star_{\phi}$ represents the fractional correlation operation. The subscript ϕ indicates that cross – correlation of $s(t)$ and $h(t)$ is computed at the fractional domain angle ϕ of the time – frequency plane. Note that for $\phi = 0$, the fractional cross – correlation simplifies to the LTI cross – correlation operation given in (2.6).

Fractional autocorrelation is similarly calculated by replacing $h(t)$ in (2.39) with $s(t)$ as,

$$\begin{aligned}\left(s \star_{\phi} s\right)(\rho) &= \left\langle s, \mathbf{R}_{\rho}^{\phi} s \right\rangle \\ &= \exp(j2\pi \frac{\rho^2}{2} \cos\phi \sin\phi) \int s(\beta) s^*(\beta - \rho\cos\phi) \exp(-j2\pi\beta\rho\sin\phi) d\beta. \end{aligned} \tag{2.40}$$

Fractional autocorrelation similarly generalizes the LTI autocorrelation for the arbitrary angle ϕ.

Formulations of fractional cross – correlation and fractional autocorrelation given by (2.39) and (2.40) are rather difficult to calculate by computer. To derive computationally efficient algorithms that approximate these fractional functions, alternative and equivalent formulations of fractional cross – and autocorrelations are used (Akay, 2000).

The first alternative equivalent formulation of fractional cross – correlation in terms of FrFT signals can be given as,

$$\left(s \star_{\phi} h\right)(\rho) = \int S^{\phi}(\beta)[H^{\phi}(\beta - \rho)]^* d\beta = \left(S^{\phi} \star_0 H^{\phi}\right)(\rho). \tag{2.41}$$

The second alternative formulation is expressed as,

$$\left(s \star_{\phi} h\right)(\rho) = \left(\mathbb{F}^{\frac{-\pi}{2}} \left\{ \left[S^{\frac{\pi}{2}+\phi}(u) \right] \left[H^{\frac{\pi}{2}+\phi}(u) \right]^* \right\} \right)(\rho). \tag{2.42}$$

In this form, to compute fractional cross – correlation at angle ϕ, first the FrFT of the signal $s(t)$ is calculated at angle $\phi + \frac{\pi}{2}$. The result is multiplied with the conjugate of the FrFT of the signal $h(t)$ calculated at angle $\phi + \frac{\pi}{2}$. Finally, a conventional inverse FT is taken. The formulation given in (2.42) helps us to define a discrete – time approximation of fractional cross – correlation based on fast Fourier transform (FFT) and the discrete FrFT algorithms.

Analogously, an alternative formulation of fractional autocorrelation is given as,

$$\left(s \star_{\phi} s\right)(\rho) = \int S^{\phi}(\beta)[S^{\phi}(\beta - \rho)]^{*} d\beta = (S^{\phi} \star_{0} S^{\phi})(\rho). \tag{2.43}$$

This equation can also be written as,

$$\left(s \star_{\phi} s\right)(\rho) = \left(\mathbb{F}^{\frac{-\pi}{2}} \left\{ \left| S^{\frac{\pi}{2}+\phi}(u) \right|^{2} \right\} \right)(\rho). \tag{2.44}$$

In this form, one FrFT with angle $\phi + \frac{\pi}{2}$ and a conventional inverse FT are used together to compute fractional autocorrelation at angle ϕ. The formulation given in (2.44) helps us to define a discrete – time approximation of fractional autocorrelation based on the FFT and fast discrete FrFT algorithms.

By computing the FT of both sides of (2.44), we can also write

$$\left(\mathbb{F}^{\frac{\pi}{2}} \left(s \star_{\phi} s\right)(\rho) \right)(u) = \left| S^{\frac{\pi}{2}+\phi}(u) \right|^{2}. \tag{2.45}$$

This equation can be considered as the fractional generalization of the autocorrelation theorem of the classical FT given in (2.8).

CHAPTER THREE

RADAR BASICS, RADAR SIGNALS AND PULSE COMPRESSION

In this chapter, principles of radars are introduced briefly. In the first section, a basic radar scenario is given and detection of radar signals using ordinary techniques are presented. In Section 2, the matched filter and the radar ambiguity function are studied. In the last section, the pulse compression techniques and the linear frequency modulated (LFM), step LFM, Frank coded and polyphase coded signals (P1, P2, P3 and P4) are discussed.

3.1 Principles of Radars

3.1.1 Radar Basics

The word radar, first used by the US Navy in 1940, is derived from *radio detection and ranging*, thus conveying these two purposes of detection and location. Modern radar goes further and is developed to classify or identify targets, and even to produce images of objects, for example mapping the ground from a satellite (Kingsley & Quegan, 1992).

The radar scenario involves a transmitter and a receiver, which are usually positioned at the same location, a target at range R, and a signal that travels the round – trip between the radar and the target. The target sometimes has a velocity relative to the radar (see Figure 3.1).

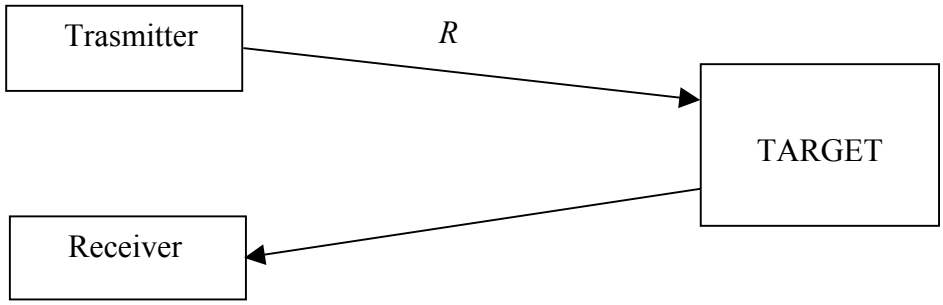

Figure 3.1: A basic radar scene.

The transmitted signal is usually an electromagnetic signal (but an acoustic one is also a possibility). The signal can be described by a carrier sine wave at frequency f_c with modulation of one or more of its parameters – amplitude, phase, and frequency (Levanon, 1988).

The changes observed in the returned signal can provide information about the target position and sometimes its character. In simple terms, the delay of the returned signal yields information on the range. The frequency shift (Doppler) yields information on the range rate (velocity). The antenna pointing direction yielding maximum return strength (or other criteria) provides the azimuth and elevation of the target relative to the radar. From the progress of some of these parameters with time, the target's trajectory can be estimated (Levanon, 1988).

How well can a radar measure the range is decided by the range accuracy and the range resolution. The *range accuracy* indicates the uncertainty in a measurement of the absolute distance to an object, whereas the *range resolution* tells us how far apart two targets have to be before we can see that there are indeed two targets rather than one larger one. For the range resolution, the time delay between the echoes from two objects must be greater than the pulse duration, T. Radar systems are normally designed to operate between a minimum range $R_{\min}$ and maximum range $R_{\max}$. The distance between $R_{\min}$ and $R_{\max}$ is divided into M range bins (gates), and the width of each bin, denoted as ΔR, corresponds to range resolution;

$$\Delta R = \frac{R_{\max} - R_{\min}}{M}. \tag{3.1}$$

Targets separated by at least ΔR will be completely resolved in range. Consider two targets located at ranges R_1 and R_2, corresponding to time delays t_1 and t_2, respectively. Denoting the difference between those two ranges as ΔR, we have

$$\Delta R = R_2 - R_1 = c\frac{(t_2 - t_1)}{2} = c\frac{\Delta t}{2} \tag{3.2}$$

where c represents the speed of light. Since the time delay between the two targets must be greater than the pulse duration, T, then (Mahafza, 2000)

$$\Delta R = \frac{cT}{2} = \frac{c}{2B} \tag{3.3}$$

where B is the bandwidth of the signal which is equal to $1/T$.

In general, radar users and designers alike seek to minimize ΔR in order to enhance the radar performance. As suggested by (3.3), in order to achieve fine range resolution one must minimize the pulse width. However, this will reduce the average transmitted power and increase the operation bandwidth. Achieving fine range resolution while maintaining adequate average transmitted power can be accomplished by using pulse compression techniques, which will be explained later in this chapter.

For the range accuracy of a system the crucial factor is the bandwidth occupied by the radar. In practice, the pulse shape and the bandwidth are related in simple pulse radars. Short pulses take up more bandwidth, B, of the radio spectrum than long pulses. It is important to be aware that the bandwidth of radar does not have to be limited. As an example, suppose we develop a system that transmits long pulses during which we sweep the frequency of the oscillator deliberately to increase the bandwidth. Such radar schemes are common and are known as chirp systems when the frequency sweep during a pulse is linear. By careful processing, chirp radars achieve high range accuracy.

The other factor determining the accuracy of the range measurement is the signal to noise ratio (SNR), due to the effect that noise has on corrupting the shape of the pulse (Kingsley & Quegan, 1992).

3.1.2 Radar Detection Basics

The radar return signal is always corrupted by noise. The detection circuit is supposed to determine the existence of a target being confused by noise. Once a target has been detected, properties such as its range and velocity are likely to be of interest.

The block diagram of a simple detection circuit is seen in Figure 3.2. It consists of a narrow band – pass filter, usually at the intermediate frequency (IF), followed by an envelope detector (which typically has a linear or square-law characteristic). The last stage is usually a threshold circuit, in which the output of the envelope detector is compared to a predetermined threshold. Whenever the envelope surpasses the threshold, the existence of a target is assumed at the corresponding delay. Whenever a noise peak is mistaken for a target, then there will be a false alarm. We can also miss one of the targets if the level of that target is below the threshold. Lowering the threshold will increase the probability of detection, but at a cost of increasing also the probability of false alarms. If the SNR were higher, which implies higher signal peaks, the smaller target return would have also crossed the threshold, and the probability of detection would have increased. Thus, there is a threefold dependency between the SNR, probability of detection and probability of false alarms (Levanon, 1988).

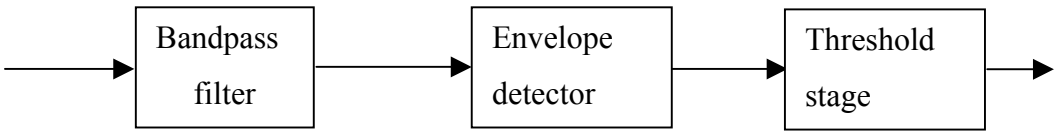

Figure 3.2: Block diagram of a basic radar detector.

The mathematical analysis of the detection circuit in Figure 3.2 can be performed using Neyman – Pearson approach of statistical signal processing. Analysis starts with an input signal consisting of a sinusoid corrupted by additive white Gaussian noise (AWGN). We seek two probability density functions (PDFs) of the envelope; one when only the noise is present and one when both signal and noise are present. These two PDFs and a selected threshold yield the probability of detection P_D, and the probability of false alarm, P_{FA} (Kay, 1998).

3.2 Matched Filter and the Radar Ambiguity Function

3.2.1 Matched Filter

The most unique characteristic of the matched filter is that it produces the maximum achievable instantaneous SNR at its output when a signal and additive white noise are present at the input. The noise does not need to be Gaussian. The peak instantaneous SNR at the receiver output can be achieved by matching the radar receiver transfer function to the received signal. In practice, it is sometimes difficult to achieve perfect matched filtering. Due to mismatching, degradation in the output SNR occurs (Mahafza, 2000).

Consider a signal, $s_i(t)$, with finite duration. Denote the pulse width by T and assume that a matched filter receiver is utilized. The received signal, $x(t)$, after the round trip is the delayed version of $s_i(t)$ with additive white noise,

$$x(t) = \alpha s_i(t - t_1) + n_i(t) \tag{3.4}$$

where

α is a constant usually known as the attenuation factor,

t_1 is the unknown time delay proportional to target range,

$n_i(t)$ is the input white noise.

Since the input noise is white, its corresponding autocorrelation and power spectral density (PSD) functions are given, respectively, by

$$R_{n_i}(t) = \frac{N_0}{2}\delta(t), \tag{3.5}$$

$$S_{n_i}(f) = \frac{N_o}{2}, \tag{3.6}$$

where $\frac{N_o}{2}$ is a constant representing the noise power. Denote the signal component and the noise component of the filter output as $s_o(t)$ and $n_o(t)$, respectively. We can compute the matched filter output as

$$y(t) = \alpha s_o(t - t_1) + n_o(t) \tag{3.7}$$

with

$$s_o(t) = s_i(t) * h(t) \tag{3.8}$$

$$n_o(t) = n_i(t) * h(t). \tag{3.9}$$

The symbol "*" indicates the convolution operation, and $h(t)$ is the filter impulse response (the filter is assumed to be LTI).

Let $R_h(t)$ denote the filter autocorrelation function. It follows that the output noise autocorrelation and PSD functions are given respectively, as

$$R_{n_o}(t) = R_{n_i}(t) * R_h(t) = \frac{N_o}{2}\delta(t) * R_h(t) = \frac{N_o}{2}R_h(t) \tag{3.10}$$

$$S_{n_o}(f) = S_{n_i}(f)\left|H(f)\right|^2 = \frac{N_o}{2}\left|H(f)\right|^2 \tag{3.11}$$

where $H(f)$ is the frequency response of the filter. The total average output noise power is equal to $R_{n_o}(t)$ evaluated at $t = 0$. Namely,

$$R_{n_0}(0) = \frac{N_o}{2}\int_{-\infty}^{\infty}\left|h(u)\right|^2 du. \tag{3.12}$$

The output signal power evaluated at time t is $\left|\alpha s_o(t - t_1)\right|^2$, and by using (3.8), we obtain

$$s_o(t-t_1)=\int_{-\infty}^{\infty} s_i(t-t_1-u)h(u)du. \tag{3.13}$$

A general expression for the output SNR at time t can be written as

$$SNR(t)=\frac{\left|\alpha s_o(t-t_1)\right|^2}{R_{n_o}(0)}. \tag{3.14}$$

Substituting (3.12) and (3.13) into (3.14) we reach at

$$SNR(t)=\frac{\alpha^2\left|\int_{-\infty}^{\infty} s_i(t-t_1-u)h(u)du\right|^2}{\frac{N_o}{2}\int_{-\infty}^{\infty}\left|h(u)\right|^2 du}. \tag{3.15}$$

Using the Cauchy – Schwartz inequality in the numerator of (3.15), we have

$$SNR(t)\le\frac{\alpha^2\int_{-\infty}^{\infty}\left|s_i(t-t_1-u)\right|^2 du\int_{-\infty}^{\infty}\left|h(u)\right|^2 du}{\frac{N_o}{2}\int_{-\infty}^{\infty}\left|h(u)\right|^2 du}=\frac{2\alpha^2\int_{-\infty}^{\infty}\left|s_i(t-t_1-u)\right|^2 du}{N_o}. \tag{3.16}$$

Cauchy – Schwartz inequality tells us that the peak instantaneous SNR occurs when

$$h(u)=s_i^*(t_o-t_1-u). \tag{3.17}$$

Thus, the maximum instantaneous SNR is found as

$$SNR(t_o)=\frac{2\alpha^2\int_{-\infty}^{\infty}\left|s_i(t_o-t_1-u)\right|^2 du}{N_o}. \tag{3.18}$$

Using the signal energy formulation

$$\mathcal{E}=\alpha^2\int_{-\infty}^{\infty}\left|s_i(t_o-t_1-u)\right|^2 du, \tag{3.19}$$

We can write the output peak instantaneous SNR as

$$SNR(t_o) = \frac{2\mathcal{E}}{N_o}. \tag{3.20}$$

Thus, the peak instantaneous SNR depends only on the signal energy and input noise power, and is independent of the waveform utilized by the radar.

Finally, we can determine the impulse response of the matched filter via (3.17). If we desire the peak to occur at $t_0 = t_1$, we get the noncausal matched filter impulse response,

$$h_{nc}(t) = s_i^*(-t). \tag{3.21}$$

Alternatively, the causal impulse response is given as

$$h_c(t) = s_i^*(T - t). \tag{3.22}$$

In this case, the peak occurs at $t_0 = t_1 + T$. The FTs of $h_{nc}(t)$ and $h_c(t)$ are

$$H_{nc}(f) = S_i^*(f), \tag{3.23}$$

$$H_c(f) = S_i^*(f)\exp(-j2\pi fT) \tag{3.24}$$

with $S_i(f)$ representing the FT of $s_i(t)$. The moduli of $H(f)$ and $S_i(f)$ are identical. However, their phase responses are opposite of each other.

The output of the matched filter, $y(t)$, in (3.7) can be expressed by the convolution integral between the filter's impulse response $h(t)$ in (3.22) and the received signal $x(t)$ in (3.4). Alternatively, the output $y(t)$ can also be interpreted as the cross – correlation between $x(t)$ and $s_i(T + t)$. That is,

$$y(t) = \int_{-\infty}^{\infty} x(u)s_i^*(T - t + u)du. \tag{3.25}$$

Therefore, the matched filter output can be computed using the cross – correlation of the received signal and an advanced replica of the transmitted waveform. If the received signal is the same as the transmitted signal, the output of the matched filter

would be the autocorrelation function of the received (or transmitted) signal (Mahafza, 2000).

3.2.2 The Radar Ambiguity Function

The radar ambiguity function represents the output of the matched filter, and it describes the interference caused by range and/or Doppler of a target when compared to a reference target of equal radar cross section. The ambiguity function evaluated at $(\tau,\nu)=(0,0)$ is equal to the matched filter output that is matched perfectly to the signal reflected from the target of interest. Here, τ is the time lag and ν represents the frequency lag (Doppler shift). In other words, returns from the nominal target are located at the origin of the ambiguity function. Thus, the ambiguity function at nonzero τ and ν represents returns from some range and Doppler different from those for the nominal target.

Radar designers normally use the radar ambiguity function as a means of studying different waveforms. It can provide insight about how different radar waveforms may be suitable for the various radar applications. It is also used to determine the range and Doppler resolutions for a specific radar waveform. The three – dimensional (3-D) plot of the ambiguity function versus the frequency and time lag is called the radar ambiguity diagram. The radar ambiguity function for signal $s(t)$ is defined as its 2-D correlation function. More precisely,

$$AF_s(\tau,\nu)=\int_{-\infty}^{\infty}s(t)s^*(t-\tau)\exp(-j2\pi\nu t)dt. \tag{3.26}$$

In this notation, the target of interest is located at $(\tau,\nu)=(0,0)$, and the ambiguity diagram is centered at the same point. Properties of the radar ambiguity function are (Mahafza, 2000):

1. The maximum value for the ambiguity function occurs at $(\tau,\nu)=(0,0)$ and is equal to $\mathcal{E}$ where $\mathcal{E}$ is the signal energy defined as $\mathcal{E}=\int_{-\infty}^{\infty}|s(t)|^2\,dt$. Then, for the maximum of the ambiguity function we have

$$\max\{AF_s(\tau,\nu)\}=AF_s(0,0)=\mathcal{E}. \tag{3.27}$$

Hence

$$AF_s(\tau,\nu)\le AF_s(0,0). \tag{3.28}$$

2. The ambiguity function is symmetric,

$$AF_s(\tau,\nu)=AF_s(-\tau,-\nu). \tag{3.29}$$

3. The total volume under the ambiguity function is constant,

$$\iint|AF_s(\tau,\nu)|^2\,d\tau d\nu=\mathcal{E}^2. \tag{3.30}$$

4. If the function $S(f)$ is the FT of the signal $s(t)$, then by using Parseval's theorem we obtain

$$AF_s(\tau,\nu)=\int S^*(f)S(f-\nu)\exp(-j2\pi f\tau)df \tag{3.31}$$

which is the equivalent frequency domain formulation of the ambiguity function.

3.3 Pulse Compression and Radar Signals

For good detection radar needs a large peak signal power to average noise power ratio. The matched filter was the best of all possible filters and it produced the maximum output SNR. This maximum ratio depended on the total transmitted energy, as in (3.20), and not on the presence of any frequency modulation (FM) on the transmitted signal. Thus, for good detection many radars seek to transmit long – duration pulses to achieve high energy. On the other hand, for good range measurement accuracy radar needs short pulses. To meet these two conflicting

conditions, a concept called pulse compression was developed. It makes use of the fact that the bandwidth of a long – duration pulse can be made larger by use of FM. Large bandwidth implies narrow effective duration. With FM, a waveform can be designed to have both long duration and small effective duration (large bandwidth). Thus, by use of FM over long transmitted pulses and a matched filter, a system can simultaneously obtain good detection performance and highly accurate range measurements (Peebles, 1998).

If a long duration pulse is frequency modulated, its spectrum can have a wider bandwidth than if no FM were present. Since increasing bandwidth corresponds to waveforms with decreased effective duration, the potential exists for a long – duration, large – bandwidth pulse to be converted to a short – duration, effective pulse. In effect, we seek to squeeze the long pulse into a short pulse. If energy can be conserved, we can even expect the shorter compressed pulse to increase in peak amplitude compared to amplitude of a long pulse. These effects can all be achieved by a signal processing technique called pulse compression.

To visualize the process of pulse compression, imagine that a long pulse $s(t)$ with duration T has a linearly varying instantaneous frequency $f_i(t)$. Its total frequency deviation over time T is Δf (Hz). This pulse is applied to a pulse compression filter that has a constant modulus transfer function but a phase with a linearly decreasing envelope delay. We may visualize the low frequencies that enter the filter first as being delayed more than those that enter later. If the slope is a match to the input signal's FM, all the frequencies can be thought of as emerging at the same time and piling up in the output. Thus, the response can be larger in amplitude. However, because the input's bandwidth is large, these frequencies can pile up for only a short time and the output quickly decreases from the peak in relation to the reciprocal of the bandwidth. Duration of the main response is smaller than T by the factor $\frac{1}{\Delta fT}$ and ΔfT is called the *time – bandwidth product* or the *pulse compression ratio* of $s(t)$. Similarly, peak power is larger by a factor of ΔfT. Outside the region of main

response, undesired responses called sidelobes occur for a time duration T on each side of the main response (Peebles, 1998).

Various types of modulations used in pulse compression are called codes. Some of the better – known codes include (Lewis, Kretschmer & Shelton, 1986):

- Barker binary phase
- Pseudorandom binary phase
- Random binary phase
- Step linear frequency modulation
- Linear frequency modulation
- Nonlinear frequency modulation
- Step-frequency-derived polyphase (Frank and P1 codes)
- Butler-matrix-derived polyphase (P2 code)
- Linear-frequency derived polyphase (P3 and P4 codes)
- Huffman codes
- Complementary codes

In this thesis, we used linear frequency modulation, step linear frequency modulation, Frank, P1, P2, P3 and P4 codes in our simulations.

3.3.1 Linear FM (Chirp) Signal

The linear frequency modulated (LFM) or chirp waveform is one of the oldest and most useful radar pulse compression waveforms due to its high range resolution (determined by the waveform bandwidth) and its tolerance to Doppler for ease in receiver processing. In this signal, the frequency varies linearly with time in the transmitted pulse. The pulse compression of the linear frequency modulated signal is equal to the product of the transmitted pulse length and the transmitted bandwidth; ΔfT . The values of ΔfT of over 10000 are achievable, although many systems use time – bandwidth products of less than a hundred or two.

The LFM pulse can be defined as,

$$s(t) = Arect(\frac{t}{T})\exp\left[j2\pi(f_o t + \frac{\mu}{2}t^2) + \phi_o \right] \tag{3.32}$$

where A, T, f_o and μ are positive constants and ϕ_o is an arbitrary phase angle. An example of the LFM signal created in discrete form with chirp rate $\mu = 0.5$, amplitude $A = 1$ and pulse duration $T = 1\mu s$ is sketched in Figure 3.3. The constant μ is related to the frequency sweep Δf and the pulse duration T via

$$\mu = \frac{2\pi\Delta f}{T}(rad/s^2). \tag{3.33}$$

The instantaneous angular frequency change $f_i(t)$ due to FM is

$$f_i(t) = \frac{1}{2\pi}\frac{d\theta(t)}{dt} = \frac{1}{2\pi}\frac{d}{dt}\left[2\pi(f_0 t + \frac{\mu}{2}t^2) \right] = f_0 + \mu t, \qquad -\frac{T}{2} \le t \le \frac{T}{2}. \tag{3.34}$$

Pulse compression is performed by convolving the received signal with a filter matched to the transmitted LFM, yielding a compressed pulse of length $\frac{1}{\Delta f}$. Hence, the compression ratio, defined as the ratio of the transmitted pulse length to the compressed pulse length is, ΔfT.

The ambiguity function (AF) defined in (3.26) which is repeated here as,

$$AF_s(\tau,\nu) = \int_{-\infty}^{\infty} s(t)s^*(t-\tau)\exp(-j2\pi\nu t)dt \tag{3.35}$$

provides a measure of the similarity between a signal $s(t)$ and its delayed (τ parameter) and Doppler shifted (ν parameter) versions. The ambiguity function is commonly used to assess the range and Doppler resolution properties of a given waveform. For the LFM signal defined in (3.32), the AF can be shown to have its primary region of support concentrated along a ridge through the origin of the delay – Doppler (frequency lag) plane with slope μ. The contour plot of the AF magnitude of the LFM signal in Figure 3.3 is shown in Figure 3.4.

Using the fact that the AF of any chirp is a line passing through the origin of the ambiguity plane with a slope equal to the sweep rate μ, a detection statistic for

detection (Wang, et. al, 1998) and sweep rate estimation of LFM signals was proposed (Akay & Boudreaux – Bartels, 2001).

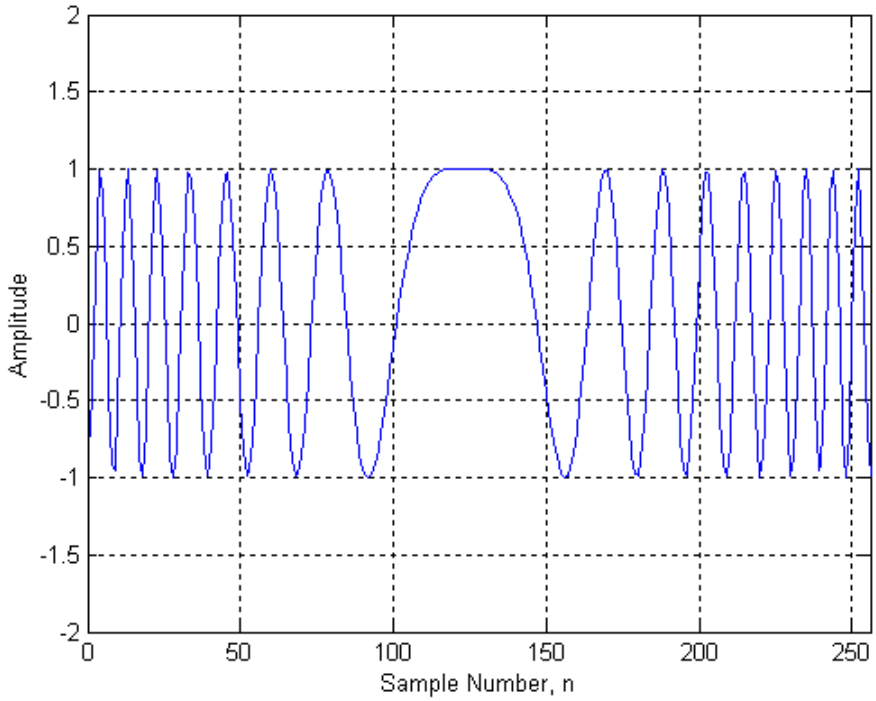

Figure 3.3: LFM signal waveform.

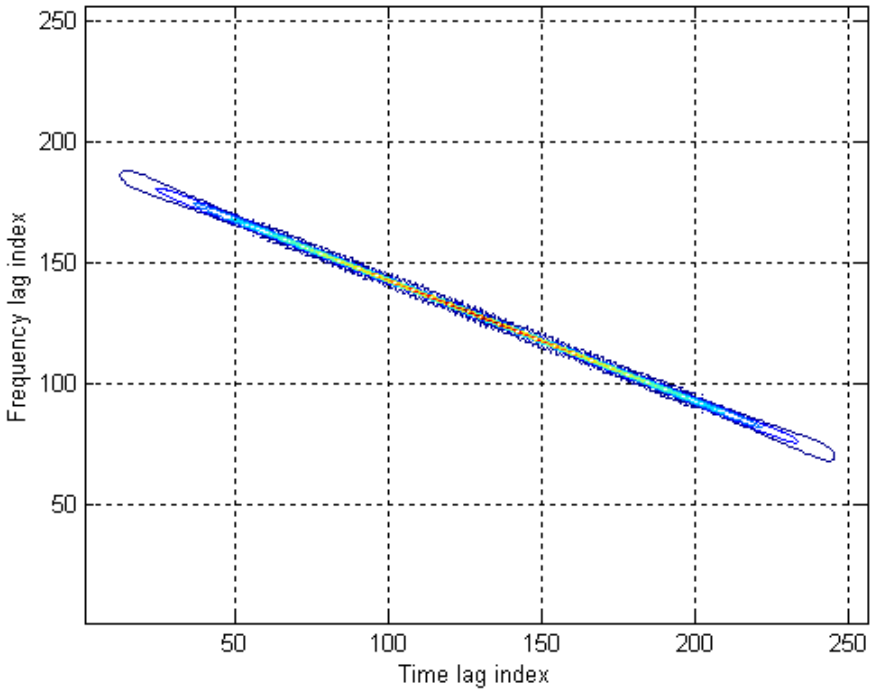

Figure 3.4: The contour plot of the ambiguity function of the LFM signal.

3.3.2 Step Linear Frequency Modulation (Step LFM) Code

The LFM is a continuous function of time over the pulse duration T. We can also build a pulse from subpulses using digital hardware. A signal of this kind is the step linear frequency modulation (LFM) code. The step LFM code, which is also known as step – chirp, provides an approximation of the chirp signal. The step – chirp waveform usually consists of a sequence of different tones or concatenated frequencies. The waveform duration T is divided into M equal – duration intervals and the waveform frequency is constant over each of these subpulses. The frequency of each subpulse differs from the adjacent subpulses by the frequency step size $\delta f = \frac{M}{T}$. The total frequency excursion of the step LFM is $M\delta f$, yielding a compression ratio of M^2. The change of the frequency step size is illustrated in Figure 3.5. The time domain waveform of the step LFM signal and the contour plot of its ambiguity function are sketched in Figure 3.6 and Figure 3.7, respectively. The duration and compression ratio are the same with the LFM signal in Figure 3.3. In

Figure 3.7, beside the main ridge at the center of the ambiguity function contour plot, there can also be seen parallel ridges. These parallel ridges are as a result of the energy spread which is a characteristic of all pulse compression codes other than the LFM signal.

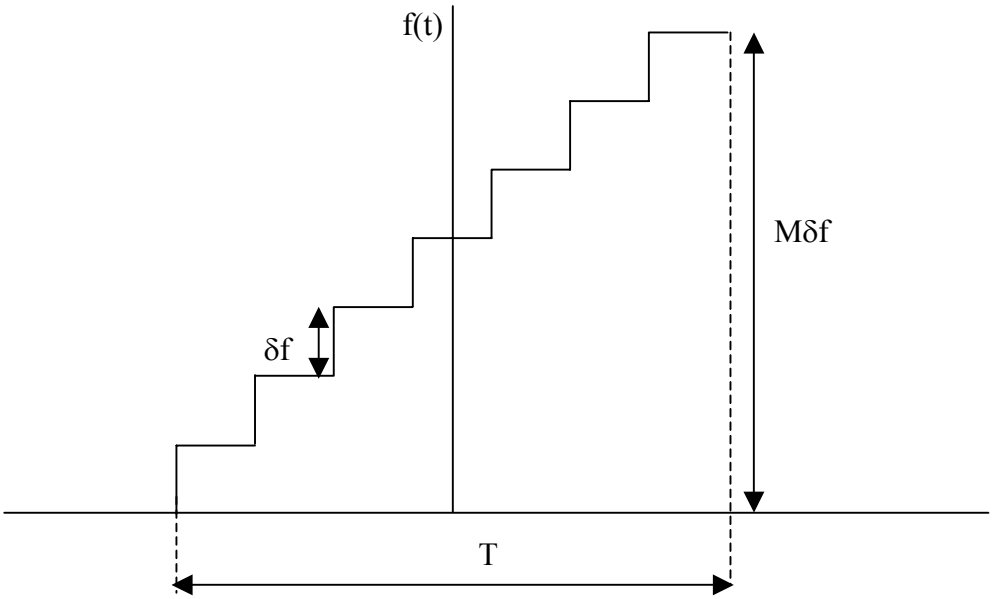

Figure 3.5: Frequency steps of the step LFM signal.

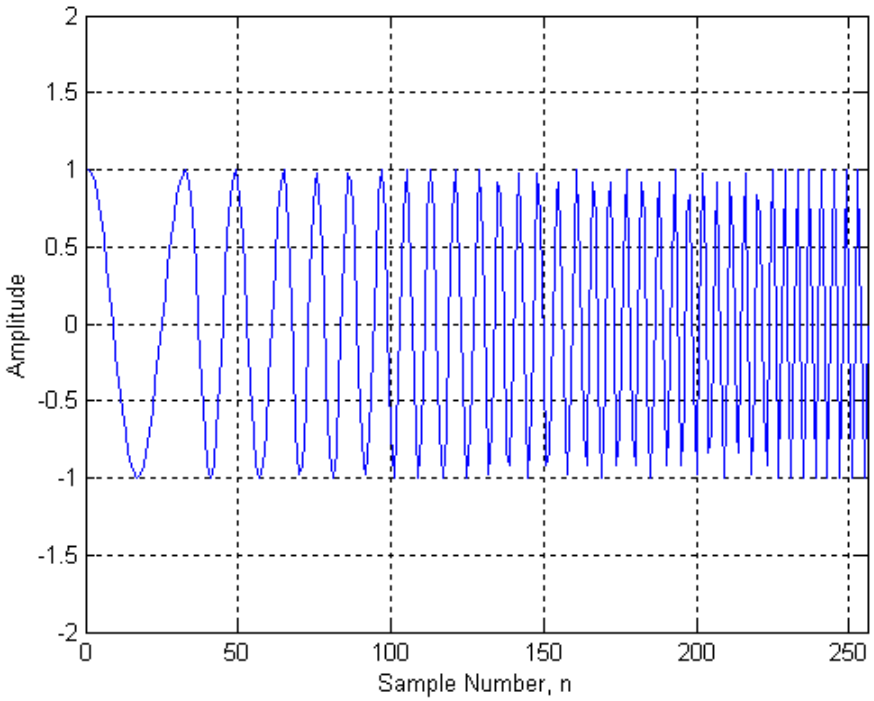

Figure 3.6: Step LFM signal waveform.

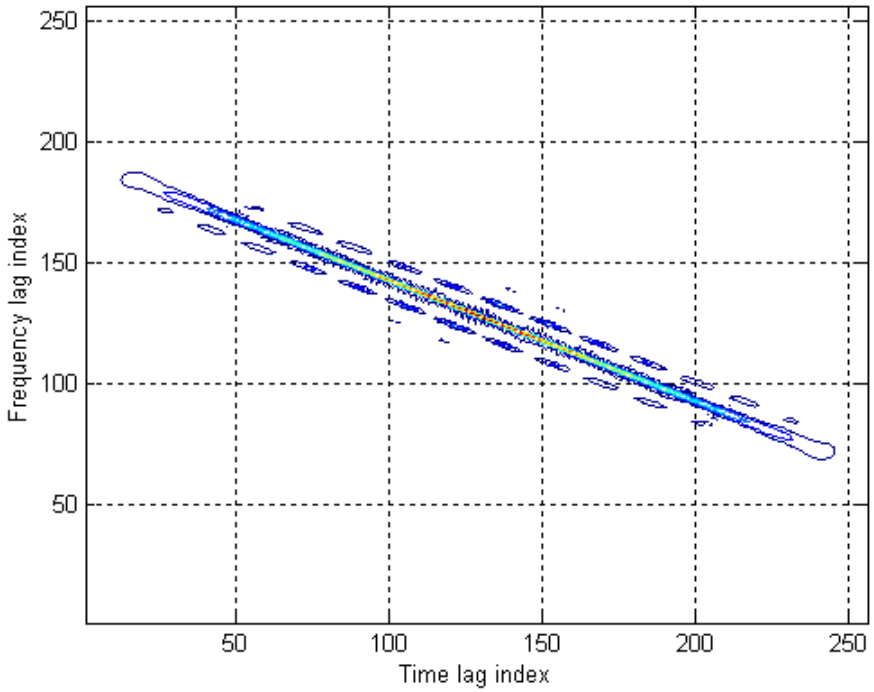

Figure 3.7: The contour plot of the step LFM ambiguity function.

3.3.3 Frank Code

The Frank polyphase coded waveform may be described and generalized by considering a hypothetically sampled step LFM waveform. In polyphase codes, a waveform of duration T is divided into N equal – length subpulses of duration $T_1 = \frac{T}{N}$ with each subpulse having one of M possible phases. For the Frank code (Frank, 1963), the length N of a codeword is equal to the square of M ;

$$N = M^2. \tag{3.36}$$

The carrier frequency remains fixed and a constant phase value is assigned to each M^2 subpulses. The compression ratio of the Frank code is given as M^2. A Frank code with unit energy is defined as

$$s(t) = \frac{1}{\sqrt{T}} \exp\left\{ j\left[2\pi f_o t + \varphi_n\right]\right\}, \qquad t \le \left|\frac{T}{2}\right|, \qquad n = 1,...,M^2. \tag{3.37}$$

The phase sequence φ_n is defined in matrix form as (Lewis, Kretschmer & Shelton, 1986)

$$\varphi_{mn} = \frac{2\pi}{M}(m-1)(n-1), \qquad m = 1,...,M \quad \text{for each} \quad n = 1,...,M. \tag{3.38}$$

For example, for $M = 4$, the phase matrix can be written as

$$\varphi_{mn} = \begin{bmatrix} 0 & 0 & 0 & 0 \\ 0 & 1 & 2 & 3 \\ 0 & 2 & 4 & 6 \\ 0 & 3 & 6 & 9 \end{bmatrix} \frac{\pi}{2}. \tag{3.39}$$

An illustration of the phase increments is shown in Figure 3.8 for $M = 4$.

The time domain plot of the Frank code and the contour plot of its ambiguity function are sketched in Figure 3.9 and Figure 3.10, respectively. The duration and compression ratio are the same with the LFM signal in Figure 3.3. In Figure 3.10, beside the main ridge at the center of the ambiguity function contour plot, there also exist parallel ridges. The number of parallel ridges is more than the one for the step LFM signal since there is more energy spread in the Frank code than the step LFM signal. The parallel lines seen in the ambiguity contour plot of the Frank code in Figure 3.10 are similar to the ones in the ambiguity contour plot of the step LFM signal. This is because the phase sequence of the Frank code is generated by sampling the phase of the step LFM signal.

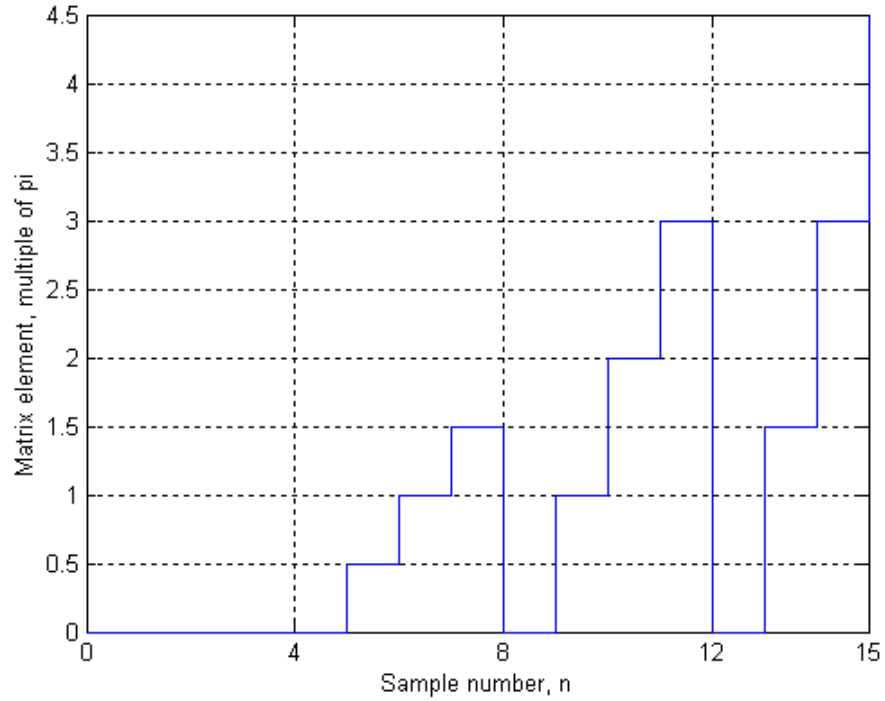

Figure 3.8: Phase increments of Frank code for M=4.

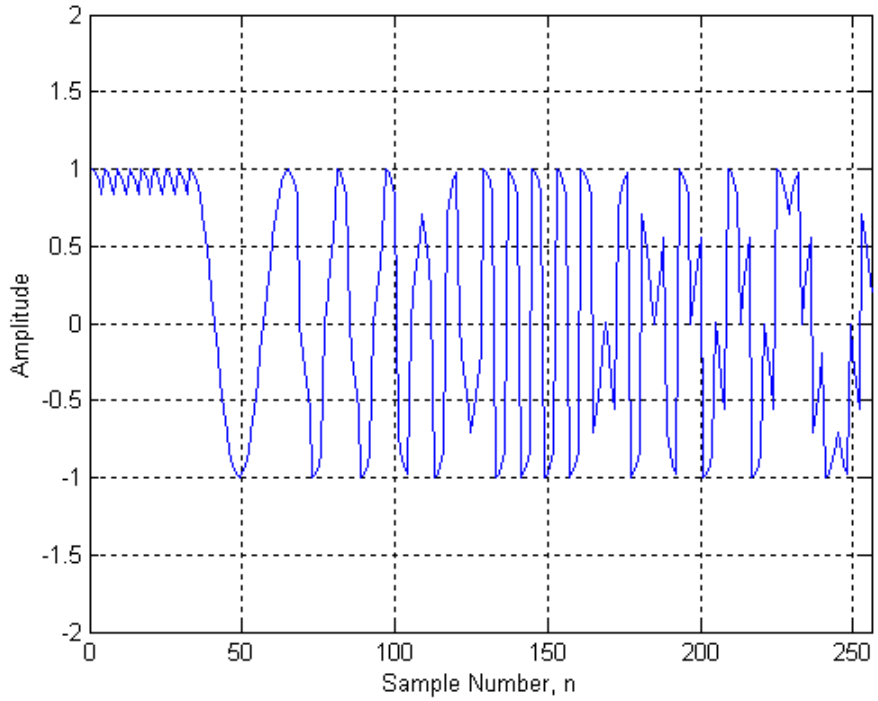

Figure 3.9: Time domain waveform of the Frank coded signal.

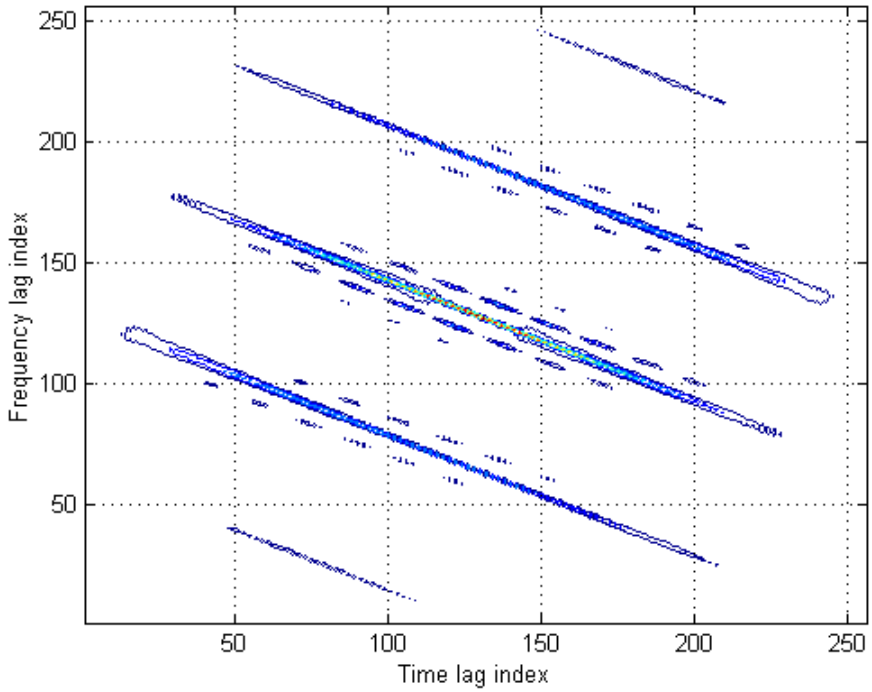

Figure 3.10: The contour plot of the Frank code ambiguity function.

3.3.4 P1 Code

The P1 codes are similar to the Frank codes in terms of the Doppler frequency tolerance and ease of implementation. In Figure 3.11(a), a Frank coded waveform is depicted, where G_k denotes the phase groups corresponding to the sampled phases of a step – chirp waveform. Each group consists of N vectors beginning with a vector at a phase angle of 0^o. The phase increments within K^{th} group, where $0 \le K \le N-1$, are

$$\Delta\phi_K = K(360^o)/N. \tag{3.40}$$

Thus, G_0 consists of N vectors at 0^o, G_1 has vectors separated by $360^o/N$, and so on, until at the center of the coded waveform the phase increments approach or become 180^o, depending on whether N is odd or even. For increments greater than 180^o, the phases are ambiguous with the result that the phasors of the phase group G_{N-K} are the conjugates of the phasors of the phase group G_K. Thus, the vectors

have the same increments, but they rotate in opposite directions. As a result, the phase increments are small at both ends of the code and become progressively larger toward the center of the code, where the increments approach 180^o from opposite directions.

The P1 code was derived using the previously described relationship between the Frank code phases and those of a sampled step – chirp waveform. The desired symmetry, having the DC or small incremental phase group at the center of the code, can be achieved by determining the phases, which result from placing the hypothetical synchronous oscillator at the band center of the step – chirp waveform. For an odd number of frequencies, the synchronous oscillator frequencies and the resulting phases are the same as in the Frank code, except that the phase groups are arranged as indicated in Figure 3.11(b). This rearrangement causes the P1 code to be more tolerant of precompression bandlimiting than the Frank code (Lewis, Kretschmer & Shelton, 1986).

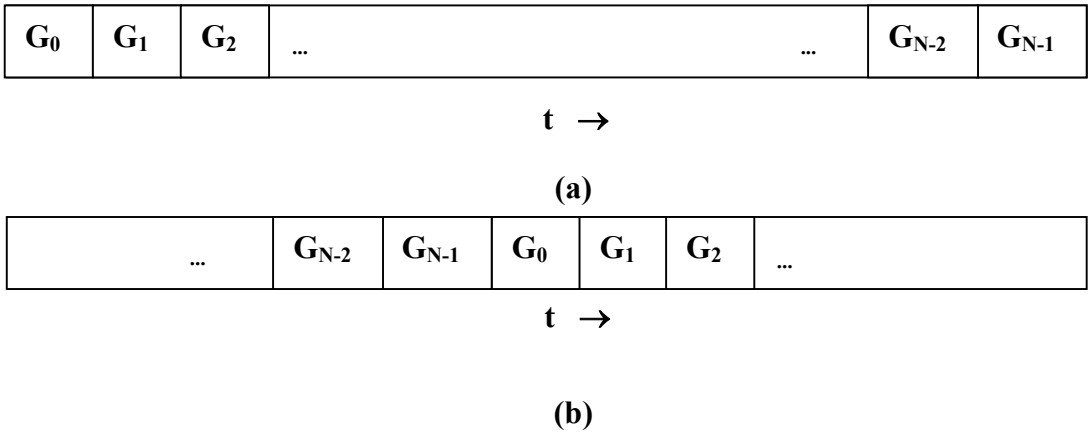

Figure 3.11: (a) Frank code phase group; (b) P1 code phase group.

Similar to the Frank code signal in (3.37), a P1 code with unit energy can be described as

$$s(t) = \frac{1}{\sqrt{T}} \exp\left\{ j\left[2\pi f_o t + \varphi_n\right]\right\}, \qquad t \le \left|\frac{T}{2}\right|, \qquad n = 1,...,M^2 \tag{3.41}$$

where the phase sequence φ_n is defined in matrix form. The m^{th} element of the n^{th} group is given in degrees by (Lewis, Kretschmer & Shelton, 1986)

$$\varphi_{mn} = \frac{\pi}{M}\left[M-(2n-1)\right]\left[(n-1)M+(m-1)\right], \quad m=1,...,M$$

$$\text{for each} \quad n=1,...,M. \tag{3.42}$$

The time domain waveform of the P1 code and the contour plot of its ambiguity function are sketched in Figure 3.12 and Figure 3.13, respectively. The duration and compression ratio are the same as with the LFM signal in Figure 3.3. In Figure 3.13, beside the main ridge at the center of the ambiguity function contour plot, there are also parallel ridges. The number of these parallel ridges is more than the one with the step LFM since there is more energy spread in P1 code as in the Frank code than the step LFM. However, compared to the Frank code, the number of these parallel ridges is still less in the P1 code. In Figure 3.13, we can see the similarity of parallel ridges of P1 with the step LFM since the phases of the P1 code are also generated from the phase samples of the step LFM signal.

3.3.5 P2 Code

The P2 code is valid for even M, and each group of the code is symmetric about the zero phase. For even M, the P2 code has the same phase increments within each phase group as the P1 code, except that the starting phases are different.

A P2 code with unit energy is described as

$$s(t) = \frac{1}{\sqrt{T}}\exp\left\{j\left[2\pi f_o t+\varphi_n\right]\right\}, \qquad t \le \left|\frac{T}{2}\right|, \qquad n=1,...,M^2 \tag{3.43}$$

where the phase sequence φ_n is defined in matrix form. The m^{th} element of the n^{th} group is given in degrees by (Lewis, Kretschmer & Shelton, 1986);

$$\varphi_{mn} = \frac{\pi}{2M}\left[M-(2n-1)\right]\left[M+1-2m\right], \quad m=1,...,M$$

$$\text{for each} \quad n=1,...,M \quad (M \quad \text{even}). \tag{3.44}$$

The requirement for M to be even in this code stems from the desire for low autocorrelation sidelobes. An odd value of M results in high sidelobes. This code has the same frequency symmetry of the P1 code.

The plot of the P2 code in time domain and the contour plot of its ambiguity function are sketched in Figure 3.14 and Figure 3.15, respectively. In Figure 3.15, the parallel ridges seen in the ambiguity contour plot of the P2 code show that similar energy spread occurs for this signal as in the Frank and P1 codes. The ambiguity contour plot is virtually similar to the contour plot of the P1 ambiguity plot in Figure 3.13. Since the phases of the P3 code is generated from the phase samples of the step LFM, the ambiguity contour plot also resembles the ambiguity plot of the step LFM shown in Figure 3.7.

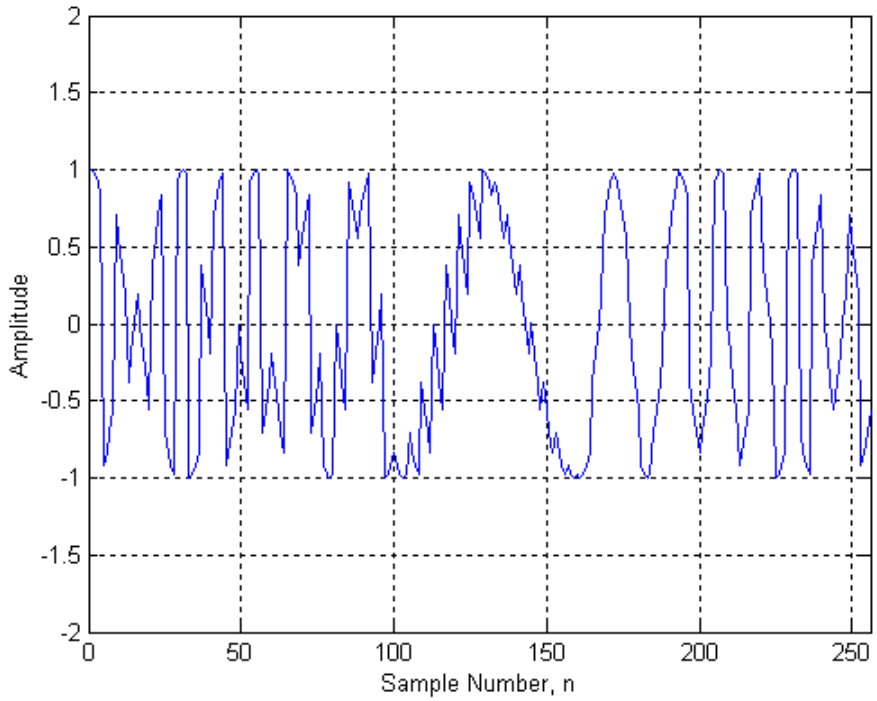

Figure 3.12: Time domain waveform of the P1 coded signal.

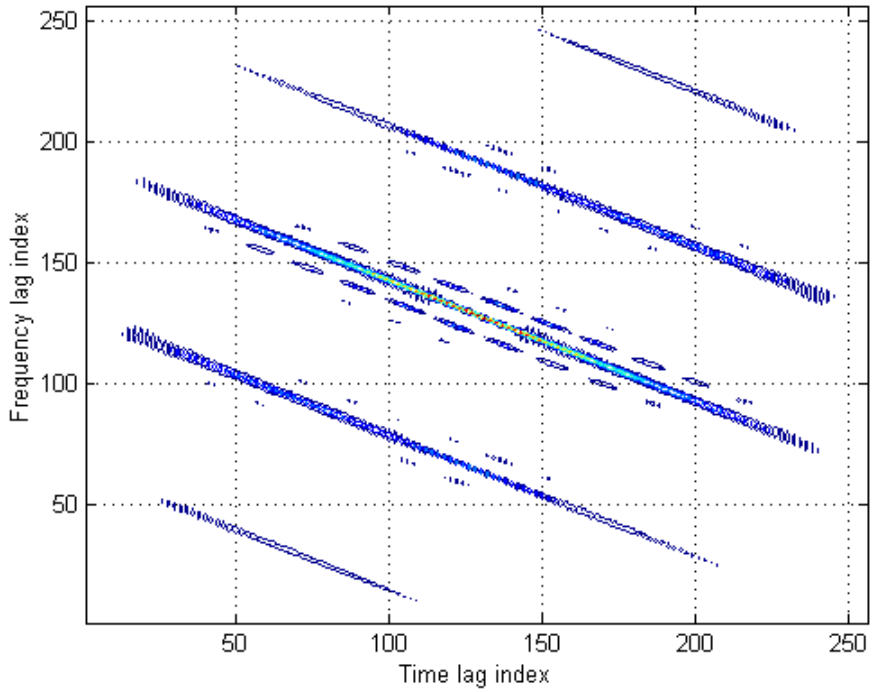

Figure 3.13: The contour plot of the P1 code ambiguity function.

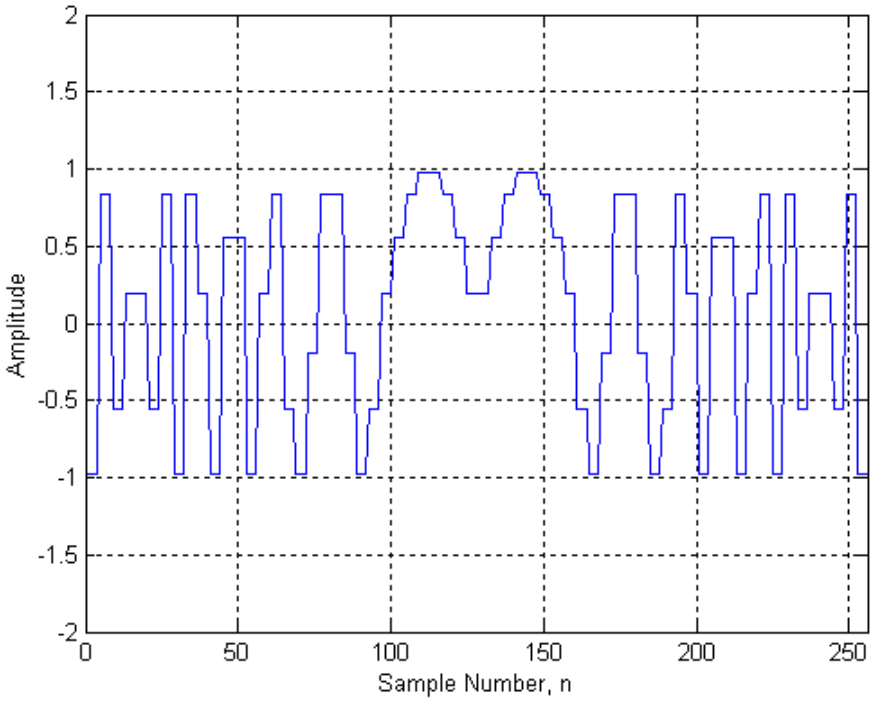

Figure 3.14: Time domain waveform of the P2 coded signal.

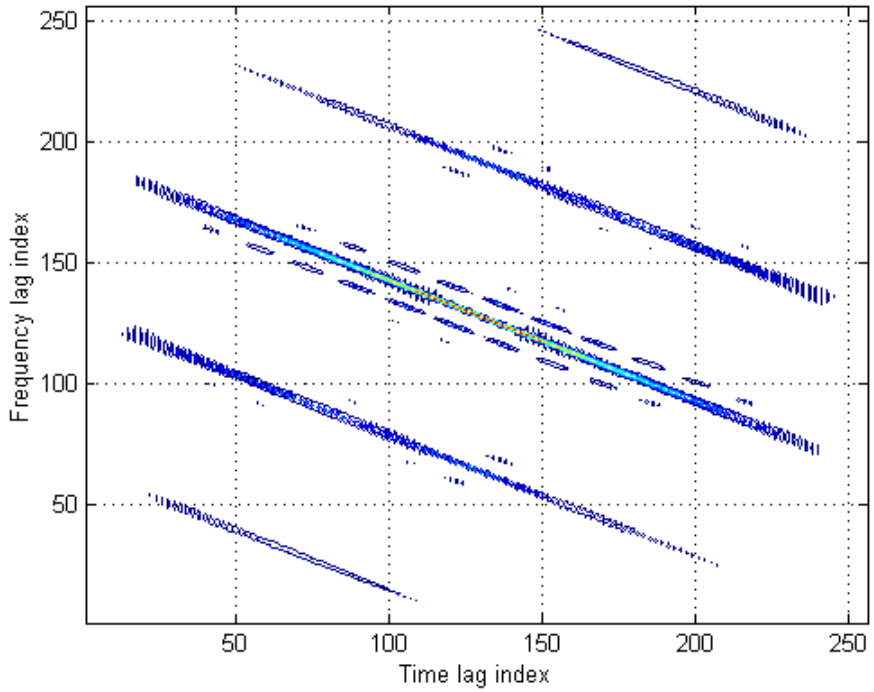

Figure 3.15: The contour plot of the P2 code ambiguity function.

3.3.6 P3 Code

The P3 code can be obtained using a linear FM waveform. The P3 code is more Doppler tolerant than the Frank, P1, and P2 codes. It is derived by converting a linear frequency modulated waveform to baseband by using a synchronous oscillator on one end of the frequency sweep and sampling the in – phase (I) and quadrature (Q) components at the Nyquist rate (Lewis, Kretschmer & Shelton, 1986).

A P3 code with unit energy is of the form

$$s(t) = \frac{1}{\sqrt{T}} \exp\left\{ j\left[2\pi f_o t + \varphi_n\right]\right\}, \qquad t \le \left|\frac{T}{2}\right|, \qquad n = 1,...,M^2 \tag{3.45}$$

where the phase sequence φ_n is defined in vector form. The n^{th} element of the phase vector is given in degrees by (Lewis, Kretschmer & Shelton, 1986)

$$\varphi_n = \frac{\pi(n-1)^2}{M^2}, \quad n = 1,...,M^2. \tag{3.46}$$

The plot of the P3 code in time and the contour plot of its ambiguity function are sketched in Figure 3.16 and Figure 3.17, respectively. In Figure 3.17, similar to other polyphase signals, there can be seen parallel ridges in the ambiguity function of the P3 signal. However, the number of parallel ridges in the P3 code is much larger than in the P1 and P2 codes. Notice that the ambiguity contour plot of the P3 code is quite similar to the ambiguity plot of the Frank code. From Figure 3.17, we see that the parallel ridges are similar to the ones in the ambiguity contour plot sketched in Figure 3.4. The reason for this can be traced to the fact that the phase sequence of the P3 code is generated by sampling the phase of the LFM signal.

3.3.7 P4 Code

The P4 code is derived from the same waveform as the P3 code. However, in the P4 code, the local synchronous oscillator frequency value is different from the P3 code (Lewis, Kretschmer & Shelton, 1986).

A P4 code with unit energy can be described as

$$s(t) = \frac{1}{\sqrt{T}} \exp\left\{ j\left[2\pi f_o t + \varphi_n \right] \right\}, \qquad t \le \left| \frac{T}{2} \right|, \qquad n = 1, ..., M^2 \tag{3.47}$$

where the phase sequence φ_n is defined in vector form. The n^{th} element of the phase vector is given in degrees by (Lewis, Kretschmer & Shelton, 1986)

$$\varphi_n = \frac{\pi (n-1)^2}{M^2} - \pi (n-1), \quad n = 1, ..., M^2. \tag{3.48}$$

The time domain plot of the P4 code and the contour plot of its ambiguity function are sketched in Figure 3.18 and Figure 3.19, respectively. In Figure 3.19, parallel lines are visible in the ambiguity contour plot showing that energy spread also exists in the P4 signal. From Figure 3.19, we see that the parallel ridges are similar to the ones in the ambiguity contour plot sketched in Figure 3.4. This is because the phase sequence of the P4 code is generated by sampling the phase of the LFM signal, similar to the P3 code.

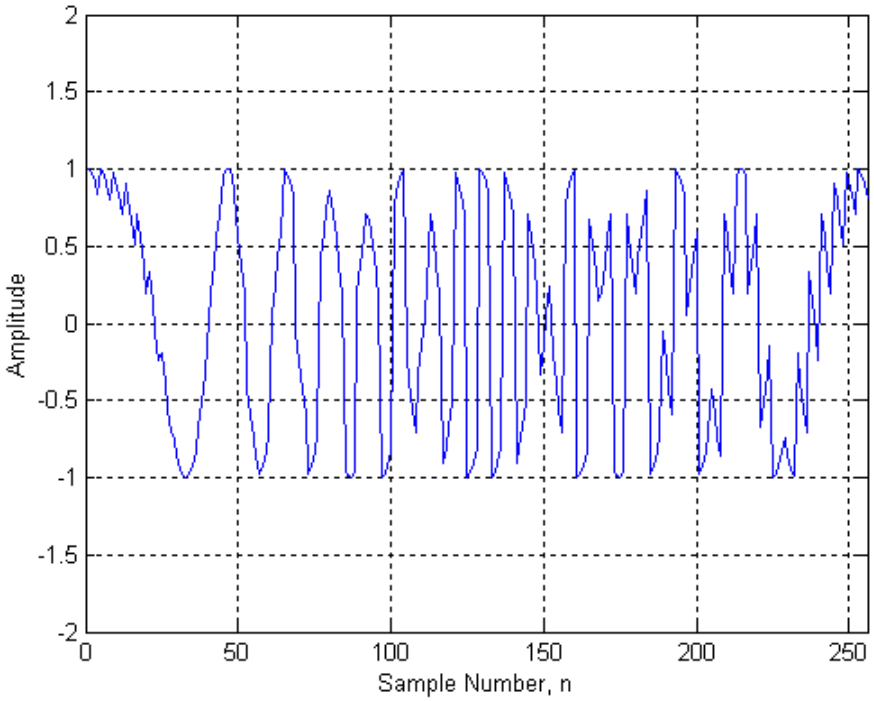

Figure 3.16: Time domain waveform of the P3 coded signal.

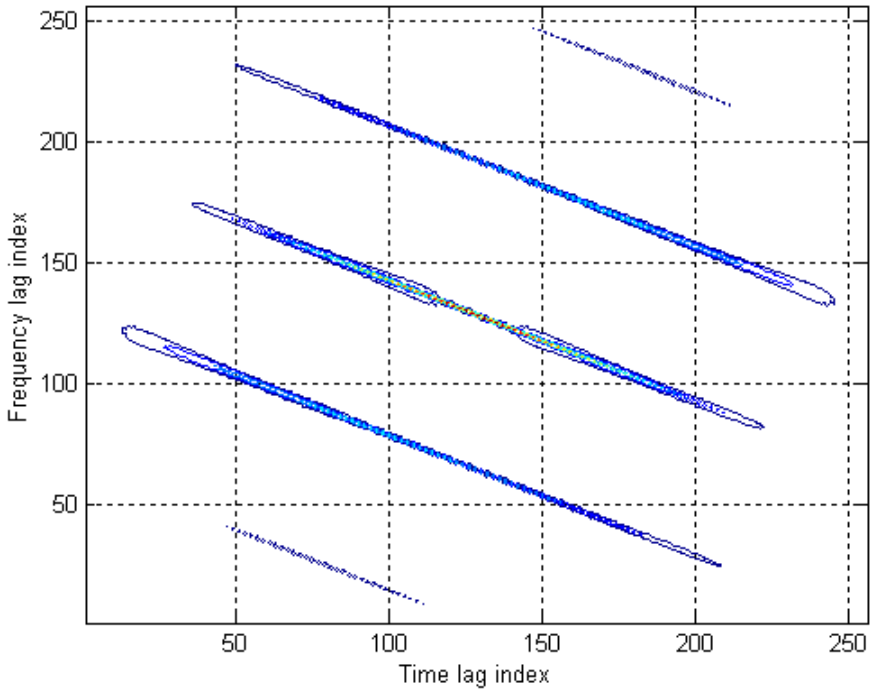

Figure 3.17: The contour plot of the P3 code ambiguity function.

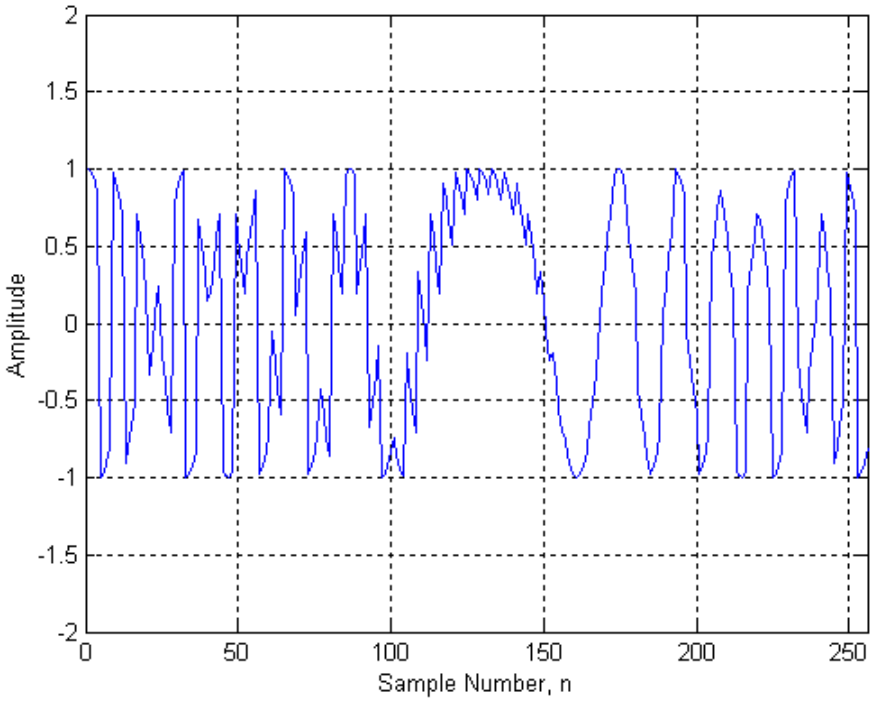

Figure 3.18: Time domain waveform of the P4 coded signal.

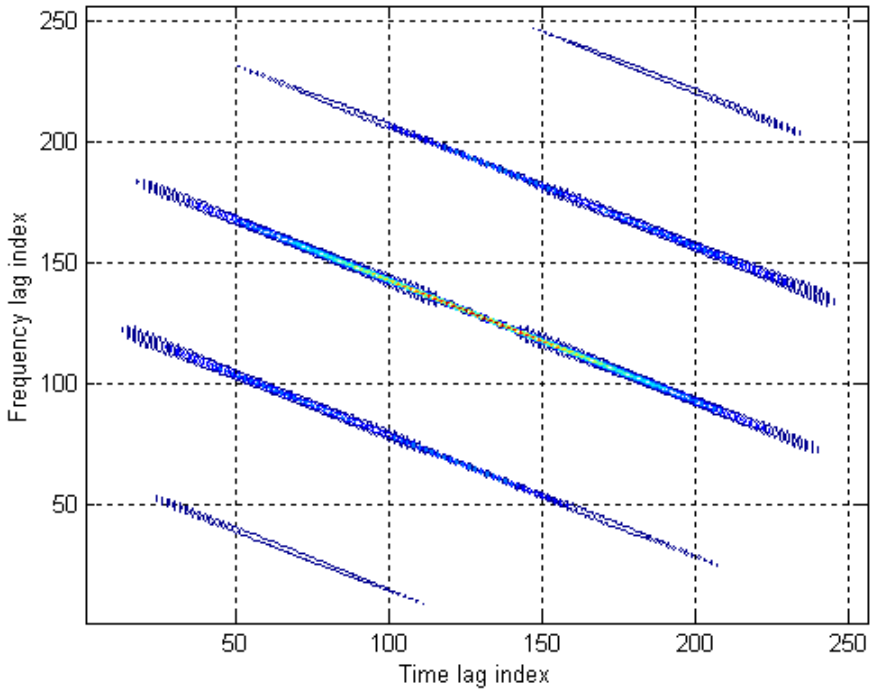

Figure 3.19: The contour plot of the P4 code ambiguity function.

CHAPTER FOUR

DETECTION OF POLYPHASE – CODED RADAR SIGNALS USING FRACTIONAL AUTOCORRELATION

In this chapter, we utilize a detection statistic which is based on fractional autocorrelation for detection of LFM, step LFM and polyphase coded signals. In Section 1, we introduce the relation between the ambiguity function and fractional autocorrelation. Then, in Section 2, we present the definition of a detection statistic based on fractional autocorrelation, which is utilized for detection of LFM signals (Akay, & Boudreaux – Bartels, 2001). We also derive the performance of this detector. In Section 3, we extend the use of the detection statistic for detection of step LFM and polyphase – coded signals (Frank, P1, P2, P3, and P4 codes) and provide simulation examples. We would like to note that some of the results in this chapter are published before as conference papers (Akay & Erözden, 2004), (Erözden & Akay, 2004).

4.1 Ambiguity Function and Fractional Autocorrelation Function

The FrFT has been shown to be related with the Wigner distribution which is a frequently used time – frequency representation (Almeida, 1994), (Özaktaş, et. al, 1994). Via fractional autocorrelation, it can also be related to the ambiguity function (AF) (Akay & Boudreaux – Bartels, 2001). The AF of a signal $s(t)$ can be considered to be a 2-D joint correlation function of time lag, τ, and frequency lag, ν (Cohen, 1995), (Hlawatsch & Boudreaux – Bartels, 1992). Definition of the AF of the signal $s(t)$ can be derived using the unitary time – shift operator, $\mathbf{T}_\tau$, and the frequency – shift operator, $\mathbf{F}_\nu$, (Baraniuk & Jones, 1995) as

$$AF_s(\tau,\nu) = \left\langle F_{-\frac{\nu}{2}} T_{-\frac{\tau}{2}} s, F_{\frac{\nu}{2}} T_{\frac{\tau}{2}} s \right\rangle = \int s\left(t+\frac{\tau}{2}\right) s^*\left(t-\frac{\tau}{2}\right) \exp\left(-j2\pi\nu t\right) dt \tag{4.1}$$

where $<\ ,\ >$ represents the inner product operation.

To obtain the relationship between the AF and fractional autocorrelation we change the integration dummy variable in (2.40) as $\beta' = \beta - \left[\left(\rho\cos\phi\right)/2\right]$. Thus, we have

$$\left(s \star_{\phi} s\right)(\rho) = \int s(\beta' + \frac{\rho\cos\phi}{2}) s^{*}(\beta' - \frac{\rho\cos\phi}{2}) \exp(-j2\pi\beta'\rho\sin\phi) d\beta'. \tag{4.2}$$

Comparing (4.1) and (4.2), fractional autocorrelation can be related to the AF as

$$\left(s \star_{\phi} s\right)(\rho) = AF_{s}(\rho\cos\phi, \rho\sin\phi). \tag{4.3}$$

By (4.3), we can conclude that fractional autocorrelation associated with the fractional domain at angle ϕ can also be recovered by taking a slice of the AF at angle ϕ on the ambiguity plane, as sketched in Figure 4.1. In particular, the cut along the time lag axis, $\phi = 0$, corresponds to temporal autocorrelation of $s(t)$. Similarly, the cut along the frequency lag (Doppler) axis, $\phi = \frac{\pi}{2}$, can be considered as spectral autocorrelation of $s(t)$. Thus, fractional autocorrelations of $s(t)$, computed using (4.2), allow us to obtain radial cuts of the AF at angles other than $\phi = 0$ and $\phi = \frac{\pi}{2}$.

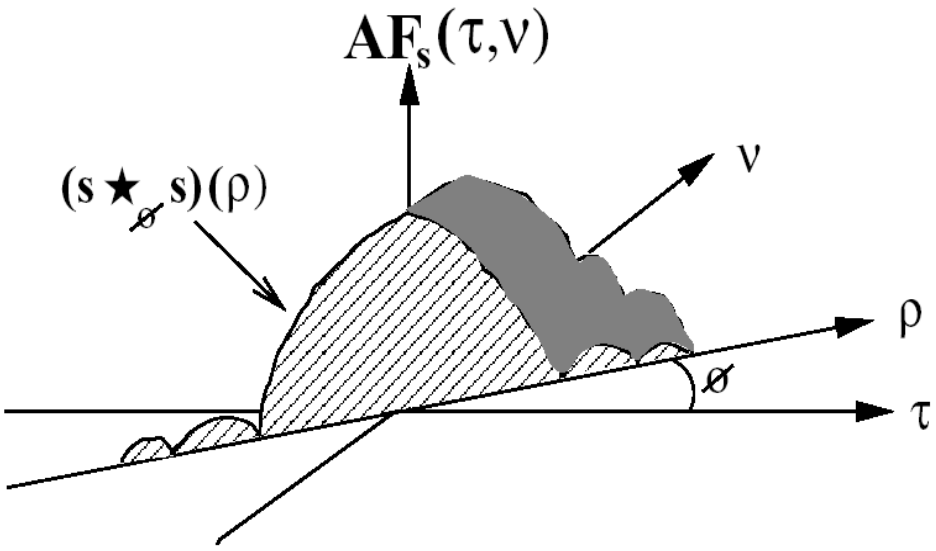

Figure 4.1: Fractional autocorrelation at angle ϕ is equal to the radial slice of the AF at angle ϕ on the ambiguity plane.

Using the property that the maximum of the AF occurs at $(\tau,\nu)=(0,0)$, we can conclude that fractional autocorrelation also has its maximum at the origin, $\rho=0$,

$$\left|\left(s\star_{\phi}s\right)(\rho)\right|\le\left(s\star_{\phi}s\right)(0). \tag{4.4}$$

The calculation of fractional autocorrelation can be accomplished efficiently using the alternative formulation in (2.44). This method uses the discrete – time approximation of the FrFT and the fast Fourier transform (FFT). The discrete FrFT algorithm proposed in (Özaktaş, et. al, 1996) has a computational load of $O(N\log N)$ for a length N discrete – time signal, making it comparable in efficiency to the fast Fourier transform (FFT) algorithm (Proakis & Monalakis, 1996). Thus, utilizing the discrete FrFT proposed in (Özaktaş, et. al, 1996) along with the FFT, a discrete – time calculation of fractional autocorrelation can be realized without excessive computational overhead. Alternatively, we can use the AF as in the right side of (4.3) to calculate fractional autocorrelation. However, it is not computationally efficient (Akay & Boudreaux – Bartels, 2001).

4.2 Detection Statistic for Detection of LFM and Polyphase – Coded Signals

It has been shown that the optimum detector for LFM signals embedded in noise, with unknown chirp rate and initial frequency, computes the integral of the Wigner distribution of the received signal along all lines on time – frequency plane (Kay & Boudreaux – Bartels, 1985). The line that produces the maximum value corresponds to the maximum likelihood estimate of the linear instantaneous frequency of the LFM. Integration of the Wigner distribution of the received signal along all lines on time – frequency plane has been named the Radon – Wigner transform (RWT) (Wood & Barry, 1994), which turns the task of tracking straight lines on the time – frequency plane into locating maxima in a two – dimensional (initial frequency versus chirp rate) plane.

Often the chirp rate is the only parameter of interest. Thus, LFM signals can be detected by locating maxima with respect to the chirp rate in many applications. In

other words, the chirp rates distinguish different LFM signals. Using this fact, for the detection of multi – LFM signals in noise a method which combines the AF and the Radon transform has been derived and called Radon – ambiguity transform (RAT) (Wang, et. al, 1998). Using the RAT, LFM signals can be detected by computing line integrals through the origin of the signal's ambiguity function magnitude. The RAT reduces the detection of LFM signals to the location of maxima over chirp rates only. Beside LFM signals, the RAT detector can also be applied for the detection of step LFM, Frank, P1, P2, P3 and P4 codes (Jennison, 2003). The detection statistic used in (Wang, et. al, 1998) and (Jennison, 2003) is given as

$$D(m) = \int \left| AF_s(\tau, m\tau) \right| d\tau \tag{4.5}$$

where AF_s denotes the AF of the received signal $s(t)$. $D(m)$ calculates a line integral of the magnitude of the AF along a radial line of slope m. When the detection statistic $D(m)$ exceeds a threshold for a certain chirp rate value, then the algorithm decides that an LFM signal, with that particular chirp rate, is present in the received signal (Wang, et al, 1998).

4.2.1 A Detection Statistic Based on Fractional Autocorrelation Function

Using the relation between the AF and fractional autocorrelation, a detection statistic based on fractional autocorrelation for the detection of LFM signals is derived (Akay & Boudreaux – Bartels, 2001), (Akay, 2000).

The integral of the AF magnitude along the radial line with angle ϕ can be expressed as

$$L(\phi) = \int \int \left| AF_s(\tau, \nu) \right| \delta(\nu \cos\phi - \tau \sin\phi) d\nu d\tau \tag{4.6}$$

where $\delta(.)$ is the Dirac delta function. Using properties of the Dirac delta function, (4.6) can be written as,

$$L(\phi) = \frac{1}{|\cos\phi|} \int \left| AF_s(\tau, \tau \tan\phi) \right| d\tau. \tag{4.7}$$

Applying the change of variable $\tilde{\tau} = \frac{\tau}{\cos\phi}$, produces

$$L(\phi) = \int \left| AF_s(\tilde{\tau}\cos\phi, \tilde{\tau}\sin\phi) \right| d\tilde{\tau}, \qquad |\phi| < \frac{\pi}{2}. \tag{4.8}$$

Using the relation between fractional autocorrelation and the AF in (4.3), we obtain,

$$L(\phi) = \int \left| (s \star_{\phi} s)(\rho) \right| d\rho. \tag{4.9}$$

If we let $\phi = \arctan(m)$ and $\overset{v}{L}(m) = L(\arctan(m))$, the final detection statistic can be expressed as,

$$\overset{v}{L}(m) = \int \left| (s \star_{\arctan(m)} s)(\rho) \right| d\rho. \tag{4.10}$$

Integrating the magnitude of the fractional autocorrelation with angle $\phi = \arctan(m)$ of the received signal $s(t)$ is equal to integrating the AF along a line with angle ϕ going through the origin.

Comparing the detection statistic in (4.5) with the detection statistic derived in (Akay & Boudreaux – Bartels, 2001) as given by (4.10), we can see that they are not completely identical. The two detection statistics can be related as (Akay & Boudreaux – Bartels, 2001)

$$\overset{v}{L}(m) = L(\arctan(m)) = \left| \sqrt{1+m^2} \right| D(m). \tag{4.11}$$

For chirp rates $|m| \le \frac{1}{2}$, the ratio between the two detection statistics is bounded by $\frac{\sqrt{5}}{2}$. However, the detection statistic in (4.10) is computationally more efficient than the one given in (4.5) since it does not require the calculation of the AF.

In simulations, we used the detection statistic in (4.10) using a normalization factor in the denumerator as

$$\overset{v}{L}(m) = \frac{\int \left| (s \star_{\arctan(m)} s)(\rho) \right| d\rho}{\int |s(t)| dt}. \tag{4.12}$$

This normalization factor allows the detection statistic to be independent of the noise power.

4.2.2 Performance of the Detection Statistic Based on Fractional Autocorrelation Function

For a given detection statistic, we conclude that a signal is present (hypothesis H_1) if the statistic exceeds a certain threshold. If not, it is decided that no signal is present (hypothesis H_0); that is, the signal contains only noise. The noise is assumed to be a zero – mean, complex, white Gaussian process with two – sided power spectral density (PSD) N_o. Performance of a detection method can be characterized with the help of the performance SNR measure

$$P(SNR) = \frac{\left| E(\overset{v}{L}(m) \mid H_1) - E(\overset{v}{L}(m) \mid H_0) \right|}{\left\{ \frac{1}{2} \left[\text{var}(\overset{v}{L}(m) \mid H_1) + \text{var}(\overset{v}{L}(m) \mid H_0) \right] \right\}^{1/2}}. \tag{4.13}$$

Here, $E(\overset{v}{L}(m) \mid H_i)$ and $\text{var}(\overset{v}{L}(m) \mid H_i)$ denote the expected value and variance of $\overset{v}{L}(m)$, respectively, for hypothesis H_i, $i = 0,1$. Large $P(SNR)$ values indicate that the average values of $\overset{v}{L}(m)$ for the two hypotheses are well separated, whereas a small variance for $\overset{v}{L}(m)$ results in improved detection (Wang, et. al., 1998).

$P(SNR)$ for the matched filter detector is equal to $\sqrt{\mathcal{E} / N_0}$, which is optimal among linear and nonlinear detectors (Wang, et. al., 1998).

For the detector $\overset{v}{L}(m)$, the performance SNR is calculated to be (the proof is given in Appendix A.1)

$$P(SNR) = \frac{\left| \mathcal{E} / |\cos\phi| \right|}{\left\{ \frac{1}{2} \left[\frac{2\mathcal{E}N_0 + N_0^2}{\cos^2\phi} \right] \right\}^{1/2}} = \frac{\mathcal{E}}{\sqrt{\mathcal{E}N_0 + N_0^2}}. \tag{4.14}$$

The performance SNR of the detector $D(m)$ in (Wang, et. al., 1998) is the same as (4.14). The plot of the performance SNR can be seen in Figure 4.2.

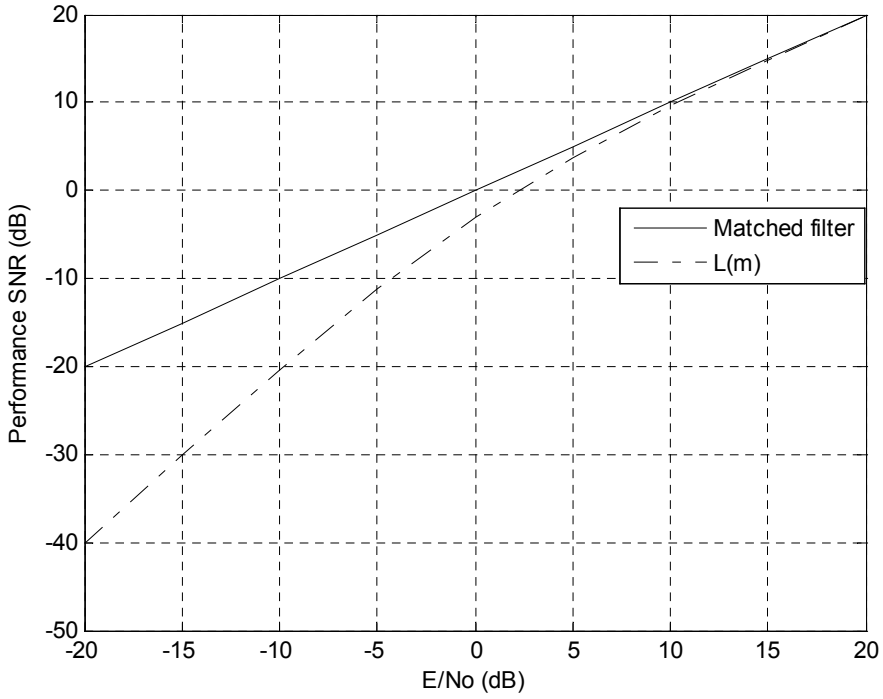

Figure 4.2: Comparison of the performance SNR of the matched filter and $\overset{v}{L}(m)$.

Another common merit of performance is the output signal to noise ratio SNR_{out}

$$SNR_{out} = \frac{output \quad signal \quad power}{\mathrm{var}(\overset{v}{L}(m) \mid H_1)} \tag{4.15}$$

which is the ratio between the output signal power and the output noise power. For the detector $\overset{v}{L}(m)$, the SNR_{out} is calculated to be (the proof is given in Appendix A.1)

$$SNR_{out} = \cos^2\phi \left(\frac{\left(\frac{\varepsilon}{N_0}\right)^2}{\frac{2\varepsilon}{N_0}+1} \right). \tag{4.16}$$

The SNR_{out} of $D(m)$ in (Wang, et. al, 1998) is almost the same as (4.16) except that the multiplication term, $\cos^2\phi$ does not appear. In Figure 4.3, SNR_{out} of the matched filter is compared with the SNR_{out} of $\overset{v}{L}(m)$ for different ϕ values.

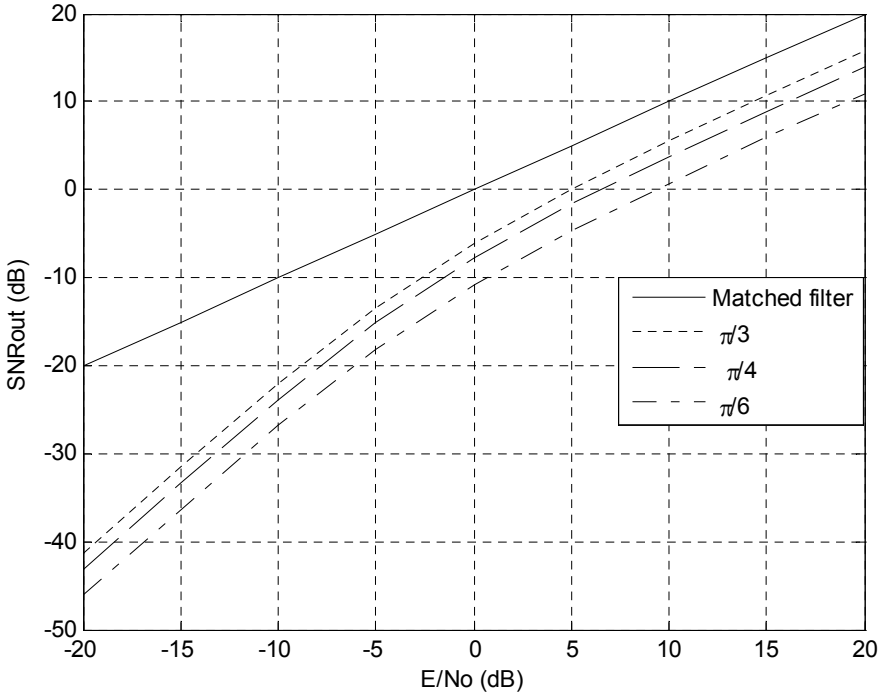

Figure 4.3: SNR_{out} of the matched filter and $\overset{v}{L}(m)$ for angles ϕ=π/3, π/4, π/6.

4.3 Detection of LFM, Step LFM and Polyphase Codes

In this section, the detection statistic, $\overset{v}{L}(m)$, given in (4.12) is digitally simulated for detection of LFM, step LFM and polyphase coded signals, namely, Frank, P1, P2, P3 and P4 codes which were described in Chapter 3. Digital computation of the detection statistic needs the digital computation of fractional autocorrelation in

(2.44). In computation of (2.44), one FrFT and one classical inverse FT are used. Hence, we need a digital computation of the FrFT. However, the discrete algorithm of the contionuous FrFT is not a purely discrete – time definition of the FrFT. Digital computation of the FrFT is an approximation of the continuous – time definition of the FrFT in (2.9) (Özaktaş, et al. 1996). In our simulations, we used the algorithm proposed in (Özaktaş, et al, 1996) to compute the FrFT digitally. We make sure that the conditions given in (Özaktaş, et al, 1996) are satisfied in order to obtain correct results.

4.3.1 Simulation Example 1

We examine the detection statistic, $\overset{v}{L}(m)$, given in (4.12) for each signal at different SNR values; 0 dB, -3 dB, -6 dB, -9 dB and -12 dB. Each signal is created digitally with 256 sample points having a sweep rate (chirp rate) of 0.5. We added zero – mean additive white Gaussian complex noise to each simulated signal. The complex noise is generated by two independent, zero – mean, random processes with a constant PSD equal to N_O. The detection statistic of the LFM signal for different SNR values is plotted in Figure 4.4. It can be seen that the detection statistic can detect the signal by producing peaks at the correct sweep rate which is 0.5. As the SNR decreases the peak value of the detection statistic also decreases but the peak occurring at the correct sweep rate value would still be visible above a suitably chosen detection threshold.

Similarly, the detection statistic of the step LFM is plotted in Figure 4.5. It also produces a peak at the correct sweep rate 0.5. However, the peak values occurred are not as high as in the LFM. The reason for this difference can be explained by comparing the AF plots of the LFM and step LFM signals given in Figures 3.4 and 3.7, respectively. The AF of a pure LFM is concentrated as a single line, however the step LFM have parallel lines, which causing on the energy spread.

The detection statistics of the polyphase coded signals Frank, P1, P2, P3 and P4 are plotted in Figure 4.6 through 4.10. Each of these detection statistics also produces a peak at the correct sweep rate as with the LFM and the step LFM plots. Similarly, the peak values occurred at the correct sweep rate are not as high as the peak values occurred in the detection statistics of the LFM signal. The reason for the decrease is explained by examining the AF plots of the polyphase codes given in Chapter 3. The AF plots of the polyphase codes have more parallel ridges than the step LFM which means more energy spread occurs for these signals. The comparison of the detection statistics for each simulated signal will be made at the next section.

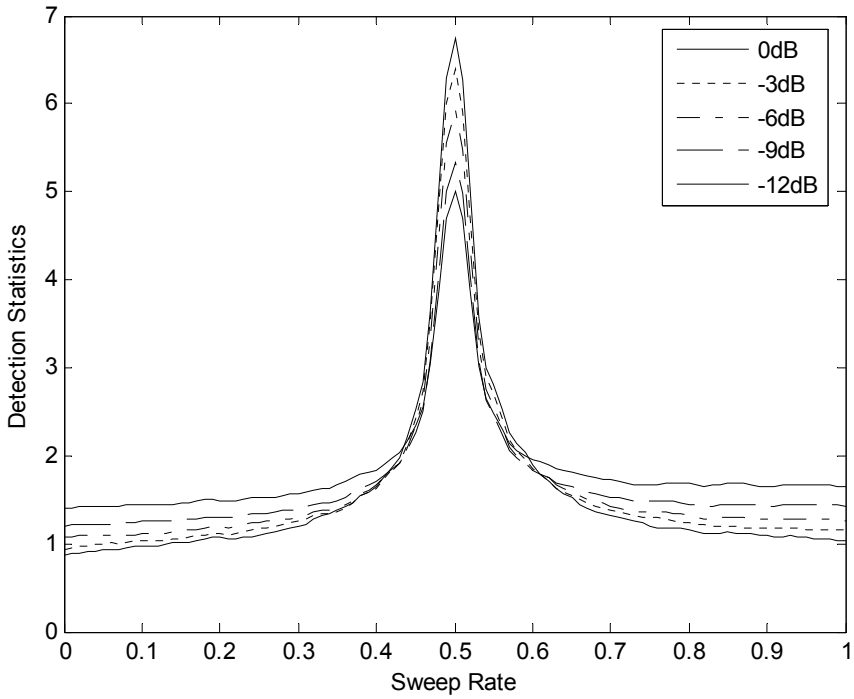

Figure 4.4: Detection statistics for the LFM signal at different SNR values.

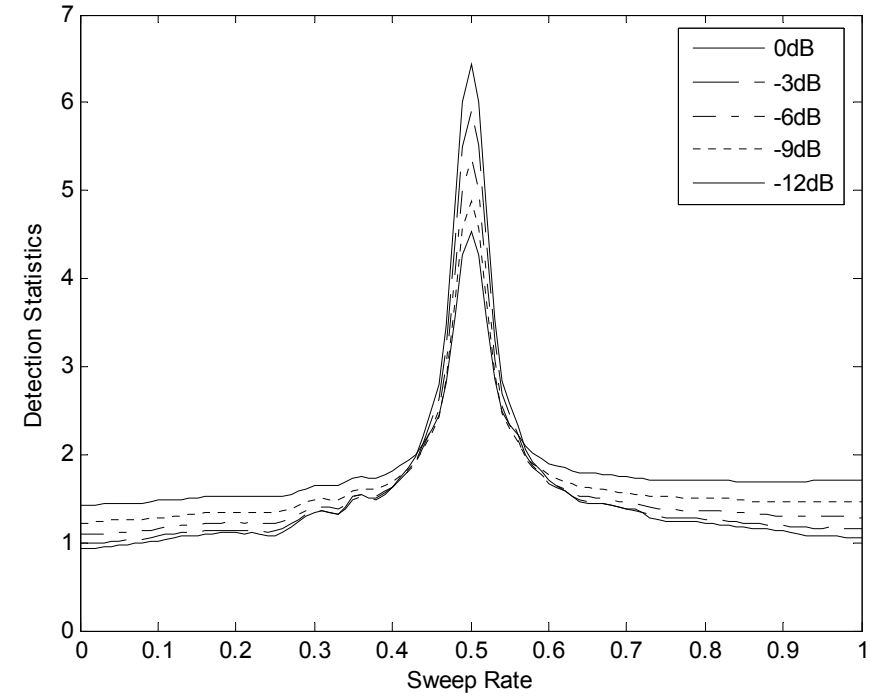

Figure 4.5: Detection statistics for the step LFM signal at different SNR values.

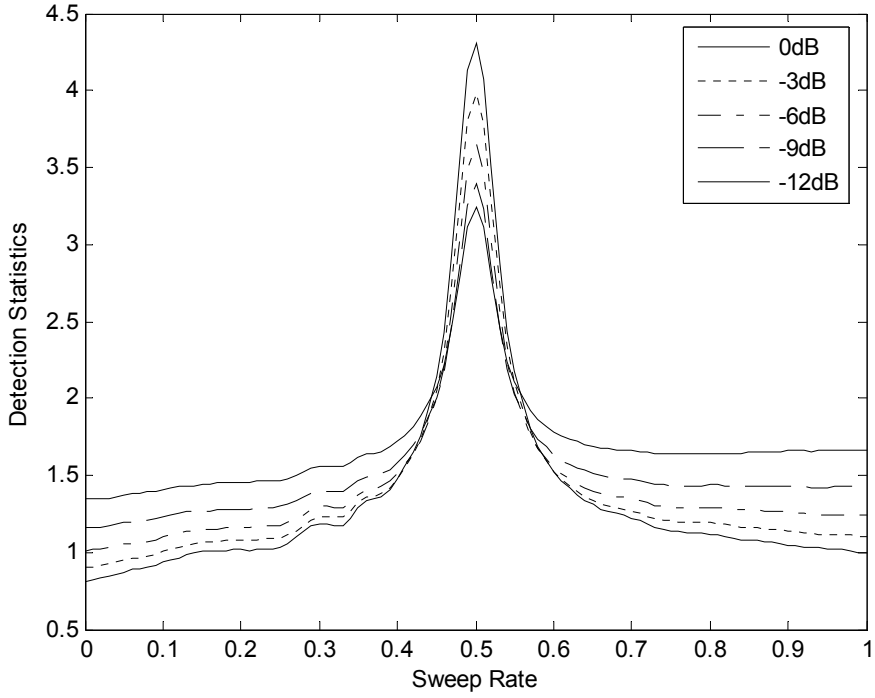

Figure 4.6: Detection statistics for the Frank code at different SNR values.

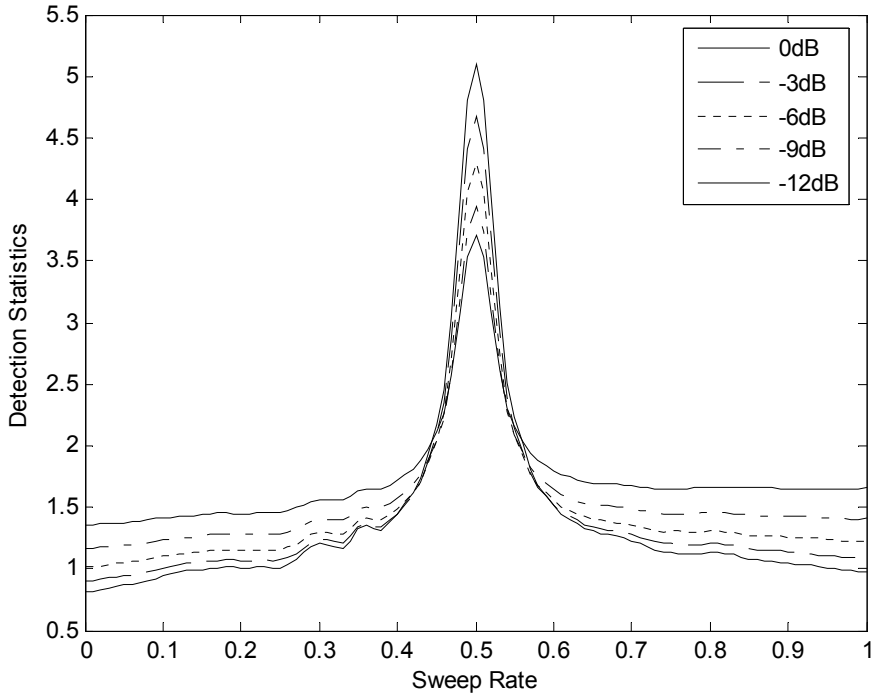

Figure 4.7: Detection statistics for the P1 code at different SNR values.

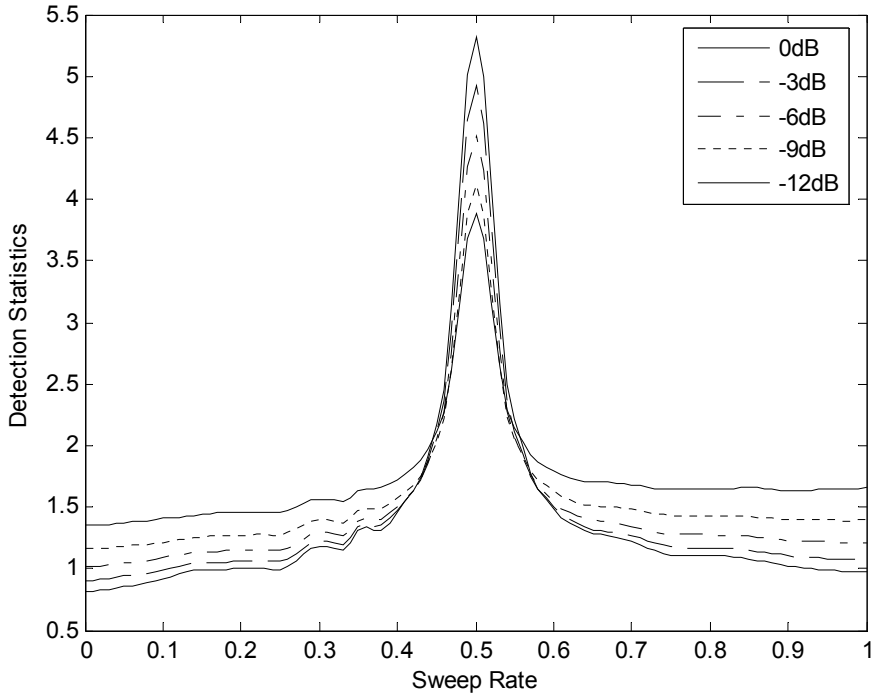

Figure 4.8: Detection statistics for the P2 code at different SNR values.

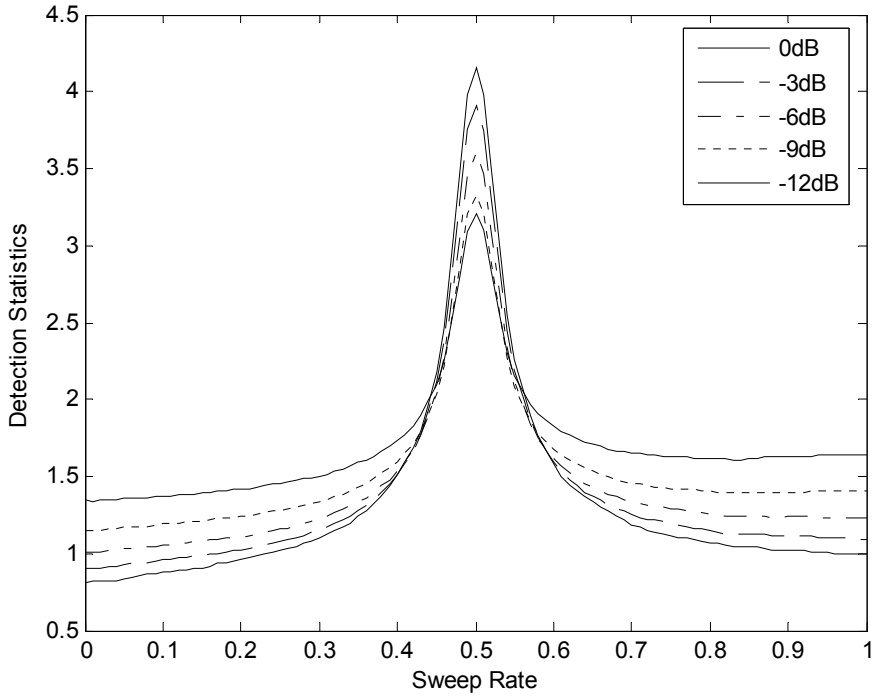

Figure 4.9: Detection statistics for P3 code at different SNR values.

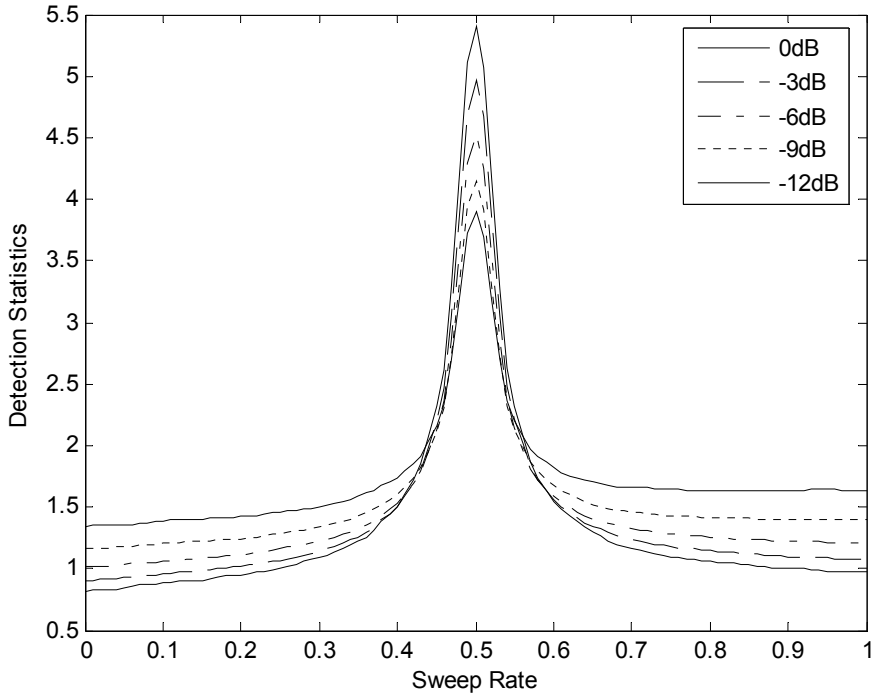

Figure 4.10: Detection statistics for the P4 code at different SNR values.

4.3.2 Simulation Example 2

In this section, we compare the detection statistic of each signal at different SNR values, 0 dB, -3 dB, -6 dB, -9 dB and -12 dB. All the signals are created digitally using 256 sample points and each has a sweep rate of 0.5. We then added zero – mean additive white Gaussian complex noise to each signal. The power of the noise is specially arranged so that the specified SNR is produced. For comparison purposes, the detection statistic is normalized with the detection statistic of the LFM signal to set the peak value as 1. The detection statistics calculated at SNR = 0 dB are plotted in Figure 4.11. It can be seen that the peak value occurred at the correct sweep rate of 0.5, and the LFM signal has the highest peak amplitude value. Then, the detection statistic peaks for the step LFM, P4, P2, P1, Frank and P3 codes come in decreasing order. The difference in the amplitude of the peaks obtained from different signals can be explained by examining the AF plots given in Chapter 3. The energy of the signals, step LFM, Frank, P1, P2, P3 and P4, are distributed among parallel lines appearing in their AF representations. Since the AF of a pure LFM is concentrated as a single line, its detection statistic produces the highest peak value. Due to the energy spread seen in the AFs of the step LFM and the polyphase codes, the peak amplitude levels in their detection statistics are lower.

The detection statistics calculated at SNR levels of -3 dB, -6 dB, -9 dB and -12 dB are plotted in Figures 4.12 through 4.15. In each plot, the similar characteristics can be observed. The peak values of the detection statistics for each signal type as a proportion of the LFM energy ε are listed in Tables 4.1 through 4.5 for different SNR values.

Table 4.1 Peak values of detection statistics as a proportion of LFM energy, ε, (SNR = 0 dB).

LFM	**Step LFM**	**Frank**	**P1**	**P2**	**P3**	**P4**
ε	0.913ε	0.613ε	0.720ε	0.766ε	0.607ε	0.768ε

Table 4.2 Peak values of detection statistics as a proportion of LFM energy, ε, (SNR = -3 dB).

LFM	Step LFM	Frank	P1	P2	P3	P4
ε	0.955ε	0.623ε	0.753ε	0.776ε	0.622ε	0.778ε

Table 4.3 Peak values of detection statistic as a proportion of LFM energy, ε, (SNR = -6 dB).

LFM	Step LFM	Frank	P1	P2	P3	P4
ε	0.896ε	0.623ε	0.723ε	0.783ε	0.634ε	0.783ε

Table 4.4 Peak values of detection statistic as a proportion of LFM energy, ε, (SNR = -9 dB).

LFM	Step LFM	Frank	P1	P2	P3	P4
ε	0.952ε	0.723ε	0.792ε	0.795ε	0.729ε	0.830ε

Table 4.5 Peak values of detection statistics as a proportion of LFM energy, ε, (SNR = -12 dB).

LFM	Step LFM	Frank	P1	P2	P3	P4
ε	0.970ε	0.613ε	0.720ε	0.766ε	0.607ε	0.768ε

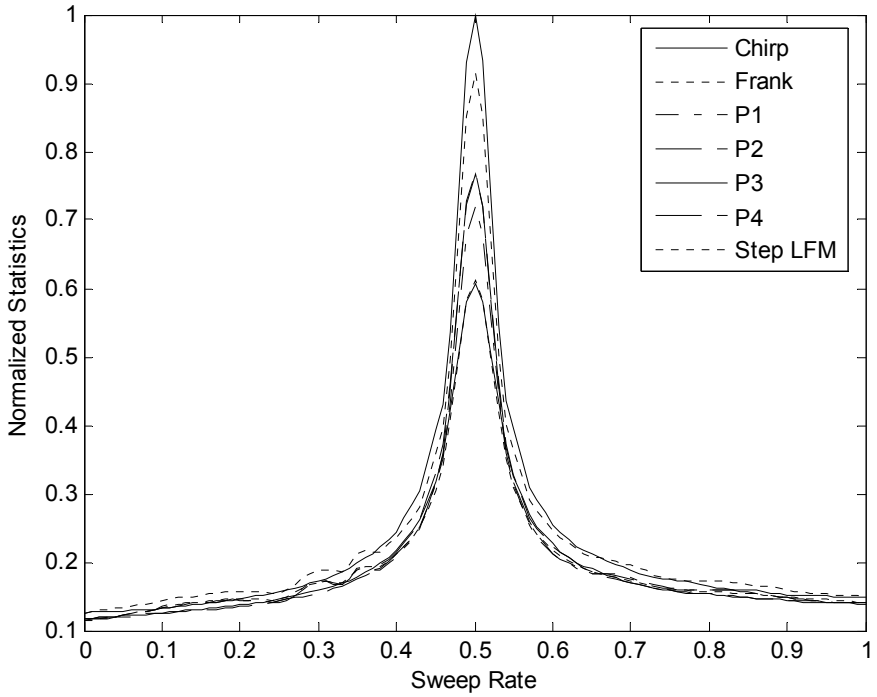

Figure 4.11: Detection statistics at SNR=0 dB.

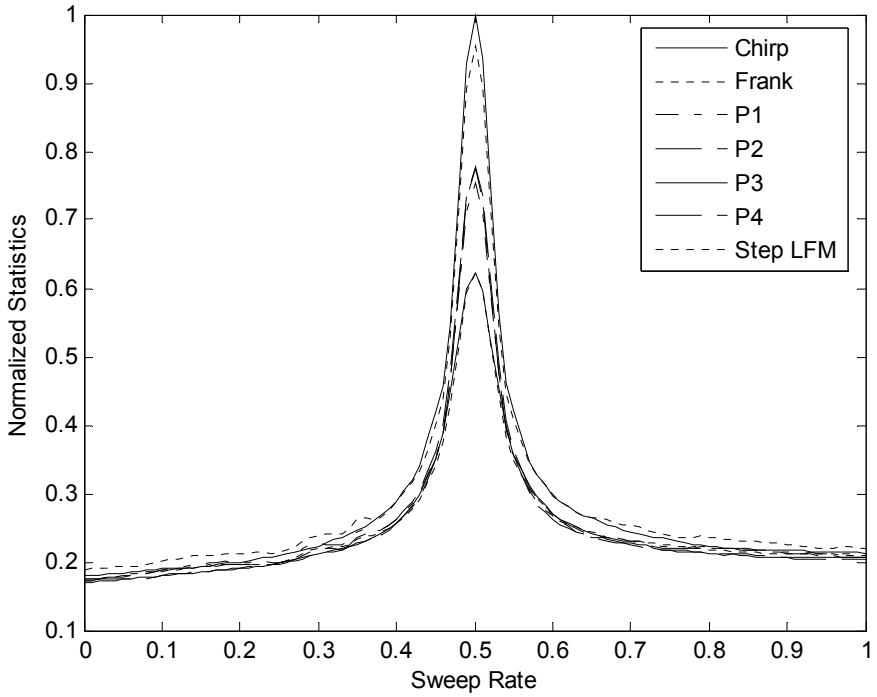

Figure 4.12: Detection statistics at SNR=-3 dB.

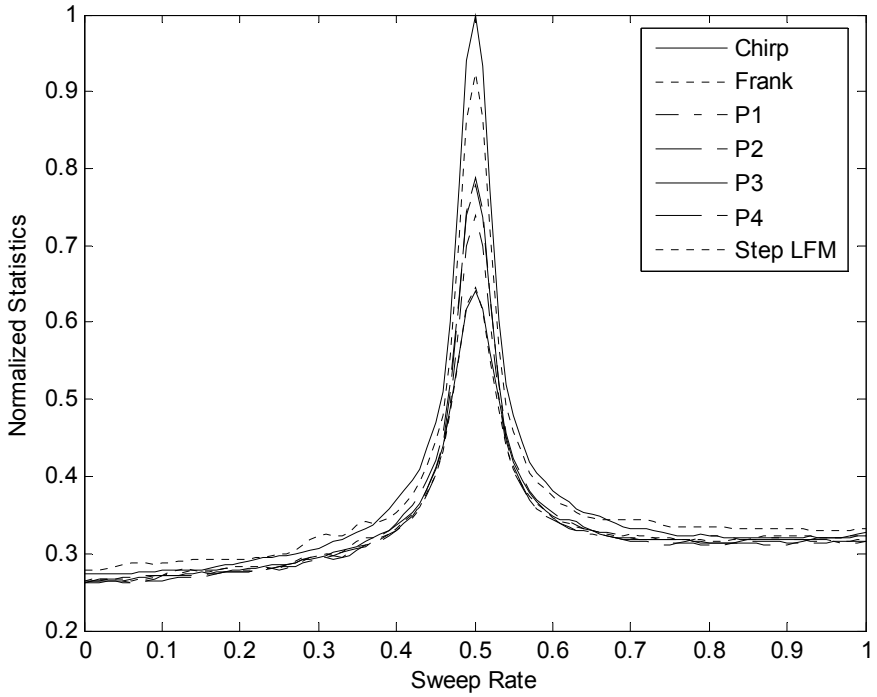

Figure 4.13: Detection statistics at SNR=-6 dB.

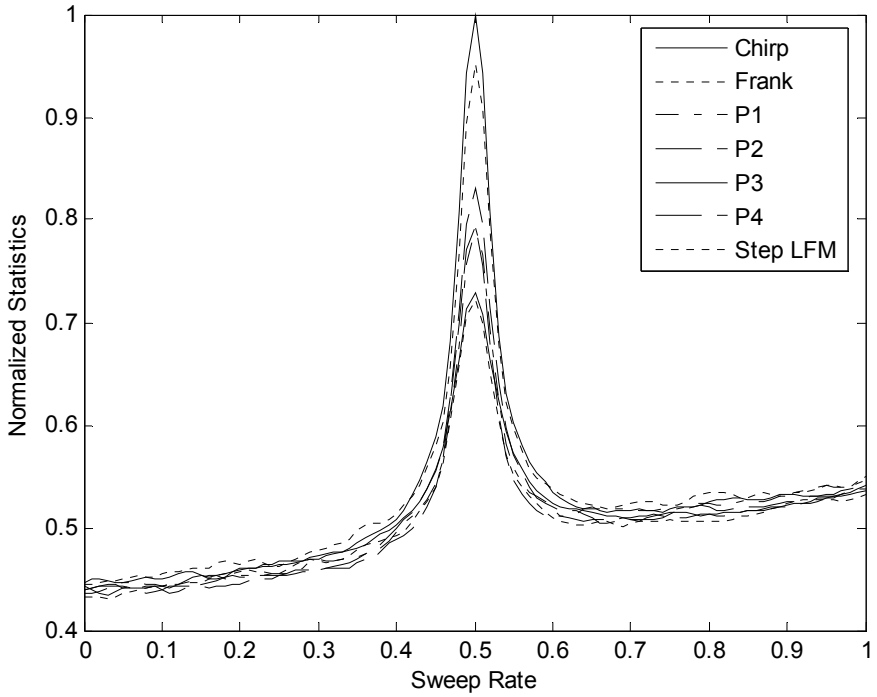

Figure 4.14: Detection statistics at SNR=-9 dB.

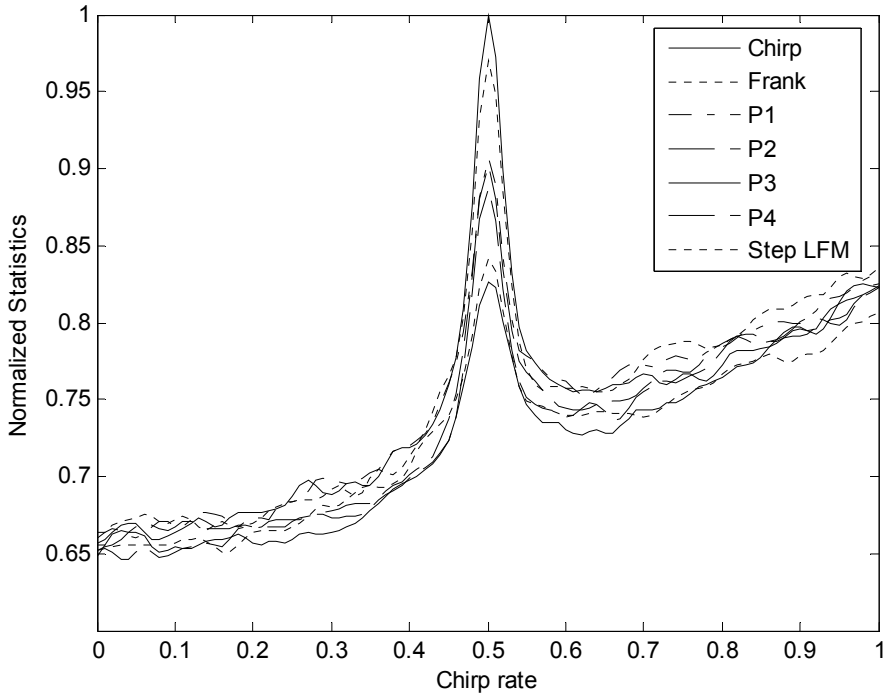

Figure 4.15: Detection statistics at SNR=-12 dB.

4.3.3 Use of Detection Statistic as a Sweep Rate Estimator

In the above simulations, we observed that the detection statistic always makes a peak at the correct sweep rate. Hence, we can use the detection statistic also to estimate the sweep rate parameter of the signals via the maximum likelihood (ML) estimate defined as

$$\hat{m} = \arg\max_{m} \; \overset{v}{L}(m). \tag{4.17}$$

We find the peak value of the detection statistic, $\overset{v}{L}(m)$, and then we determine the sweep rate, m, for which this maximum is obtained.

In simulations, the SNR value is changed between -12 dB and 0 dB with steps of 3 dB. The signal length is 256 samples, and the sweep rate is set as $m = 0.5$. 1000 Monte Carlo runs were carried out to estimate the sweep rate.

Figure 4.16 shows the performance of the estimator as a function of the SNR in estimating the sweep rate of the different signal types that we used. The presence of a threshold effect for low SNRs, which is typical of every nonlinear estimation algorithm, is evident in Figure 4.16. The mean square error (MSE) becomes a decreasing line after about SNR is at -6 dB. In Figure 4.17, the estimated sweep rates at different SNR values are plotted. The best performance is obtained for the LFM signal. Then, the other pulse compression signals come in decreasing order as the step LFM, P4, P2, P1, Frank and P3 code.

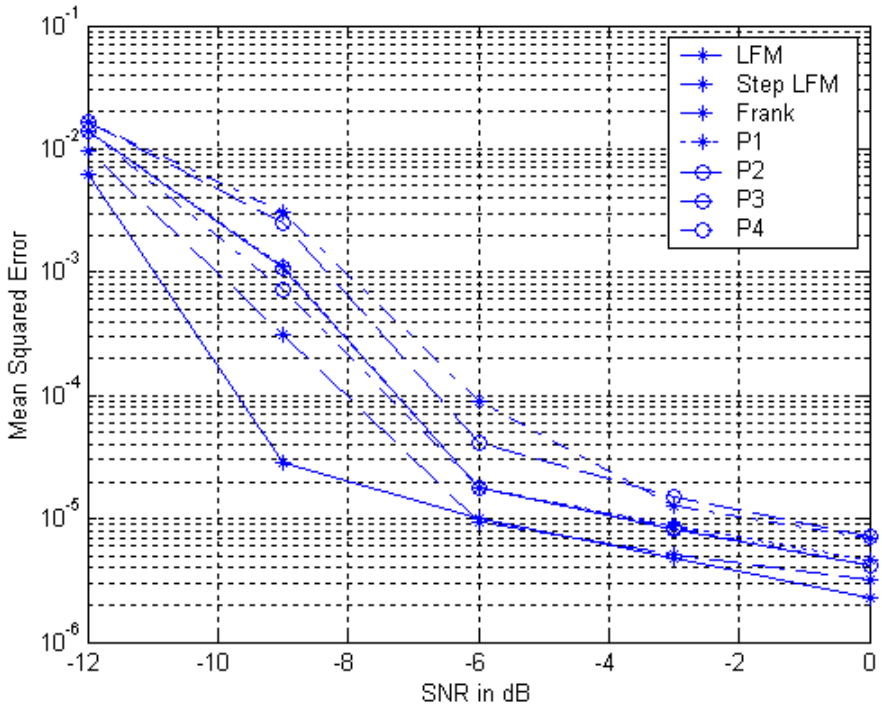

Figure 4.16: MSE for different SNR values.

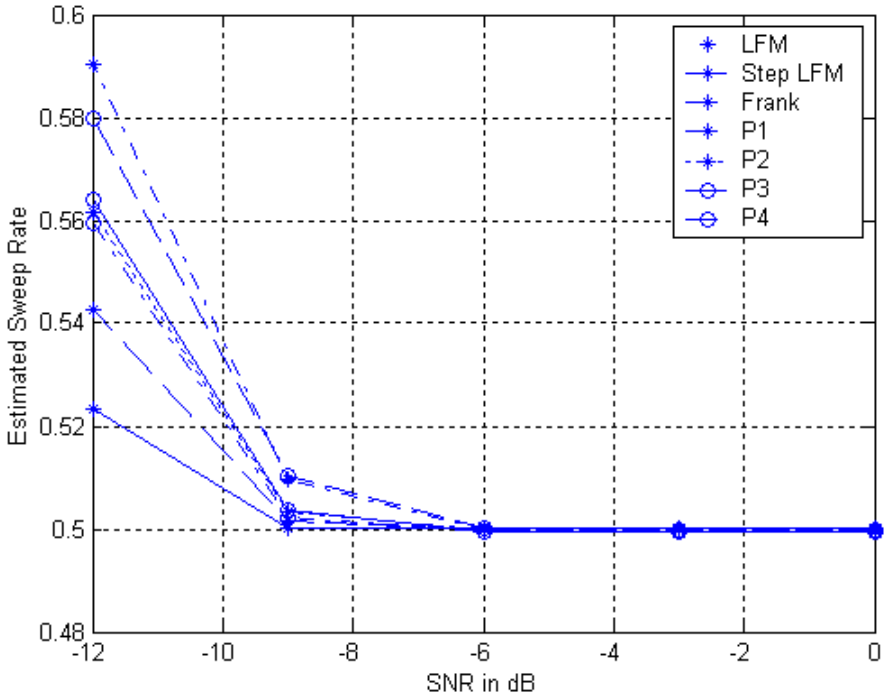

Figure 4.17: Sweep rate estimation at different SNR values.

Performance of the estimator for different sample size values, 64, 256 and 1024, and at different SNR values, 0, -3, -6, -9, -12 dB, is also simulated. 500 Monte Carlo runs were carried out to estimate the sweep rate and 500 grid points were taken for the sweep rate in the range of [0,1] .

In Figure 4.18 through 4.27, the mean square error (MSE) and the estimated sweep rate are plotted for SNR values of 0, -3, -6, -9, -12 dB. It can be seen that as the sample size increases the MSE value of the estimator decreases linearly and the estimates of the sweep rate approach to the correct value. The best performance is attained with the LFM signal. Then, the step LFM, P4, P2, P1, Frank and P3 codes come in decreasing order. This performance loss for the polyphase signals can be attributed to the energy spread in their AF representations.

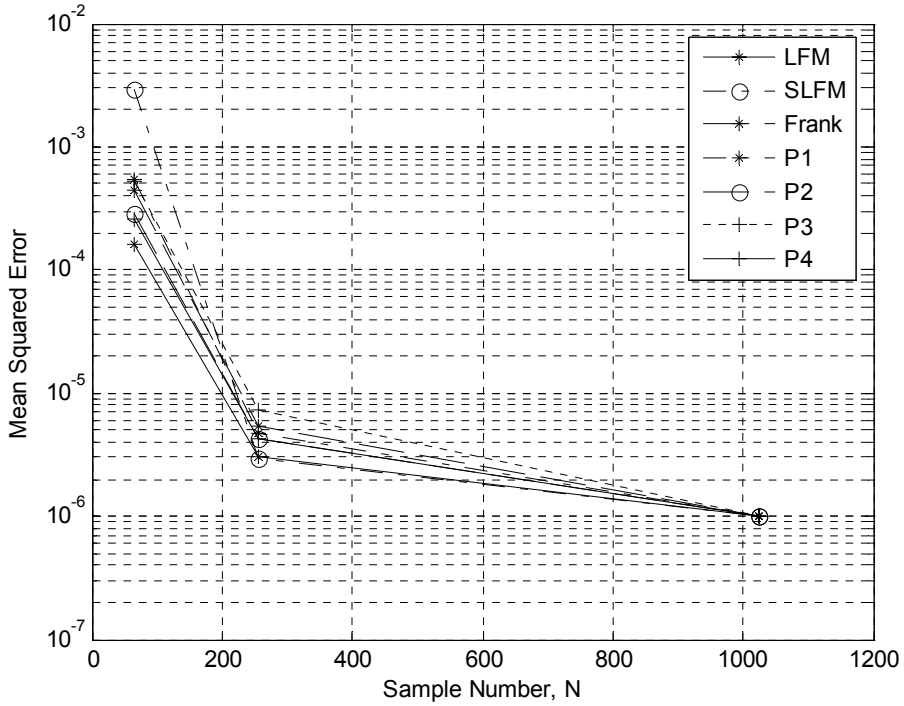

Figure 4.18: MSE for different sample sizes (SNR = 0 dB).

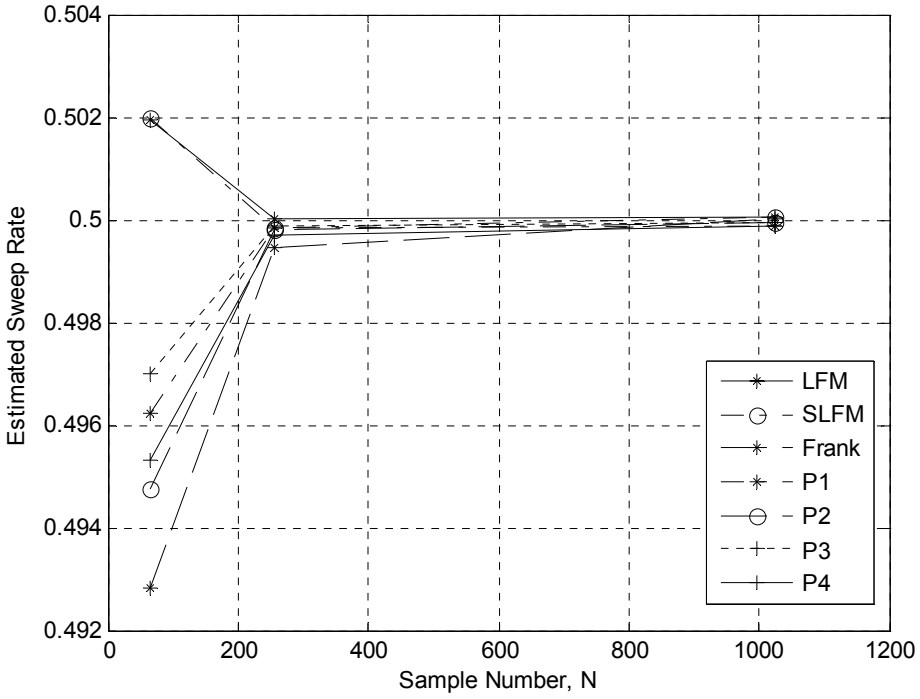

Figure 4.19: Estimated sweep rate for different sample sizes (SNR=0 dB).

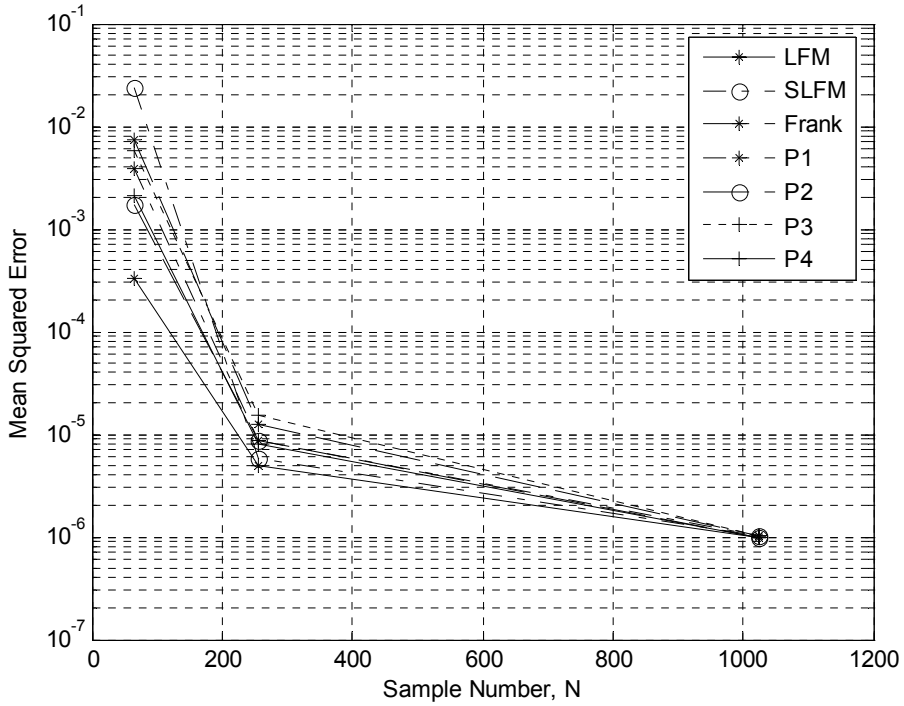

Figure 4.20: MSE for different sample sizes (SNR = -3 dB).

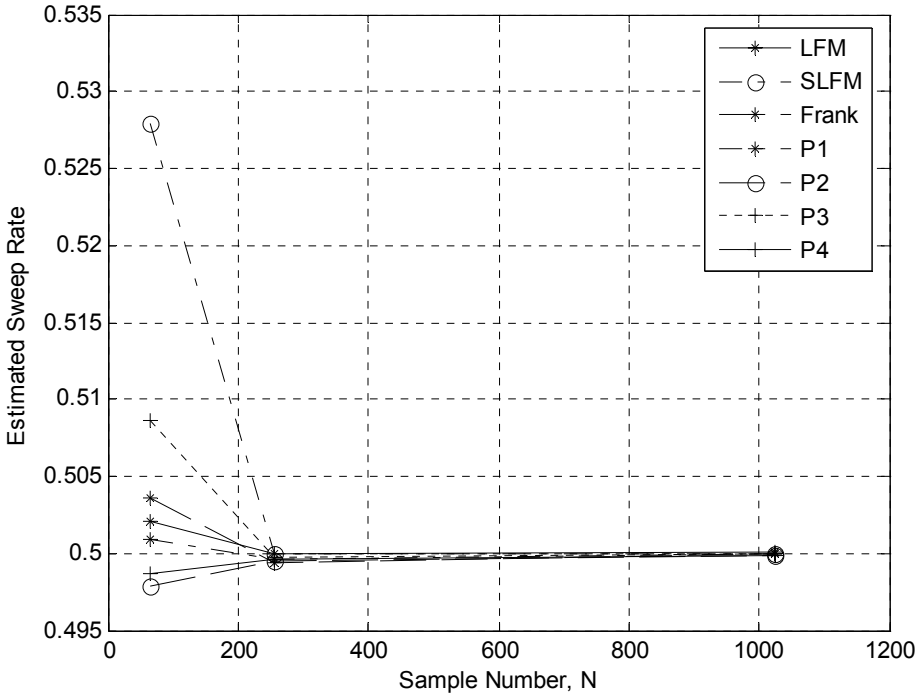

Figure 4.21: Estimated sweep rate for different sample sizes (SNR=-3 dB).

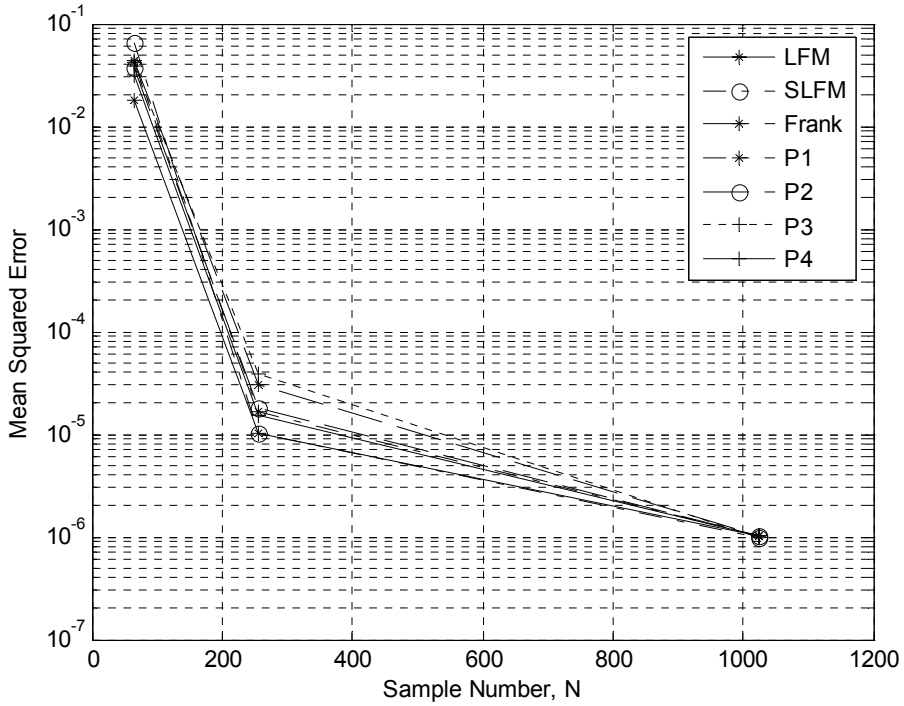

Figure 4.22: MSE for different sample sizes (SNR = -6 dB).

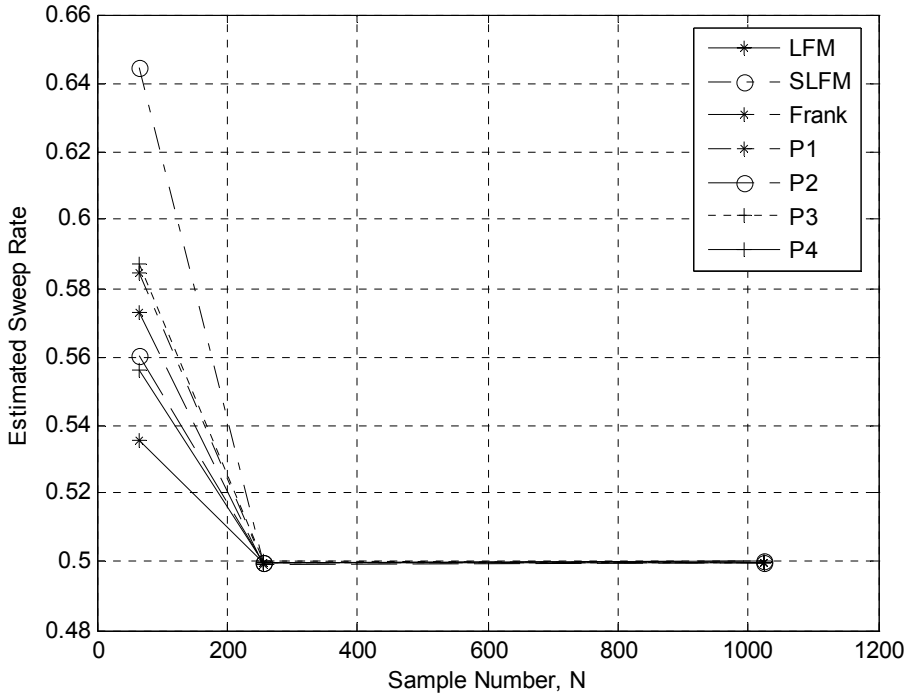

Figure 4.23: Estimated sweep rate for different sample sizes (SNR=-6 dB).

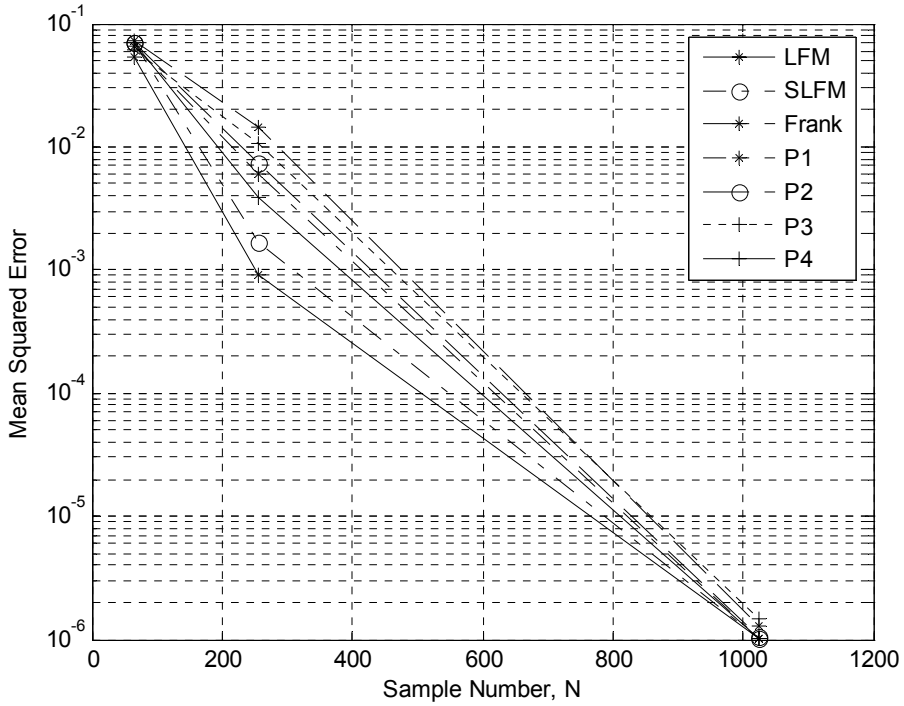

Figure 4.24: MSE for different sample sizes (SNR = -9 dB).

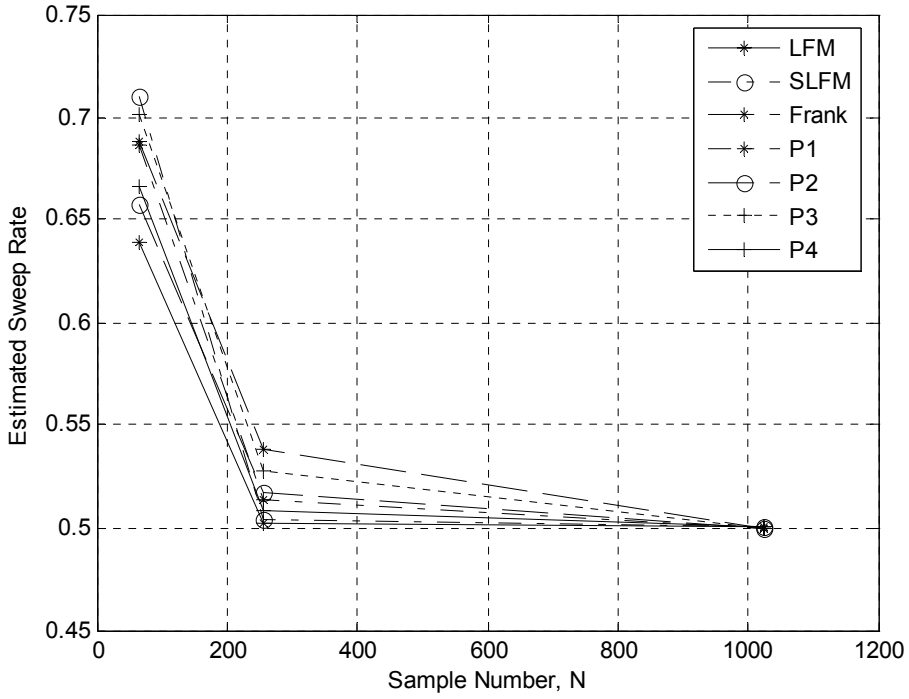

Figure 4.25: Estimated sweep rate for different sample sizes (SNR=-9 dB).

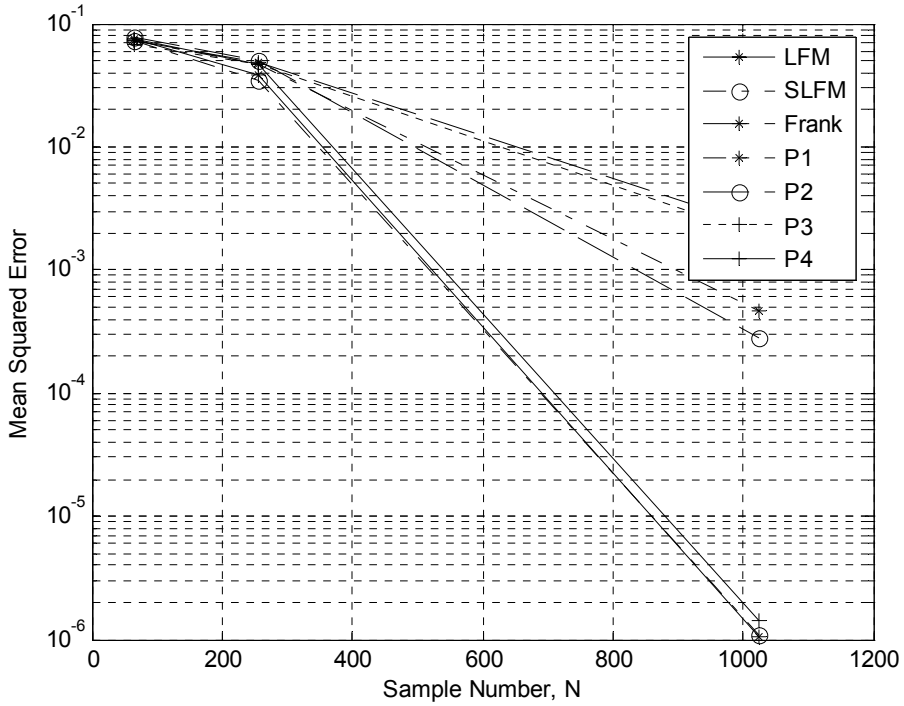

Figure 4.26: MSE for different sample sizes (SNR = -12 dB).

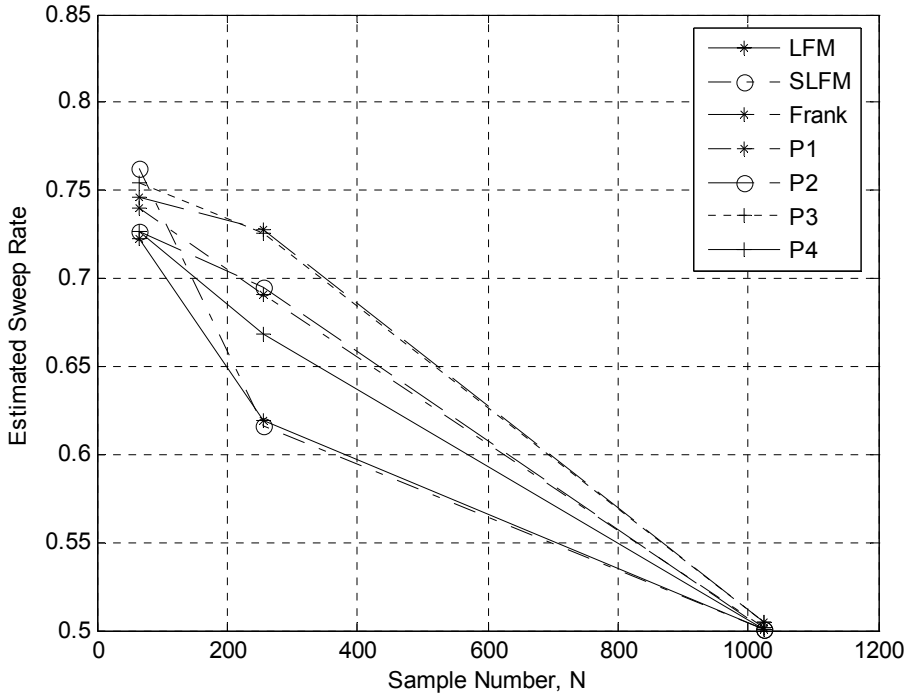

Figure 4.27: Estimated sweep rate for different sample sizes (SNR=-12 dB).

4.4 Maximization of the Fractional Autocorrelation Function for the LFM Signals

It is known that the AF of an LFM signal is a line which goes through the origin of the ambiguity plane. The maximum value of our detection statistic, $\overset{v}{L}(m)$, given in (4.12) usually occurs at the correct sweep rate of the LFM signal. This is because when the sweep rate of the LFM is matched to the calculation angle of the detection statistic, the detection statistic calculates the integral of the line passing through the origin of the AF plane. It is shown in Appendix A.3 that this peak value that occurs at the matched angle is dependent on the amplitude value A, time duration T, and the sweep rate, m, of the LFM signal in the ambiguity plane. This peak value is found in Appendix A.3 as

$$\overset{v}{L}(m = m_o) = \frac{AT}{2\cos\phi}. \tag{4.18}$$

The detection statistics in Figure 4.28 calculated for LFM signals having the same amplitude and time duration but different sweep rate values of 0.4, 0.6 and 0.8 show that as the angle increases the peak value of the detection statistic also increases slightly as a result of the $\cos\phi$ term in the denominator of (4.18).

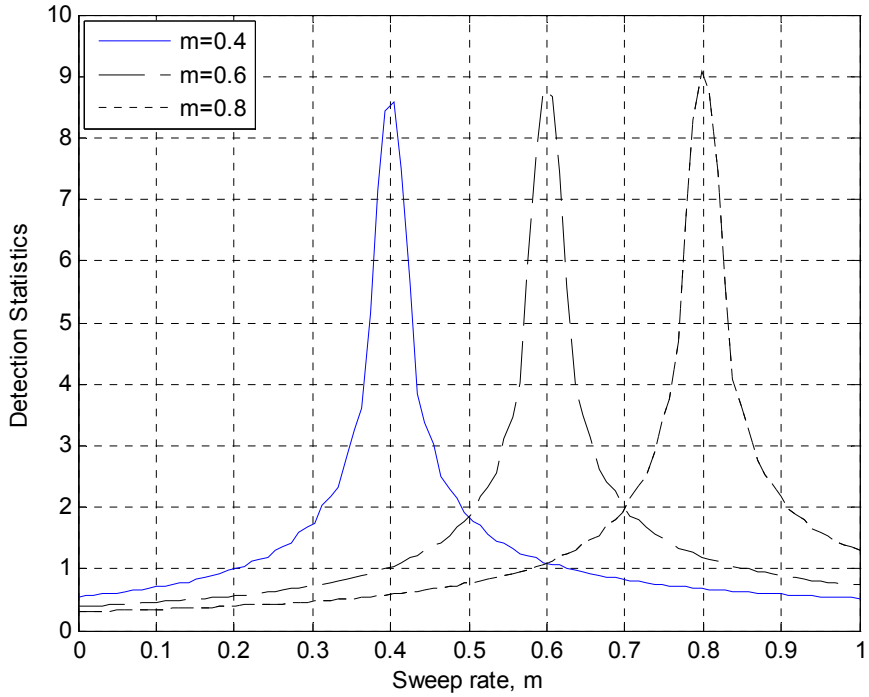

Figure 4.28: Detection statistics for LFM signals at different sweep rates.

CHAPTER FIVE

USE OF FRACTIONAL CROSS – CORRELATION IN RANGE ESTIMATION

In this chapter, we extend the use of fractional cross – correlation in radar signal processing for range estimation employing the LFM and polyphase coded signals. Range estimation via fractional cross – correlation for the LFM signal is studied before (Akay, 2003). Here, we extend this work for polyphase coded signals. Through simulations, we compare the performance of fractional cross – correlation with the performance of the conventional LTI cross – correlation.

5.1 Delay Estimation for One Target

Calculation of fractional cross – correlation for a rectangular pulse at different angles is studied before (Akay, 2001). The use of fractional cross – correlation for delay estimation employing the LFM signal was proposed and a simulation example for only one realization was given (Akay, 2001), (Akay, 2003). Here, we extend these works for multiple realizations via Monte Carlo simulations.

In the simulations, we created the LFM signal in (3.32) digitally. The sweep rate is taken as 0.5. The discrete sequence for the transmitted waveform is denoted as $x[k]$. The received signal sequence can be expressed as

$$y[k] = \alpha x[k-D] + w[k] \tag{5.1}$$

where α is an attenuation factor and D represents the round – trip delay. The received signal is corrupted by additive white Gaussian noise (WGN) denoted by $w[k]$. For simplicity of analysis, we use the attenuation factor $\alpha = 1$.

In simulations, we generate $w[k]$ as complex white Gaussian noise with SNR values of -12 dB. The number of samples for discrete LFM signal is 512 and the

round trip delay is set as $D = 100$. 1000 Monte Carlo simulations are performed and the results are presented as the mean of individual simulations.

In the following figures, the top subplots show the result of conventional cross – correlation, and the results obtained using fractional cross – correlation are plotted at the bottom subplots.

The horizontal axis of fractional cross – correlation is normalized as $\frac{k}{\sin[\arctan(\mu)]}$ in order to make the fractional axis, r, comparable with the time axis, t. The normalization factor is equal to sine of the arctangent of the sweep rate, μ. This is dictated by the angle parameter ϕ of the fractional cross – correlation operation. This axis arrangement must be performed whenever a fractional cross – correlation is used to determine the amount of the time delay correctly. In calculation of fractional cross – correlation, selection of the angle parameter ϕ is critical. To match the angle of fractional cross – correlation with the sweep rate of the LFM signal, we assigned the angle value as $\phi = \arctan(\mu)$.

In Figure 5.1, the simulation results are plotted for $SNR = -12 \ \ dB$. It is seen that the conventional cross – correlation produces a peak at the correct delay value of 100. The peak is also visible at the correct delay value using the fractional cross – correlation but with a lower peak value.

We expected that fractional cross – correlation should produce a higher peak value than the conventional cross – correlation since the angle parameter of the fractional cross – correlation matches with the sweep rate of the LFM signal. But since we estimate the sweep rate parameter before taking the fractional cross – correlation operation, performance loss as compared with the regular cross – correlation operation is occured. Similar results can be observed in the simulation examples performed using step LFM, Frank, P1, P2, P3 and P4 codes. This kind of estimation can be used in passive radar applications.

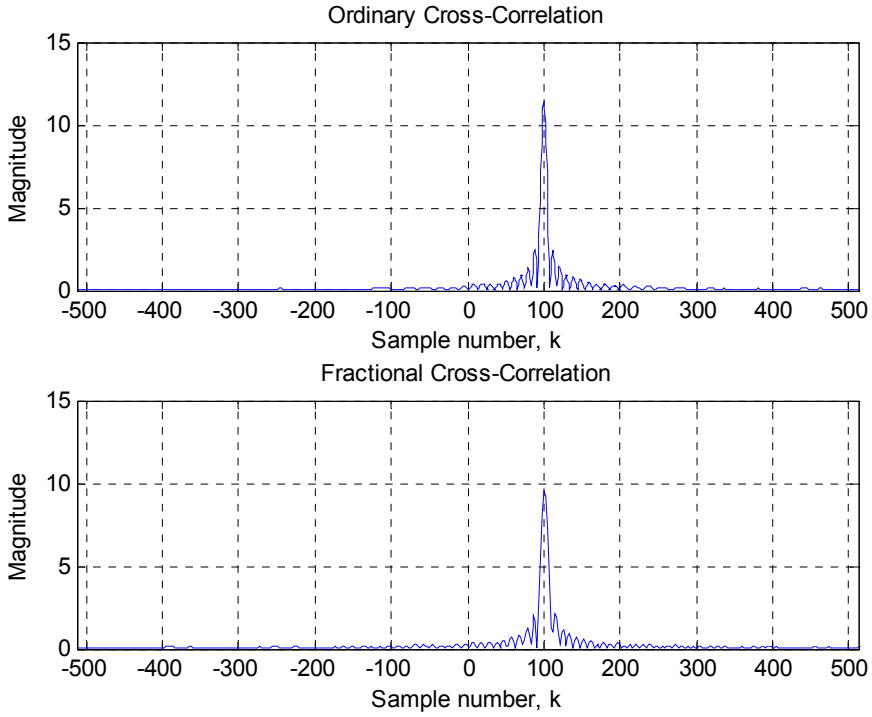

Figure 5.1: Comparison of conventional and fractional cross – correlations for LFM signal delay estimation (SNR = -12 dB).

If we assume that we know the sweep rates of the transmitted and received signals , then there is no need to estimate the sweep rate parameter. Thus, if we perform this simulation for known sweep rate for both transmitted and received LFM signals, then performance of both operations are nearly similar. The simulation result for the LFM signal with sweep rate 0.5, $SNR = -12$ and delay value of 100 is shown in Figure 5.2. In simulations, 500 Monte Carlo runs were carried out.

The fractional cross – correlation method is extended here to estimate the range information of a target by using the step LFM signal as the transmitted pulse. In Figure 5.3, the results obtained for $SNR = -12$ dB are plotted using the conventional and fractional cross – correlation. Both methods correctly estimate the true range delay value but the conventional cross – correlation produces a visibly larger peak than the fractional cross – correlation.

In Figures 5.4 through 5.8 the simulations for SNR value of -12 dB with a delay value of $D = 100$ are performed using the Frank, P1, P2, P3 and P4 codes, respectively, as the transmitted pulse. It can be seen that fractional – cross correlation produces a peak at the correct range value, but the peak value found using the conventional cross – correlation is larger.

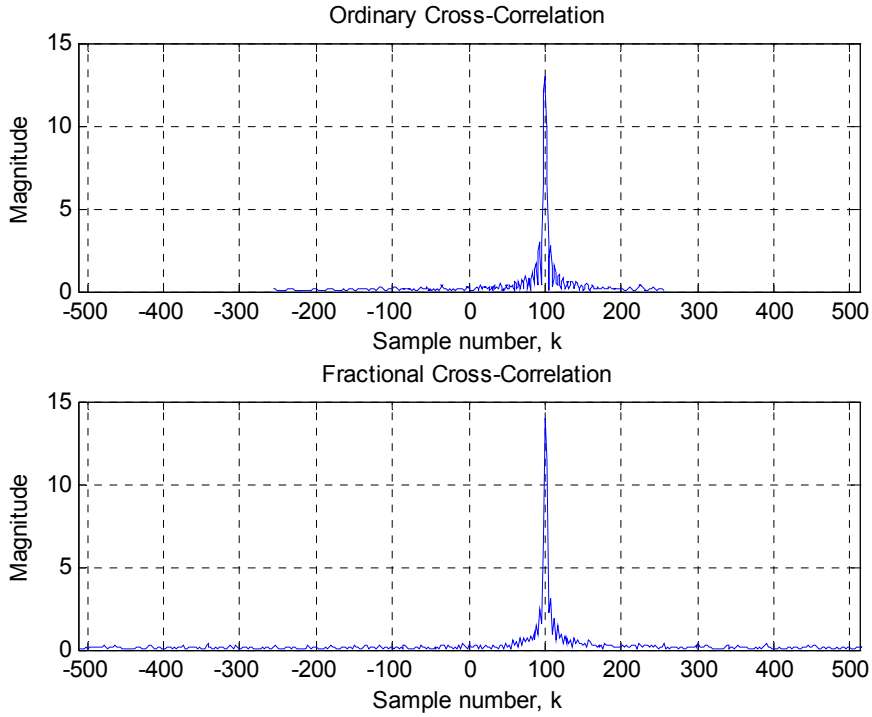

Figure 5.2: Comparison of conventional and fractional cross – correlations for LFM signal delay estimation with known sweep rate (SNR = -12 dB).

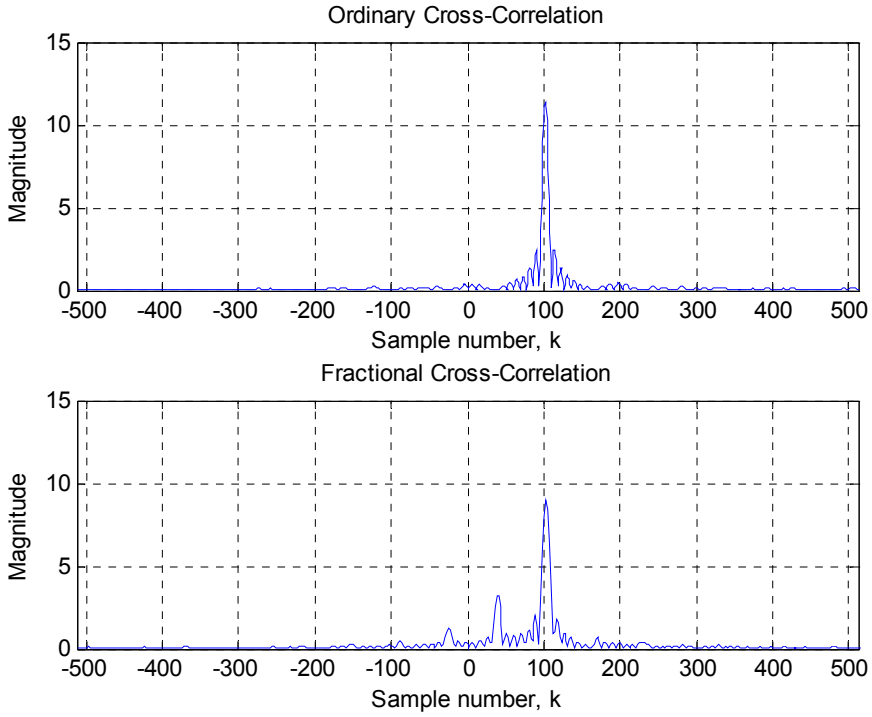

Figure 5.3: Comparison of conventional and fractional cross – correlations for step LFM signal delay estimation (SNR = -12 dB).

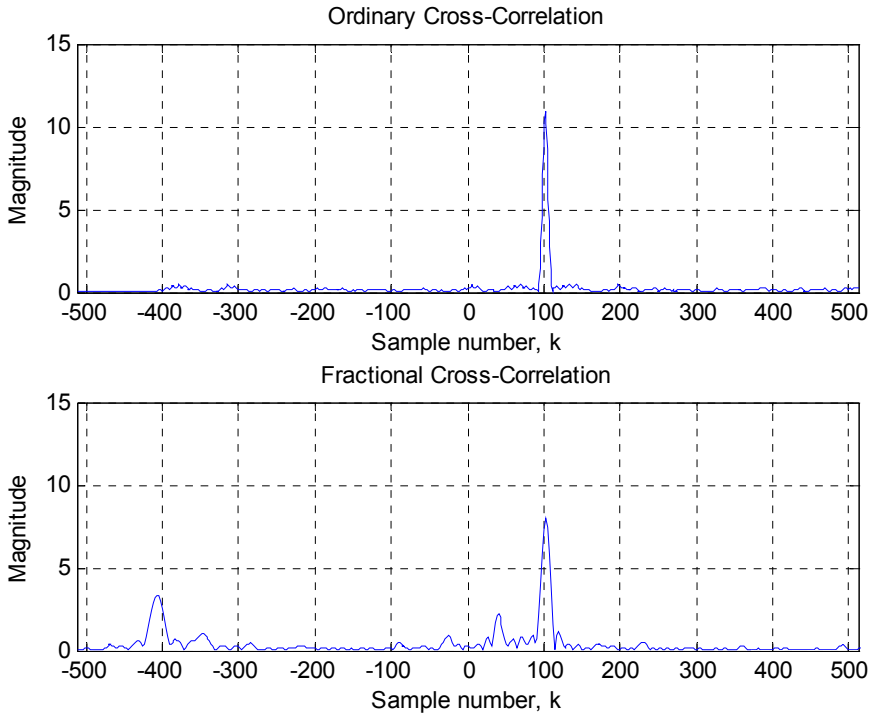

Figure 5.4: Comparison of conventional and fractional cross – correlations for the Frank code delay estimation (SNR = -12 dB).

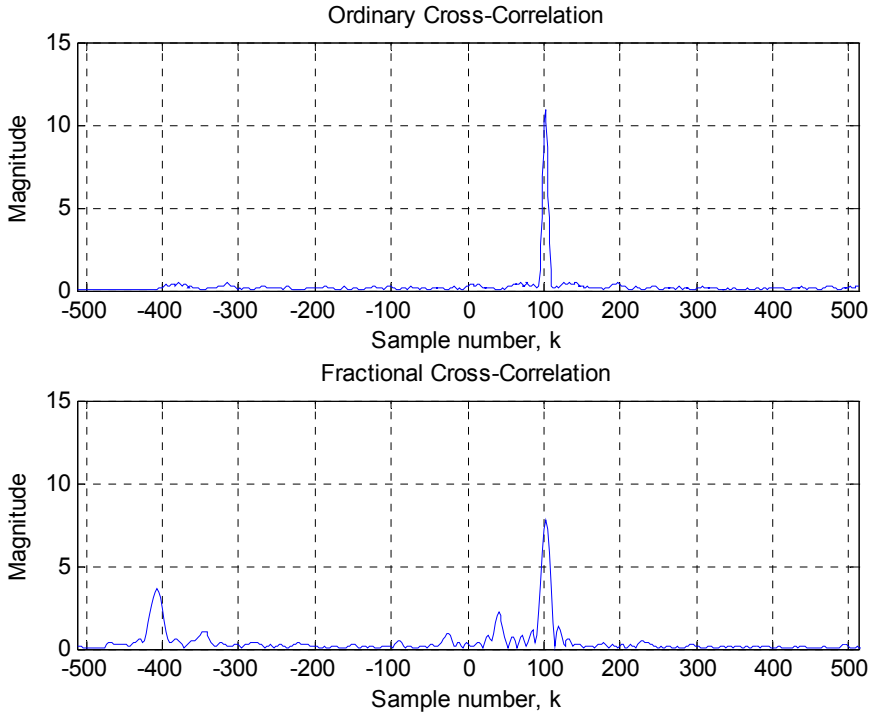

Figure 5.5: Comparison of conventional and fractional cross – correlations for the P1 code delay estimation (SNR = -12 dB).

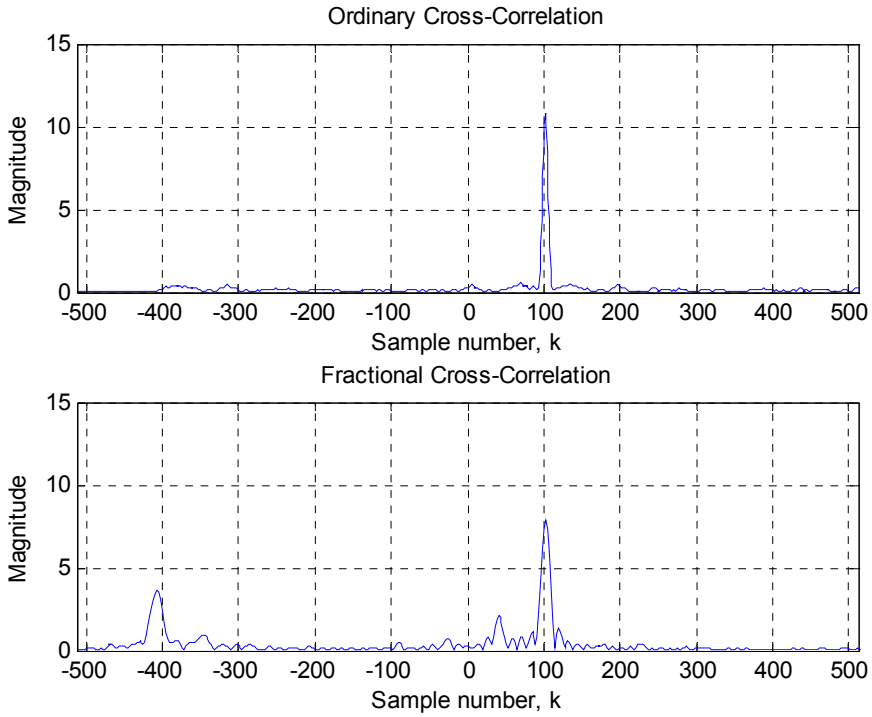

Figure 5.6: Comparison of conventional and fractional cross – correlations for the P2 code delay estimation (SNR = -12 dB).

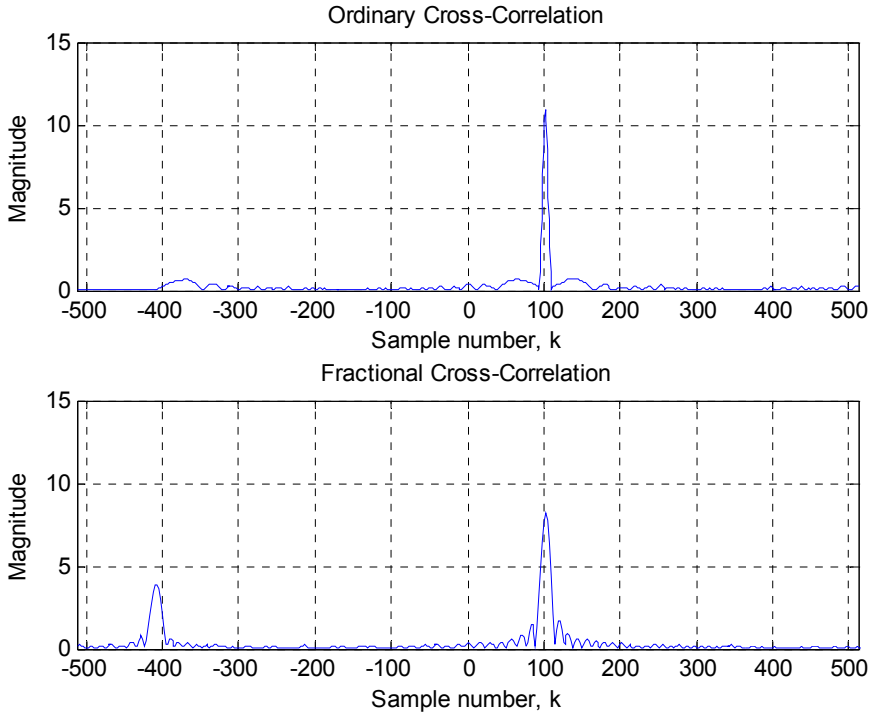

Figure 5.7: Comparison of conventional and fractional cross – correlations for the P3 code delay estimation (SNR = -12 dB).

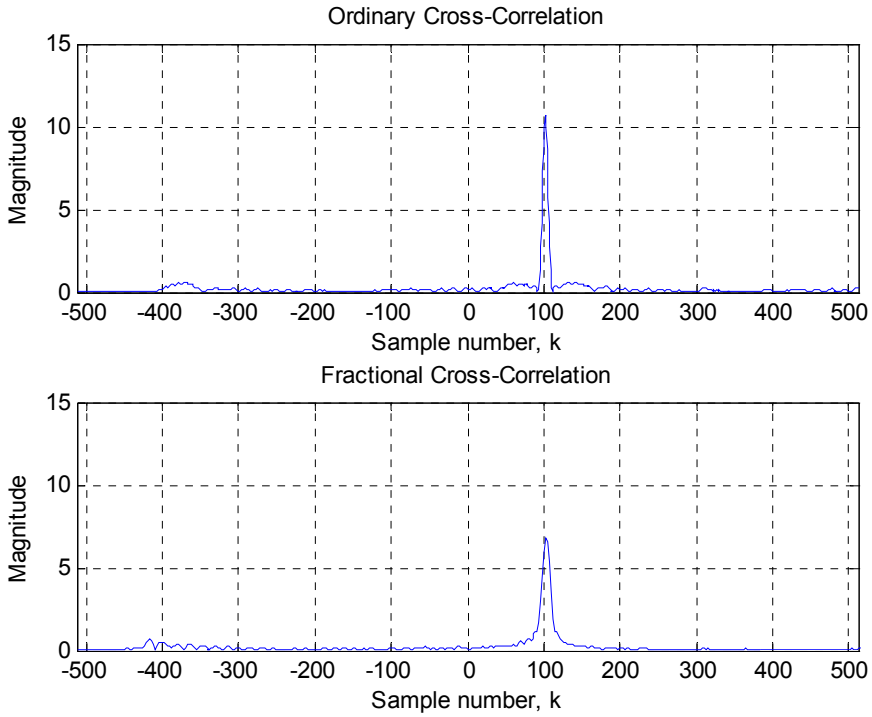

Figure 5.8: Comparison of conventional and fractional cross – correlations for the P4 code delay estimation (SNR = -12 dB).

5.2 Delay Estimation for Two Targets

In this section, we simulated our algorithm for the case of two targets. We compare the delay estimation performance of convetional cross – correlation and fractional cross – correlation again for the LFM signal and the step LFM, Frank, P1, P2, P3 and P4 codes. The simulations are performed for two targets; one has a delay of 100 and the other 120. AWGN with -12 dB SNR is added to the signals which have 1024 samples. In simulations, 500 Monte Carlo runs are performed. The simulation results are plotted in Figures 5.9 through 5.15.

It can be seen that both conventional and fractional cross – correlations can resolve the two targets at the correct delays, but similar to the one target case, conventional cross – correlation produces a higher peak value than fractional cross – correlation. In Figure 5.9, we can see that fractional and conventional cross – correlation algorithms produce nearly equal peak values for the LFM signal.

However, for other codes, the peak values found using fractional cross – correlation are lower than the peaks of the conventional cross – correlations. This might be attributed to the fact that the polyphase codes and the step LFM signal suffer from energy spread as demonstrated by their ambiguity function plots.

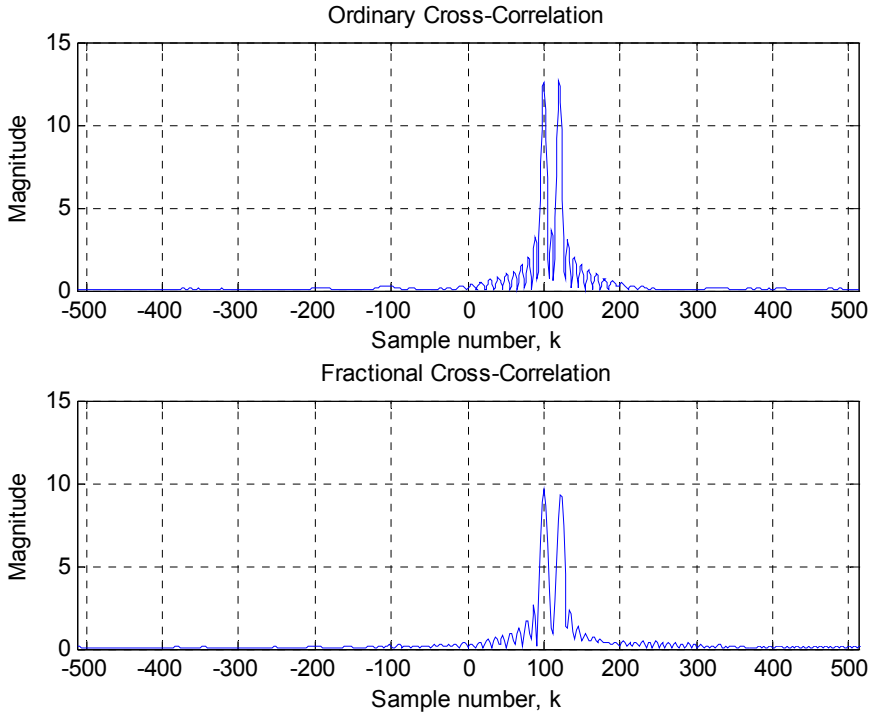

Figure 5.9: Comparison of conventional and fractional cross – correlations using LFM signal for two targets.

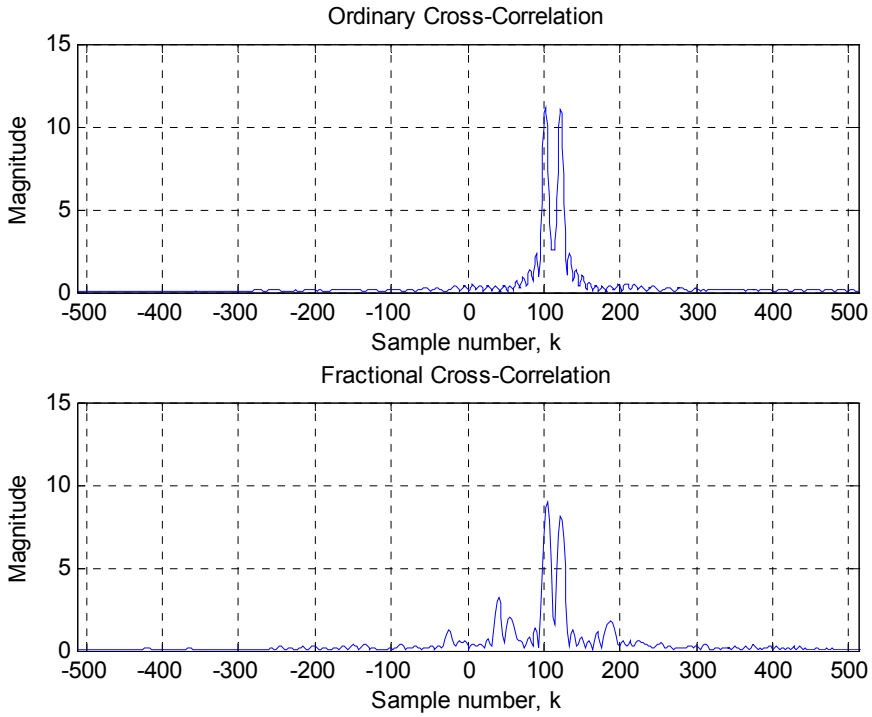

Figure 5.10: Comparison of conventional and fractional cross – correlations using step LFM signal for two targets.

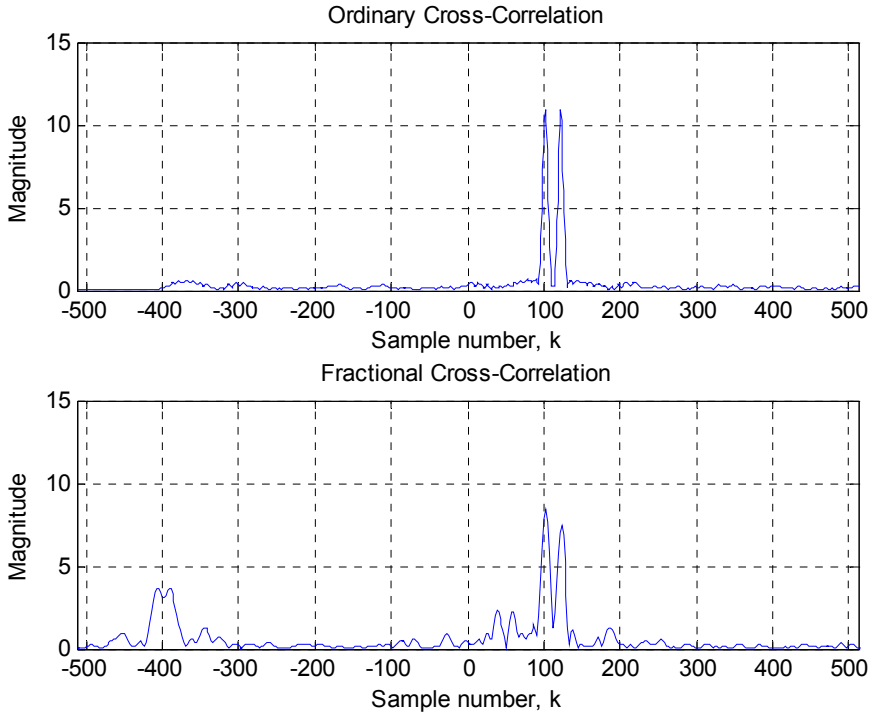

Figure 5.11: Comparison of conventional and fractional cross – correlations using Frank code for two targets.

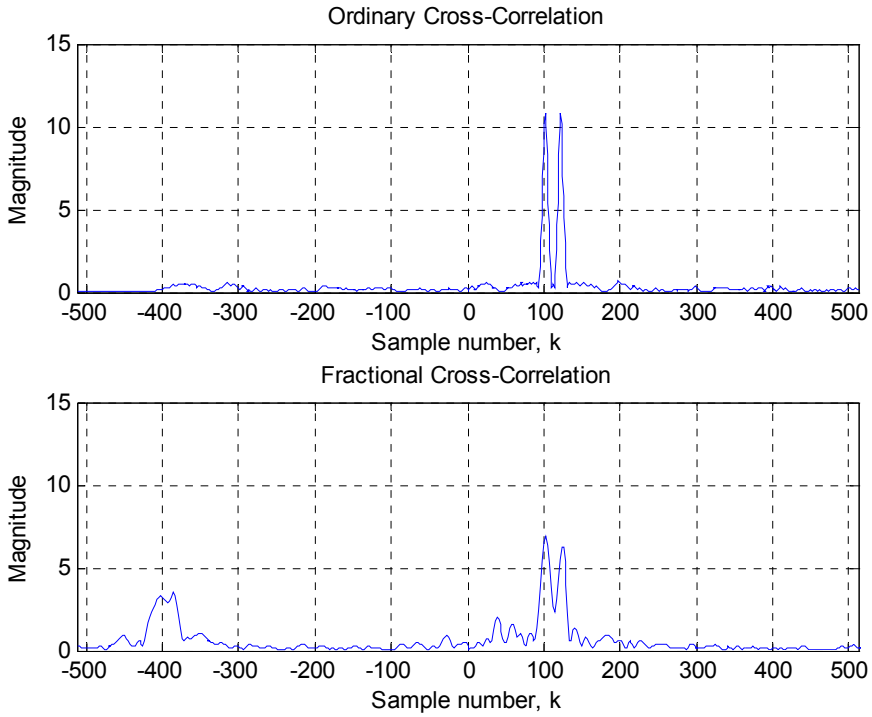

Figure 5.12: Comparison of conventional and fractional cross – correlations using P1 code for two targets.

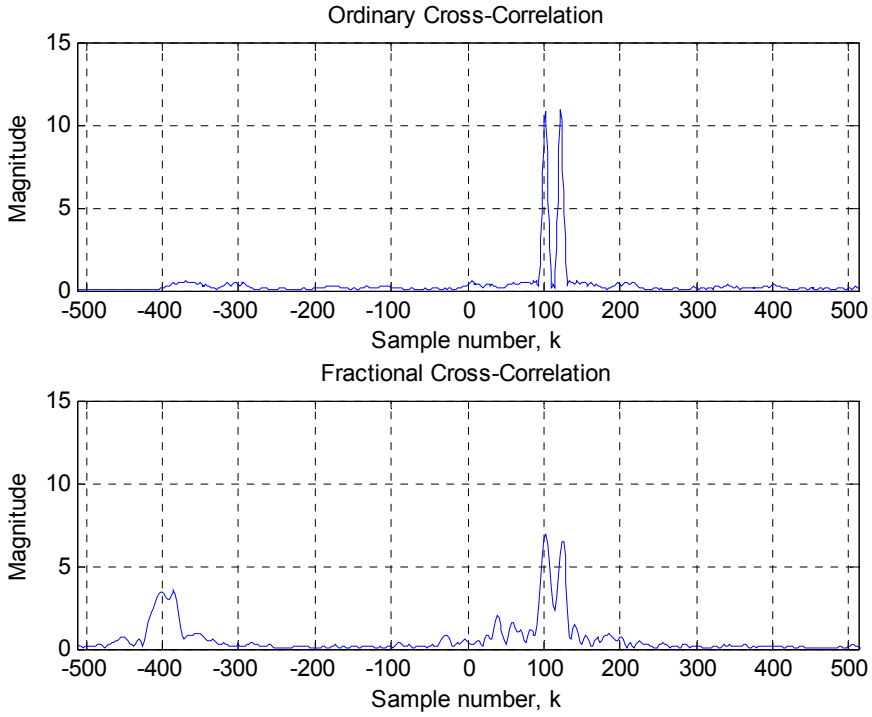

Figure 5.13: Comparison of conventional and fractional cross – correlations using P2 code for two targets.

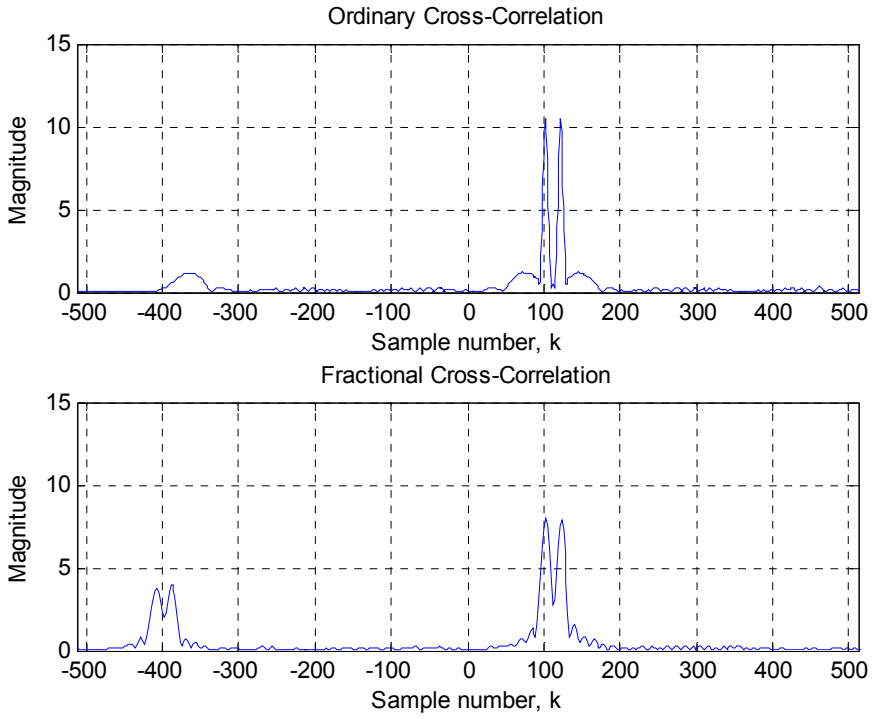

Figure 5.14: Comparison of conventional and fractional cross – correlations using P3 code for two targets.

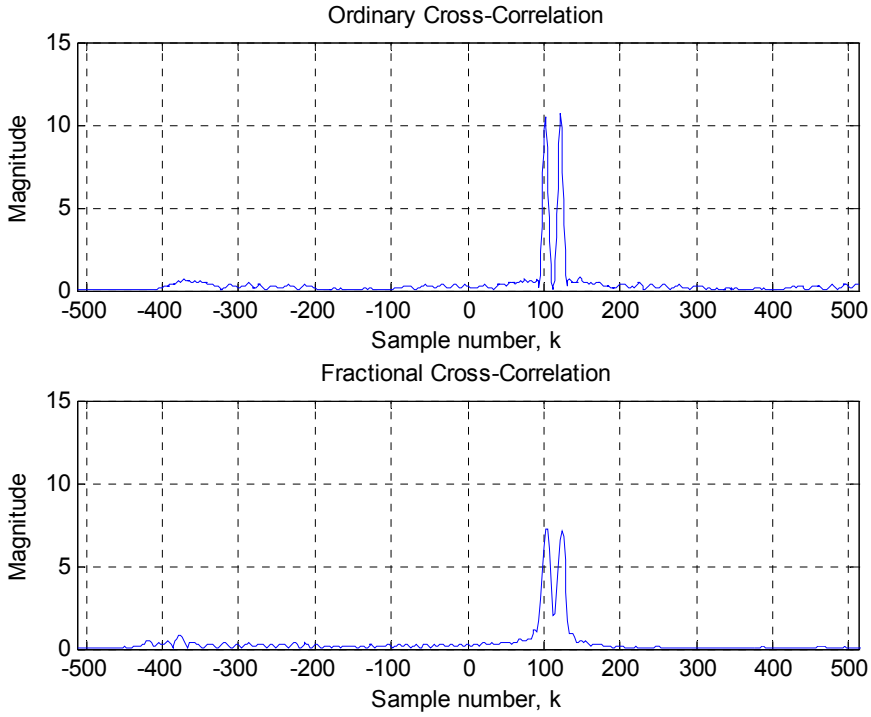

Figure 5.15: Comparison of conventional and fractional cross – correlations using P4 code for two targets.

CHAPTER SIX

CONCLUSIONS

In this thesis, our aim was to investigate the performance of a detection statistic, based on fractional autocorrelation for detection of pulse compression waveforms. To obtaion good range and Doppler accuracy simultaneously, the pulse compression technique is used to ensure the requirements of large bandwidth and time duration. The most commonly used pulse compression waveform in radars is the linear frequency modulated (LFM) signal. The ambiguity function (AF) of any LFM signal is a line going through the origin of the ambiguity plane. The slope of the line is determined by the sweep rate of the LFM signal. This fact helped in proposing a detection statistic for detection and sweep rate parameter estimation of LFM signals (Akay & Boudreaux – Bartels, 2001). Since fractional autocorrelation corresponds to the cuts of the AF along radial lines going through the origin, we could integrate fractional autocorrelations at different angle values and search for a peak value. Observing a strong peak above a threshold level would indicate the presence of an LFM at the specific angle value for which the integration was carried out. The integration angle value corresponds to the slope of the AF of the LFM signal. Therefore, position of the peak directly provides an estimate of the sweep rate of the LFM signal.

Motivated by the fact that the step LFM and the polyphase – coded signals have ambiguity functions involving lines in the ambiguity plane, we can expect to detect these signals using our detector and estimate the sweep rate parameter in the same manner as the LFM.

Performance of the detector was investigated for different pulse compression waveforms at various SNR values. We observed that the detector produces a peak at the correct sweep rate as expected. By determining a suitable threshold value we were able to detect each of these signals. Performance comparison of the detector was also carried out using all the signals at the same SNR value. It is seen that the

highest peak value and the best performance is obtained for the LFM signal. This is because all the energy of the LFM signal is contained in only one linear component that goes through the origin of the ambiguity plane. The peak values for other pulse compression signals are less than the LFM since some of the energy of these signals is spread to secondary lines which are parallel to the main component passing through the origin. The peak values from highest to lowest are ordered as the LFM signal, the step LFM signal, P4 code, P2 code, P1 code, Frank code and the P3 code.

Performance of the detection statistic as a sweep rate estimator was also investigated at different SNR values. It was seen that as the SNR value increased the mean square error (MSE) of the estimator decreased. For various values of sample numbers the detection statistic also behaves expectedly. As the number of samples of the signal is increased the performance of the estimator also increases by producing smaller MSEs.

As a delay parameter estimator, performance of the fractional cross – correlation function was compared with the classical cross – correlation through simulations. It was seen that both methods can estimate the delay correctly. However, the peak amplitude value that occured at the correct delay value was higher for the classical cross – correlation operation. Since our method can estimate the sweep rate parameter of the received signal before calculating the fractional cross – correlation, we can also use this estimator in passive radar applications.

REFERENCES

Akay, O., (Haziran 2003). Kesirli çapraz korelasyonun radar sinyal işlemede kullanılması. *11. Sin. İşl. Uyg. Kur. (SIU 2003)*, 789 – 792.

Akay, O. & Erözden, E. (February 2004). Use of fractional autocorrelation in efficient detection of pulse compression radar signals. *First International Symposium on Control, Communications and Signal Processing, 2004,* 33 – 36.

Akay, O. (2000). *Unitary and Hermitian Fractional Operators and Their Extensions*. Ph. D. Thesis. University of Rhode Island.

Akay, O., & Boudreaux – Bartels, G. F. (December 1998). Unitary and Hermitian fractional operators and their relation to the fractional Fourier transform. *IEEE Signal Processing Letters*, *5*, 312 – 314.

Akay, O. & Boudreaux-Bartels, G. F. (May 2001). Fractional convolution and correlation via operator methods and an application to detection of linear FM signals. *IEEE Trans. on Sig. Proc.*, *49*, 979-992.

Almedia, L. B. (November 1994). The fractional Fourier transform and time – frequency representations. *IEEE Trans. on Sig. Proc.*, *42*, 3084-3091.

Baraniuk R. G. & Jones D. L. (October 1995). Unitary equivalence: A new twist on signal processing. *IEEE Trans. on Sig. Proc.*, *43*, 2269-2282.

Cohen L. (1995) ,*Time – Frequency Analysis*, Englewood Cliffs, NJ, Prentice Hall.

Erözden, E. & Akay, O. (April 2004). Use of fractional autocorrelation for efficient detection and parameter estimation of polyphase-coded radar signals. *Proceedings of the IEEE 12th Signal Processing and Communications Applications Conference, 2004.* 41 – 44.

Frank, R. L. (January 1963). Polyphase codes with good nonperiodic correlation properties. *IEEE Transactions on Information Theory*, *9*, 43-45.

Hlawatsch F. & Boudreaux – Bartels G. F. (April 1992). Linear and quadratic time – frequency signal representations. *IEEE Signal Processing Magazine*, *9*, 21 – 67.

Jennison B. K. (January 2003). Detection of polyphase pulse compression waveforms using the Radon – ambiguity transform. *IEEE Trans. on Aerospace and Electronics*, *39*, 335 – 343.

Kay S. M. (1998), *Fundamentals of Statistical Signal Processing Volume II - Detection Theory*. NJ, Prentice Hall.

Kay S. & Boudreaux – Bartels G. F. (April 1985). On the optimality of the Wigner distribution for detecting a chirp signal. *Proc. IEEE ICASSP*, *10*, 1017 – 1020.

Kingsley S. & Quegan S. (1992), *Understanding Radar Systems*, Cambridge, McGraw Hill.

Kutay M. A., Özaktaş H. M., Arıkan O. & Onural L. (May 1997). Optimal filtering in fractional Fourier domains. *IEEE Trans. on Sig. Proc.*, *45*, 1129-1143.

Levanon N. (1988), *Radar Principles*, NY, John Wiley and Sons.

Lewis B. L., Kretschmer F. F. & Shelton W. W. (1986), *Aspects of Radar Signal Processing*, Artech House.

Li W. (August 1987). Wigner distribution method equivalent to dechirp method for detecting a chirp signal. *IEEE Trans. Acoust., Speech, Signal Processing*, *35*, 1210 – 1211.

Mahafza B. R. (2000), *Radar Systems Analysis and Design Using Matlab*, USA, Chapman & Hall/CRC.

McBride, A. C. & Kerr, F. H. (1987). On Namias' fractional Fourier transforms. *IMA J. Appl. Math.*, *39*, 159-175.

Namias, V. (1980). The fractional order Fourier transform and its application to quantum mechanics. *J. Inst. Math. Appl.*, *25*, 241-265.

Özaktaş H. M., Zalevsky Z. & Kutay M. A. (2000). *The Fractional Fourier Transform with Applications in Optics and Signal Processing*, NY, Wiley.

Özaktaş H. M., Barshan B., Mendlovic D. & Onural L. (February 1994). Convolution, filtering, and multiplexing in fractional Fourier domains and their relationship to chirp and wavelet transforms. *Journal Optical Society of America. 11*, 547 – 559.

Özaktaş H., Arıkan O., Kutay M. A. & Bozdağı G. (September 1996). Digital computation of the fractional Fourier transform. *IEEE Transactions on Signal Processing*, *44*, 2141-2150.

Qian S. & Chen D., (1996), *Joint Time – Frequency Analysis, Methods and Applications*, NJ, Prentice Hall.

Peebles P. Z. (1998), *Radar Principles*, USA, John Wiley & Sons.

Proakis J. G. & Manolakis D. G. (1996), *Digital Signal Processing Principles, Algorithms, and Applications*, NJ, Prentice Hall.

Poularikas, A. D., (2000). *The Transforms and Applications Handbook, (2nd Edition) Electrical Engineering Handbook Series*, CRC Press.

Sayeed A. M. & Jones D. L. (June 1996). Integral transforms covariant to unitary operators and their implications for joint signal representations. *IEEE Trans. on Sig. Proc.*, *44*, 1365-1377.

Wang M., Chan A. K. & Chui C. K. (March 1998). Linear frequency modulated signal detection using Radon - ambiguity transform. *IEEE Trans. on Sig. Proc.*, *46*, 571 – 586.

Wood J. C. & Barry D. T. (November 1994). Radon transformation of time – frequency distributions for analysis of multicomponent signals. *IEEE Trans. Signal Processing*, *42*, 3166-3177.

APPENDIX A

MATHEMATICAL DERIVATIONS

A.1 Performance of the Detection Statistic $\overset{v}{L}(m)$

Performance of a detection statistic can be determined using two different criteria. One of them is the performance SNR measure which is formulated as

$$P(SNR) = \frac{\left| E(\eta \left| H_1 \right.) - E(\eta \left| H_0 \right.) \right|}{\left\{ \frac{1}{2} \left[\text{var}(\eta \left| H_1 \right.) + \text{var}(\eta \left| H_0 \right.) \right] \right\}^{1/2}}, \qquad (A.1.1)$$

where η denotes a detection statistic and H_0 and H_1 represents the noise only hypothesis and the signal plus noise hypothesis, respectively. The values $E(\eta \left| H_i \right.)$ and $\text{var}(\eta \left| H_i \right.)$ denote the expected value and the variance of the detection statistic, η.

The other merit of performance is the output signal to noise ratio (SNR). It is defined as

$$SNR_{out} = \frac{output \quad signal \quad power}{\text{var}(\eta \mid H_1)}, \qquad (A.1.2)$$

which is the ratio between the output signal power and the output noise power (Wang, et al., 1998).

Using (A.1.1) and (A.1.2), we can determine the performance of our detection statistic given in (4.12) which is rewritten below;

$$\overset{v}{L}(m) = \frac{\int \left| (s \star_{\arctan(m)} s)(\rho) \right| d\rho}{\int \left| s(t) \right| dt}. \qquad (A.1.3)$$

To calculate the performance of the detection statistic $\overset{v}{L}(m)$ using (A.1.1) and (A.1.2), we must first determine the expected value and variance values. The quantities, which must be calculated, are

$$E(\overset{v}{L}(m); H_0), \tag{A.1.4}$$

$$E(\overset{v}{L}(m); H_1), \tag{A.1.5}$$

$$\text{var}(\overset{v}{L}(m); H_0), \tag{A.1.6}$$

$$\text{var}(\overset{v}{L}(m); H_1). \tag{A.1.7}$$

These quantities can be calculated more easily using the relationship given in (4.11) as,

$$\overset{v}{L}(m) = \left|\sqrt{1+m^2}\right| D(m). \tag{A.1.8}$$

The expected value of the detection statistic $\overset{v}{L}(m)$ for hypothesis H_0 can be calculated as

$$E\left(\overset{v}{L}(m); H_0\right) = E\left(\left|\sqrt{1+m^2}\right| D(m); H_0\right) = \left|\sqrt{1+m^2}\right| E\left(D(m); H_0\right)$$
$$= \left|\sqrt{1+m^2}\right| (N_0) = \frac{N_0}{\left|\cos(\phi)\right|}, \tag{A.1.9}$$

where $\sqrt{1+m^2} = \dfrac{1}{\cos\phi}$ (Akay, 2000) and $E(D(m); H_1) = N_0$ which is the constant power spectral density of additive white Gaussian noise (Wang, et. al., 1998).

For hypothesis H_1, the expected value of $\overset{v}{L}(m)$ is found as

$$E\left(\overset{v}{L}(m); H_1\right) = E\left(\left|\sqrt{1+m^2}\right| D(m); H_1\right) = \left|\sqrt{1+m^2}\right| E\left(D(m); H_1\right)$$
$$= \left|\sqrt{1+m^2}\right| (\boldsymbol{\mathcal{E}} + N_0) = \frac{\boldsymbol{\mathcal{E}} + N_0}{\left|\cos(\phi)\right|}, \tag{A.1.10}$$

where $\boldsymbol{\mathcal{E}}$ is the energy of the signal. N_0 is the constant power spectral density of additive white Gaussian noise and $E(D(m); H_1) = \boldsymbol{\mathcal{E}} + N_0$ (Wang, et. al., 1998).

Variance values of the detection statistic $\overset{v}{L}(m)$ for hypothesis H_0 and H_1 are also derived below.

$$\text{var}\left(\overset{v}{L}(m);H_0\right)=\text{var}\left(\left|\sqrt{1+m^2}\right|D(m);H_0\right)=\left(\left|\sqrt{1+m^2}\right|\right)^2\text{var}\left(D(m);H_0\right)$$

$$=\left(1+m^2\right)N_0^2=\frac{N_0^2}{\cos^2(\phi)}, \qquad (A.1.11)$$

where $\text{var}\left(D(m);H_0\right)=N_0^2$ (Wang et. al., 1998).

$$\text{var}\left(\overset{v}{L}(m);H_1\right)=\text{var}\left(\left|\sqrt{1+m^2}\right|D(m);H_1\right)=\left(\left|\sqrt{1+m^2}\right|\right)^2\text{var}\left(D(m);H_1\right)$$

$$=\left(1+m^2\right)(2\mathcal{E}N_0+N_0^2)=\frac{(2\mathcal{E}N_0+N_0^2)^2}{\cos^2(\phi)}, \qquad (A.1.12)$$

where $\text{var}(D(m);H_1)=(2\mathcal{E}N_0+N_0^2)^2$ (Wang et. al., 1998).

Using the results in (A.1.9) through (A.1.12) with (A.1.1) and (A.1.2), the performance SNR and the output SNR of our detection statistic given in (A.1.8) can be found as

$$P(SNR)=\frac{\left|\mathcal{E}\big/\left|\cos\phi\right|\right|}{\left\{\frac{1}{2}\left[\frac{2\mathcal{E}N_0+N_0^2}{\cos^2\phi}\right]\right\}^{1/2}}=\frac{\mathcal{E}}{\sqrt{\mathcal{E}N_0+N_0^2}}, \qquad (A.1.13)$$

$$SNR_{out}=\frac{\mathcal{E}^2}{\left(\frac{2\mathcal{E}N_0+N_0^2}{\cos^2\phi}\right)}=\frac{\left(\left(\frac{\mathcal{E}}{N_0}\right)^2\cos^2\phi\right)}{\left(\frac{2\mathcal{E}}{N_0}+1\right)}=\cos^2\phi\left(\frac{\left(\frac{\mathcal{E}}{N_0}\right)^2}{\frac{2\mathcal{E}}{N_0}+1}\right). \qquad (A.1.14)$$

A.2 Calculation of Fractional Autocorrelation for the LFM Signal

The fractional autocorrelation function of a signal $s(t)$ at an angle ϕ is calculated as

$$(s \star_{\phi} s)(\rho) = \exp\{j\pi\rho^2 \cos\phi \sin\phi\} \int s(\beta) s^*(\beta - \rho\cos\phi) \exp\{-j2\pi\beta\rho\sin\phi\}\, dt, \qquad (A.2.1)$$

which was also given in (2.40).

Thus, to calculate fractional autocorrelation of a signal $s(t)$, we first shift it by $\rho\cos\phi$ and conjugate the result and then multiply these two signals. Finally, the integration in (A.2.1) is carried out.

Here, we use an LFM signal denoted by $s(t)$. An LFM (chirp) signal is defined as,

$$s(t) = A\exp\left\{j\left(2\pi f_0 t + \frac{m_o t^2}{2}\right)\right\} rect\left(\frac{t}{T}\right), \qquad |t| \le \frac{T}{2}. \qquad (A.2.2)$$

If we delay this LFM signal by an amount of $\rho\cos\phi$, we obtain,

$$s(t-\rho\cos\phi) = A\exp\left\{j\left[2\pi f_0 (t-\rho\cos\phi) + \frac{m_o (t-\rho\cos\phi)^2}{2}\right]\right\} rect\left(\frac{t-\rho\cos\phi}{T}\right), \qquad |t-\rho\cos\phi| \le \frac{T}{2}. \qquad (A.2.3)$$

After taking the complex conjugate of (A.2.3) and performing some simplifications, we finally reach at

$$s^*(t-\rho\cos\phi) = A\exp\left\{-j2\pi f_0 t + j2\pi f_0 \rho\cos\phi - j\frac{m_o t^2}{2} + j m_o t\rho\cos\phi - j\frac{m_o \rho^2 \cos^2\phi}{2}\right\} rect\left(\frac{t-\rho\cos\phi}{T}\right), \qquad |t-\rho\cos\phi| \le \frac{T}{2}. \qquad (A.2.4)$$

The envelope of these two signals $s(t)$ and $s(t-\rho\cos\phi)$ can be seen in Figure A.1 and Figure A.2, respectively.

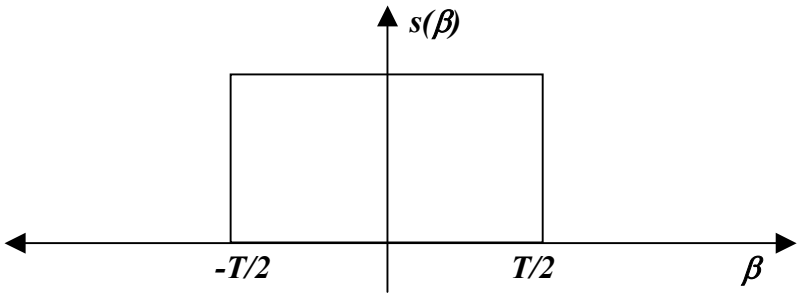

Figure A.1: The envelope of *s(β)*.

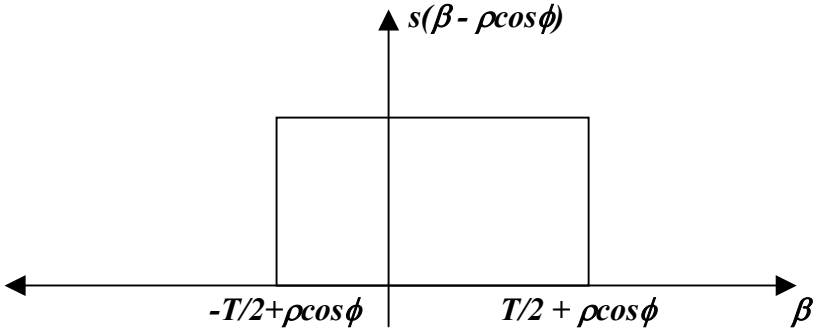

Figure A.2: The envelope of *s(β-ρcosϕ)*.

We can now calculate fractional autocorrelation for the chirp signal using (A.2.1). We have to consider the following four cases for the calculations:

Case I: *s(β)* and *s(β-ρcosϕ)* do not overlap: $T/2+\rho\cos\phi < -T/2$ *OR* $\rho\cos\phi < -T$

Case II: *s(β)* and *s(β-ρcosϕ)* overlap: $-T/2 \le T/2+\rho\cos\phi \le T/2$ OR $-T \le \rho\cos\phi \le 0$

Case III: *s(β)* and *s(β-ρcosϕ)* overlap: $-T/2 \le -T/2+\rho\cos\phi \le T/2$ OR $0 \le \rho\cos\phi \le T$

Case IV: *s(β)* and *s(β-ρcosϕ)* do not overlap: $T/2 < -T/2+\rho\cos\phi$ OR $\rho\cos\phi > T$

Calculations are need to be performed only for Case II and Case III, since Case I and Case IV result in zero due to nonoverlapping rectangular regions.

For Case II:

The limits are given as

$-T/2 \le T/2+\rho\cos\phi \le T/2$.

For ρ; $-T/\cos\phi \le \rho \le 0$ (the delay is negative),

For β; $-T/2 \le \beta \le T/2+\rho\cos\phi$.

For Case III:

The limits are given as

$-T/2 \le T/2+\rho\cos\phi \le T/2$.

For ρ, $0 \le \rho \le T/\cos\phi$ (the delay is positive),

For β, $-T/2 +\rho\cos\phi \le \beta \le T/2$.

Using (A.2.1), (A.2.2) and (A.2.4), we can calculate fractional autocorrelation of the LFM signal. Then, using this function and the limits above given for Case II and Case III, we can compute the desired fractional autocorrelations.

$$(s \star_\phi s)(\rho) = \exp\left\{j\pi\rho^2 \cos\phi \sin\phi\right\} \int A \exp\left\{j2\pi f_0\beta + j\frac{m_o\beta^2}{2}\right\} rect\left(\frac{\beta}{T}\right)$$
$$A \exp\left\{-j2\pi f_0\beta + j2\pi f_0\rho\cos\phi - j\frac{m_o\beta^2}{2} + jm_o\beta\rho\cos\phi - j\frac{m_o\rho^2\cos^2\phi}{2}\right\}$$
$$rect\left(\frac{\beta-\rho\cos\phi}{T}\right) \exp\left\{-j2\pi\beta\rho\sin\phi\right\} d\beta. \qquad (A.2.5)$$

After cancelling some terms and taking the terms independent of β outside of the integral; we reach at,

$$(s \star_\phi s)(\rho) = A^2 \exp\left\{j\pi\rho^2 \cos\phi \sin\phi\right\} \exp\left\{j2\pi f_0\rho\cos\phi - j\frac{m_o\rho^2\cos^2\phi}{2}\right\}$$
$$\int \exp\left\{jm_o\beta\rho\cos\phi\right\} \exp\left\{-j2\pi\beta\rho\sin\phi\right\} rect\left(\frac{\beta}{T}\right) rect\left(\frac{\beta-\rho\cos\phi}{T}\right) d\beta. \quad (A.2.6)$$

Now we can evaluate fractional autocorrelation for Cases II and III given above and we can use these results in the calculation of the peak value of the detection statistic.

A.3 Evaluation of the Peak Amplitude Value of the Detection Statistic

The detection statistic formula is given as

$$\overset{v}{L}(m)=\frac{\int\left|(s\star_{\arctan(m)}s)(\rho)\right|d\rho}{\int|s(t)|\,dt}. \qquad (A.3.1)$$

When we evaluate this statistic at the angle matched with the sweep rate of the LFM signal, that is at $m=m_0$, it produces a peak given as $\overset{v}{L}(m=m_o)$. Since m_0 is the sweep rate of the LFM signal, it can be related to ϕ by

$$m_0=2\pi\tan\phi=2\pi\,(\frac{\sin\phi}{\cos\phi}). \qquad (A.3.2)$$

Here, ϕ is the angle of the line that the support of the LFM signal make with the time axis in the time – frequency plane.

Using the limits of β and ρ given for Case II and Case III, and the sweep rate m_0 in the detection statistic, we can find the maximum value of $\overset{v}{L}(m)$ as

$$\overset{v}{L}(m=m_o)=\frac{\int\left|(s\star_{\arctan(m_o)}s)(\rho)\right|d\rho}{\int|s(t)|\,dt}. \qquad (A.3.3)$$

To find this value, we need to calculate the absolute value of the fractional autocorrelation function in (A.2.6) at the angle $\phi=\arctan(m_0)$. Using (A.2.6) with m_0 replaced by $2\pi\tan\phi=2\pi(\frac{\sin\phi}{\cos\phi})$ and taking the absolute value, we obtain

$$\left|(s\star_{\phi}s)(\rho)\right|=$$
$$A^2\left|\int\exp\left\{j2\pi\frac{\sin\phi}{\cos\phi}\beta\rho\cos\phi\right\}\exp\{-j2\pi\beta\rho\sin\phi\}\,rect\left(\frac{\beta}{T}\right)rect\left(\frac{\beta-\rho\cos\phi}{T}\right)d\beta\right|. \qquad (A.3.4)$$

After canceling the cosine terms we have

$$\left|(s\star_{\phi} s)(\rho)\right| = A^2\left|\int \exp\{j2\pi\sin\phi\beta\rho\}\exp\{-j2\pi\beta\rho\sin\phi\}\,rect\left(\frac{\beta}{T}\right)rect\left(\frac{\beta-\rho\cos\phi}{T}\right)d\beta\right|. \tag{A.3.5}$$

If we look at (A.3.5) carefully, we can see that the exponential terms in the integral are in the same form but have different signs. Hence, they also cancel each other. Finally, we are left with only the rectangular functions in the integral;

$$\left|(s\star_{\phi} s)(\rho)\right| = A^2\left|\int rect\left(\frac{\beta}{T}\right)rect\left(\frac{\beta-\rho\cos\phi}{T}\right)d\beta\right|. \tag{A.3.6}$$

Now we can use (A.3.6) in (A.3.1) to calculate the peak amplitude value of the detection statistic. Using the limits for β at Case II we can evaluate this integral;

$$\begin{aligned}\left|(s\star_{\phi} s)(\rho)\right| &= A^2\left|\int_{-T/2}^{T/2+\rho\cos\phi} rect\left(\frac{\beta}{T}\right)rect\left(\frac{\beta-\rho\cos\phi}{T}\right)d\beta\right| \\ &= A^2\left|\frac{T}{2}+\rho\cos\phi-(-\frac{T}{2})\right| = A^2(T+\rho\cos\phi).\end{aligned} \tag{A.3.7}$$

Using (A.3.7) in (A.3.3) and the limits for ρ given in Case II, we can calculate the peak amplitude value of the detection statistic as

$$\begin{aligned}\overset{v}{L}(m=m_o) &= \frac{\int_{-T/\cos\phi}^{0} A^2(T+\rho\cos\phi)d\rho}{\int_{-\infty}^{\infty}\left|s(t)\right|dt} = \frac{A^2\left\{T\rho+\frac{\rho^2}{2}\cos\phi\right\}_{-T/\cos\phi}^{0}}{AT} \\ &= \frac{A^2\dfrac{T^2}{2\cos\phi}}{AT} = \frac{AT}{2\cos\phi}.\end{aligned} \tag{A.3.8}$$

Thus, the maximum value of the detection statistic is found as $\dfrac{AT}{2\cos\phi}$ for Case II.

We can perform the same calculations for Case III using the limits given for Case III. (A.3.6) also holds for Case III, and the absolute value of the fractional autocorrelation for Case III is found as

$$\left|(s \star_{\phi} s)(\rho)\right| = A^2 \left| \int_{-T/2+\rho\cos\phi}^{T/2} rect\left(\frac{\beta}{T}\right) rect\left(\frac{\beta-\rho\cos\phi}{T}\right) d\beta \right|$$

$$= A^2 \left| \frac{T}{2} - (-\frac{T}{2} + \rho\cos\phi) \right| = A^2 (T - \rho\cos\phi). \qquad (A.3.9)$$

Using (A.3.9) in (A.3.3) and considering the limits for ρ in Case III, we can compute the peak amplitude value of the detection statistic as

$$\overset{v}{L}(m = m_o) = \frac{\int_0^{T/\cos\phi} A^2 (T - \rho\cos\phi) d\rho}{\int_{-\infty}^{\infty} |s(t)| dt} = \frac{A^2 \left\{ T\rho - \frac{\rho^2}{2}\cos\phi \right\}_0^{T/\cos\phi}}{AT}$$

$$= \frac{A^2 \frac{T^2}{2\cos\phi}}{AT} = \frac{AT}{2\cos\phi}. \qquad (A.3.10)$$

This shows that we obtain the same result both for Case II and Case III.

We can conclude that for both cases the detection statistic yields a peak amplitude value at the same level as given in (A.3.8) and (A.3.10). This peak level is dependent on the signal amplitude A and duration of the signal, T, directly. Cosine of the angle, ϕ, that the LFM signal makes with the time axis in the time – frequency plane, is inversely proportional with the peak level.

Consequently, for two chirp signals with the same amplitude and duration in time, the one that has a larger angle value produces a larger peak value for the detection statistic since $\cos\phi$ decreases as ϕ goes from 0 to $\pi/2$.